APPLICATIONS OF FORCE FEEDBACK STEERING FOR STEER-BY-WIRE VEHICLES WITH ACTIVE STEERING

A DISSERTATION
SUBMITTED TO THE DEPARTMENT OF MECHANICAL ENGINEERING
AND THE COMMITTEE ON GRADUATE STUDIES
OF STANFORD UNIVERSITY
IN PARTIAL FULFILLMENT OF THE REQUIREMENTS
FOR THE DEGREE OF
DOCTOR OF PHILOSOPHY

Avinash Balachandran

June 2015

This dissertation is online at: http://purl.stanford.edu/wz736wf4893

I certify that I have read this dissertation and that, in my opinion, it is fully adequate in scope and quality as a dissertation for the degree of Doctor of Philosophy.

J Gerdes, Primary Adviser

I certify that I have read this dissertation and that, in my opinion, it is fully adequate in scope and quality as a dissertation for the degree of Doctor of Philosophy.

Mark Cutkosky

I certify that I have read this dissertation and that, in my opinion, it is fully adequate in scope and quality as a dissertation for the degree of Doctor of Philosophy.

Allison Okamura

Approved for the Stanford University Committee on Graduate Studies.

Patricia J. Gumport, Vice Provost for Graduate Education

This signature page was generated electronically upon submission of this dissertation in electronic format. An original signed hard copy of the signature page is on file in University Archives.

தந்தை மகற்காற்று நன்றி அவையத்து
முந்தி இருப்பபச் செயல். --- திருக்குறள் 67

This dissertation is dedicated to my parents.

Acknowledgement

Going through a PhD is a unique and humbling experience. Though it may sometimes be the abode of desperation and despair, those of us who are engaged it in know that it is more often an arena of great ideas and noble pursuits. We spend years in graduate school attempting to contribute in someway to human knowledge and our dissertation is the crowning glory of that work. Writing the dissertation has provided me an opportunity to look back at my time in graduate school. Reflecting on my journey so far, I am faced with one immutable truth; I owe a great deal to a great many people. I hope to do as many of them justice as I can in this section.

Firstly, I would like to thank my advisor, Professor Chris Gerdes. Chris has that unique combination of deep technical skill and wide-eyed enthusiasm that makes him a great advisor. He is an invaluable resource for anything related to dynamics, modeling and controls. Beyond that, his opinion about jobs, academia and life in general has been very insightful (and frequently entertaining!). Chris also has the rare skill of being able to convey highly technical information to the general public and its been a pleasure seeing that skill in action during his various talks, interviews etc. My hope is that some of that skill has rubbed off on me, for what is a successful researcher if not a person who can communicate his ideas to others. Perhaps the aspect of Chris I appreciate the most is his enthusiasm. He is so fired up about research (to be fair, its about cars that drive themselves so who wouldn't be) but I have never left a meeting with Chris without feeling more enthusiastic than when I entered. Chris once mentioned to me that a PhD came with a 'lifetime warranty', so I intend to use that and keep him as a life resource!

I am also grateful to my defense committee. Professor Allison Okamura was on my

qualifying examination committee and followed my progress since the earliest days of my PhD. It was her class in haptics and corresponding feedback on the shared control system that resulted in the later third of my work in predictive haptic cues. Professor Mark Cutkosky and the BDML which he leads has proven to be an invaluable resource as well. His insight into tying my work with the tele-operation literature has been very useful. Furthermore, working with one of his students, Chris Ploch, to continue my work in predictive feedback has made the last few years of my PhD all that more enjoyable. Professor Steve Rock, who served as my committee chairman, taught the classes that would form the foundation of my controls knowledge at Stanford. Without his guidance and teaching, I would not have the necessary skills to conduct much of my research. Professor Erin MacDonald has provided valuable feedback in creating human subject experiments and I look forward to seeing her insights incorporated into future experiments to answer more complex and compelling questions.

I cannot go too far without thanking the members of the Dynamic Design Lab (DDL). Doing the kind of work that we do, with actual complex test vehicles, breeds a lab culture of collaboration. Having lab members that you can work with during the day and grab a beer with at night is indeed a pleasure. It has been especially rewarding to see the DNA of the lab change over the years but still have the same core strands that Chris implanted 20 years ago. The lab has a great support network of administrators/engineers/program directors (Erina, Adele, Jo, Jennifer, Elizabeth, Reilly, Sven, Godwin, Larry) that have made it an awesome place to work. The DDL alumni network has also been a great resource for research and job hunting. 'Once a DDLer, always a DDLer' and I look forward to continuing interaction with the lab going forward.

My time at Stanford would not be complete without mentioning my friends. It is not the easiest to spend five years away from home in a foreign country. However, I have been fortunate to have the very best of friends to keep me company along the way. These are the people that made my Stanford experience great by helping me keep perspective and being there in the best of times and the worst of times. Thanks for keeping me motivated and entertained during my years at Stanford.

I have saved the most important acknowledgment for last. My family. They have

been exceptionally supportive during my journey. Everyone of my family has brought a little bit of home here when they have visited me multiple times over my life at Stanford. Beyond that, I must thank my sister and brother-in-law for providing me a refuge in London, UK (where they live) whenever I needed time away. Taking the time in London to be with family has proven relaxing but also productive as I have also written two papers while there! For my parents words alone will never suffice for thanks. How do you thank the people who raised you in a few lines (or even paragraphs)? Nonetheless, I will try. They have been beyond supportive, visiting me a few times a year and bringing the sights, sounds and smells of home and home cooking to Stanford. They always have a listening ear and are invaluable sources of feedback, insight and most importantly encouragement. Perhaps their most important contribution has been to show me, by example, that I should always pursue my dreams and stay the course even when the going gets tough. For that lesson and many more, I shall always be in their debt.

Contents

List of Tables

List of Figures

Chapter 1

Introduction

1.1 Motivation

Modern life relies heavily on the automobile. They provide an unparalleled means of personal mobility without which many functions of daily life like commuting to work, getting groceries, traveling etc. become much more challenging. Thinking beyond the present and into the future, automobiles will continue to play an important role in personal mobility. Ensuring that they improve in terms of safety and comfort is the continuing mission of all automobile manufacturers and suppliers. Based on current trends, this mission seems like a success. From 2005 - 2011 the total number of automobile fatalities decreased every year to a historic low of 32,367 in 2011. Despite this encouraging trend, more can still be done. In particular, over a similar period from 2005 - 2008, Wilson and Stimpson showed that fatalities attributed to distracted driving rose 28% [78]. Furthermore, this work showed that texting alone resulted in an additional 16,000 deaths from 2001 - 2007. As more interactive mobile phones and computing devices permeated our lives, ensuring that vehicle safety is not compromised by distracted driving is a key challenge.

Safety systems like Electronic Stability Control (ESC) and Anti-lock Braking Systems (ABS), which seek to prevent loss of vehicle control, can do little to prevent collisions stemming from a distracted driver. Rather, to reduce these collisions, the first step involves having vehicles that are aware of their surroundings. Recent advances

in perception technologies like radar, cameras, and lidars provide detailed information to the vehicle about its surroundings [44], [45], [9]. These systems provide this information in real-time and in situations where human perception may be reduced due to distraction or challenging environmental conditions like poor lighting or fog. With this information about its environment, a vehicle now has the ability to generate feasible trajectories to ensure its safety and stability.

On calculating these safe trajectories, a vehicle needs to have some means of actualizing these trajectories in the event of an emergency where the driver's action will lead to collision. Therefore, the vehicle needs a means of augmenting the driver's steering command. This capability exists and is known as active steering. With active steering, a vehicle is able to intervene in emergency scenarios to prevent a distracted driver from colliding with the environment. This can improve the safety of a vehicle and reduce fatalities due to distracted drivers.

1.2 Conventional Steering Systems

To understand steering and, in particular, active steering capability, it is useful to discuss the evolution of steering systems over the last century. Figure 1.1 shows this evolution. Conventional steering systems like manual steering and power steering continue to dominate the market though new technologies like steer-by-wire are beginning to penetrate the production fleet.

Figure 1.1(a) illustrates a manual steering system. This was the earliest form of steering system where the driver, via the handwheel, mechanically turned the roadwheels. These systems formed the simplest of all steering systems as the handwheel command, after accounting for the steering ratio, is directly used to mechanically turn the roadwheels. This direct mechanically connection meant that drivers felt all the moments acting on the roadwheels during operation. This made manual steering systems hard to turn for the driver particularly when performing maneuvers like parallel parking which require a lot of steering effort.

In order to aid the driver and reduce steering effort, power steering systems were introduced later (illustrated in Figure 1.1(b)). In these systems, the handwheel was

still mechanically connected to the roadwheels. However, a power steering unit located on the steering column helped the driver lower his required torque command on the handwheel, when necessary, to increase the ease of turning. These units began as hydraulic systems which used hydraulic fluid as a means of assisting the driver and reducing his torque input on the handwheel during steering. These units would release hydraulic fluid to aid in turning the roadwheels when a simple torque measuring element called a torsion bar indicated that the difference between the driver's torque input and the torque acting on the roadwheels was beyond a certain amount. The characteristic of how the assist varied with this difference in torque was carefully designed to give a vehicle its particular power assistance 'feel'. More recently, hydraulic power assist has give way to Electronic Power Steering (EPS) systems. These

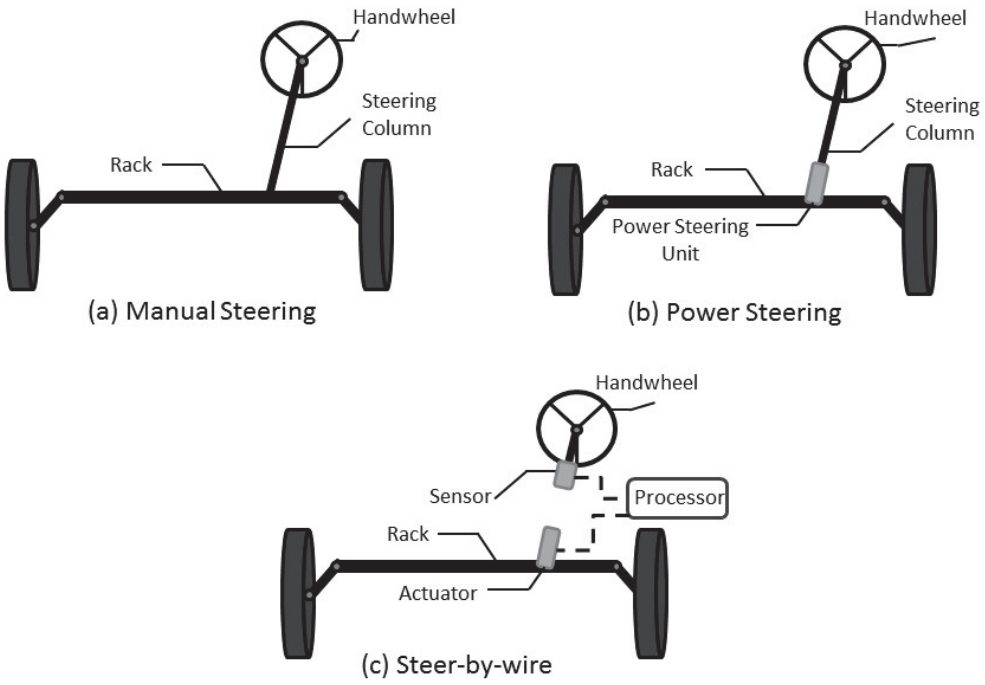

Figure 1.1: Evolution of steering systems

replace the hydraulic systems of the past with electronic motors that serve the same function of reducing the amount of torque a driver needs to input during turning. EPS systems form the backbone of the production vehicle fleet today.

Power steering systems still maintain a mechanical connection between the handwheel and roadwheel making active steering capability challenging to implement. Nonetheless, active steering can be achieved using cleverly designed mechanical steering systems like that created by ZF Lenksysteme and BMW AG [42]. This system can change the driver's steering command to the roadwheel despite the mechanical connection. Koehn and Eckrich showed that this system could aid in some vehicle stabilization tasks [42].

1.3 Steer-by-wire

In the 1990s, interest in replacing traditional steering systems on automobiles with by-wire systems grew [70]. This idea, known as steer-by-wire, replaces the traditional mechanical steering linkages between the handwheel and front tires with electronic sensors and actuators [4]. This technology has been used extensively by the aircraft industry since the 1970s [61], when electro-mechanical control systems replaced the traditional hydro-mechanical systems on aircraft. These systems not only saved weight and improved safety through better redundancy techniques, but they also allowed many pilot tasks to be automated. This led to the introduction of extensive stability augmentation and flight envelope limiting controllers [23].

Figure 1.1(c) illustrates a steer-by-wire system. These systems measure the driver's handwheel angle electronically and use a processor to calculate the required roadwheel angle which is realized using actuators. By severing the mechanical connection between the roadwheel and handwheel, steer-by-wire systems removed the need for the long steering columns associated with the conventional steering systems. This freed up space in the heavily packed front-end of the vehicle and also improved vehicle efficiency by reducing weight.

Steer-by-wire offers another means of achieving active steering interventions. The mechanical decoupling of the handwheel from the roadwheels allows steer-by-wire

systems to augment the driver's steering command by any arbitrary amount through roadwheel steering corrections. This capability is limited only by the physical limits on the roadwheel motion due to mechanical interference. The flexibility offered by this kind of active steering system creates opportunities to improve vehicle control and stability in a wide variety of different scenarios. Ackermann et al. showed that active steering can aid vehicle control in various situations like yaw control and rollover avoidance [2]. More recently, Anderson et al. [5] and Erlien et al. [22] showed that active steering can be used for sharing control between the driver and the vehicle, specifically for obstacle avoidance scenarios which typically require large active steering interventions. Therefore, active steering capability afforded by steer-by-wire systems can result in improvements in the safety and stability of a vehicle.

A major concern about implementing steer-by-wire systems is that, by removing the mechanical connection between the handwheel and roadwheels, critical system failure could have catastrophic results as the driver then has no means of lateral control over the vehicle. However, the recent development of good fault detection algorithms and redundancy systems for steer-by-wire vehicles has decreased the safety concerns about implementing this technology on consumer vehicles [26]. Therefore, though firmly in the research realm for many years, steer-by-wire systems are now finding their way to production vehicles on the road (see Figure 1.2) [21].

Figure 1.2: 2014 Infiniti Q50: World's first steer-by-wire production car

1.4 Steer-by-wire and Steering Feedback Torque

In a conventional steering system, the driver experiences a steering feedback torque (known as 'steering feel') on the handwheel that reflects the force and moments acting on the tires. Drivers use steering feel extensively to obtain useful information about the road and tire dynamics, which aids them in performing various driving tasks. Using a driving simulator, Liu and Chang demonstrated that having steering torque feedback results in better curve negotiation and skid recovery by a driver [46]. Forsyth and MacLean used a driving simulator and observed that without steering feedback, drivers became disoriented in tight turns [25]. Furthermore, Gordon showed that after visual feedback, steering torque feedback was rated as the next highest source of input for drivers [28]. Therefore, automobile manufacturers spend a lot of time and effort on designing good steering feedback torque on their vehicles. Similar results have also been found for driver assistance systems. For instance, Switkes et al. showed that steering feedback must be carefully designed to ensure the stability of a lane-keeping controller [73]. Clearly, designing good steering feedback torque is important for driver comfort and safety.

Though steer-by-wire technology has many benefits, the severing of the mechanical connection also disrupts this steering feedback torque. Now there is no direct mechanical channel for the forces and moments acting on the tire to be fed back to the driver. Since this feedback torque is important, creating a means of artificially

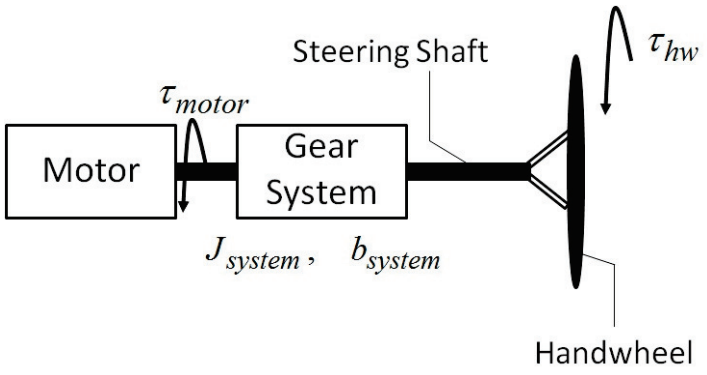

Figure 1.3: Force Feedback (FFB) steering system

re-creating this torque on a steer-by-wire vehicle is crucial. A force feedback (FFB) steering system mounted on a steer-by-wire vehicle can be used to create any arbitrary steering feedback torque on the handwheel that can be felt by the driver. Figure 2.2 illustrates a schematic of a typical FFB steering system and Appendix A details the design of the FFB system used for this work. A motor provides the ability to create any arbitrary torque that is applied directly to the handwheel and is felt by the driver. Since a FFB steering system can create any arbitrary steering feedback torque, what kind of torque to create is a natural question.

1.5 Thesis Overview

The question of what kind of torque to create on a FFB steering system for a steer-by-wire vehicle is a broad one. Figure 1.4 illustrates the approach taken in this dissertation to address this issue. As a first step, since steer-by-wire vehicles have no

Figure 1.4: Approach taken to develop torques on the FFB steering system for a steer-by-wire vehicle

inherent steering feel like conventional steering vehicles, creating an artificial steering feel is important. This allows a steer-by-wire vehicle to 'feel' like a conventional steering vehicle and gives the driver the same kinds of information that he is used to getting from those vehicles. Once a realistic and stable artificial steering feel can be created on steer-by-wire vehicles to mimic conventional steering vehicles (i.e. the first level in Figure 1.4), the question of active steering can be addressed (i.e. the second level in Figure 1.4). Conventional steering systems reflect the actual moments acting on the roadwheels in their steering feel. However, during an active steering intervention, the handwheel and roadwheels are no longer in sync, begging the question of what moments should be reflected in the steering feel then. This dissertation shows that using the concept of a virtual wheel to feed back the driver's intended tire moments, rather than the actual tire moments, results in a supportive steering feel. Realizing the second level in Figure 1.4 implies that a steering feel that supports scenarios with and without active steering can be implemented on steer-by-wire vehicles. The third level in Figure 1.4 builds on the prior two levels by overlaying this supportive steering feel with predictive haptic cues to aid in the obstacle avoidance task.

1.6 Contributions

The contributions of this dissertation are as follows:

I An easily tunable artificial steering feel model based on objective steering feel performance measures for use on actual steer-by-wire vehicles

II Lyapunov stability analysis of the artificial steering feel model along with stability guarantees incorporating the tire saturation limit and power assist effect

III The virtual wheel technique for generating supportive steering feel in scenarios with and without active steering

IV A novel technique for generating predictive haptic feedback based on a Model Predictive shared control framework for obstacle avoidance

V Design and conduct of an on-road experimental driver study to investigate the efficacy of predictive haptic feedback on the obstacle avoidance task

1.7 Dissertation Outline

The chapters in this disseration are organized as follows:

Chapter 2: Generating Artificial Steering Feel

Chapter 2 tackles the problem of creating a realistic artificial steering feel on steer-by-wire vehicles. It does this by creating a model for generating steering feel that is based on mirroring the moments acting on the tires that form the basis of steering feel in conventional steering systems. Identifying the appropriate level of model fidelity required to generate a realistic steering feel involves understanding what elements of steering feel are important like power assist. This chapter proposes using objective steering feel measures used in industry as a means of understanding which elements of steering feel are most important. The measures are used to inform the creation of the artificial steering feel model to have the appropriate fidelity to capture these important elements of steering feel while remaining intuitive to tune objectively with a small set of parameters. A simulation based design approach generates steering feel with desired characteristics for steer-by-wire vehicles while experimental data validates this technique as a means of generating steering feel on an actual steer-by-wire vehicle.

Chapter 3: Artificial Steering Feel Stability

Before this steering feel model can be put on the road, stability guarantees of performance must be obtained. This ensures that the model proposed will not result in unbounded outputs of the vehicle states during operation, leading to catastrophic results. Chapter 3 uses a Lyapunov stability analysis, that incorporates the inherent nonlinearities present in the system, to obtain such stability guarantees that hold even at tire saturation. These guarantees manifest as four

bounds on various design parameters in the model that, when met, guarantee stability. Furthermore, this approach yields bounds on the amount of power assist allowable for stability, providing guidance on how to design the power assistance effect.

Chapter 4: Supportive Steering Feel for Active Steering

Steer-by-wire enables active steering interventions that result in improved vehicle safety and stability especially during distracted driving. Steering feel in conventional steering systems, and consequently the proposed artificial steering feel model, reflects the actual moments acting on the roadwheels. During an active steering intervention, the roadwheel is incremented to something other than the handwheel command. Therefore, there exists a disconnect between the driver's command and the vehicle's motion, potentially resulting in driver confusion. Chapter 4 investigates the impact of active steering on steering feel and this disconnect between the driver and the vehicle. In these scenarios, a steering feel should support the intervention by reducing this disconnect between the driver's command and the controller. This chapter presents the virtual wheel as an approach that results in supportive steering feel during scenarios with and without active steering intervention. The virtual wheel ensures that the steering feel model reflects the driver's *intended* tire moments rather than the *actual* tire moments. Simulations and experiments show that this approach results in a supportive steering feel for active steering while giving intuition into why feeding back the actual tire moments is undesirable.

Chapter 5: Predictive Haptic Feedback for Obstacle Avoidance

Haptic steering cues can help improve safety during distracted driving scenarios by alerting the driver to on-coming obstacles early so that he can avoid them. Predictive shared controllers use both the vehicle's perception of the environment and active steering to work with the driver to ensure a safe and collision-free vehicle trajectory. These shared control systems must constantly balance the

sometimes competing objectives of following the driver's command and maintaining a feasible trajectory for the vehicle. The earlier the system intervenes, the smoother the intervention but the more it interferes with the driver's control authority. Ideally, predictive controllers should intervene late but also indicate early to the driver that these two objectives are in conflict so that he may modify his actions to reduce this conflict. Chapter 5 presents a novel technique for creating haptic steering feedback, based on future differences between the predictive controller and the driver. This feedback mirrors the tension between the sometimes competing controller objectives of following the driver and maintaining a feasible path. Simulation results indicate the inherent trade-offs of predictive haptic feedback and qualitatively discuss its impact. A driver study is performed to act as a proof-of-concept that this predictive feedback can result in improved driver performance in the obstacle avoidance task.

Chapter 6: Conclusion

This chapter summarizes the contributions of each of the preceding chapters. It clearly lists the contributions in each chapter and also details future directions and extensions of this work.

Appendix A: X1 Force Feedback Steering System

This appendix gives an overview into the mechanical and electrical design of the Force Feedback (FFB) steering system designed and implemented on X1. It gives specifications on the system and documents the system identification process used to obtain inherent system properties like inertia, damping and friction.

Chapter 2

Generating Artificial Steering Feel

By mechanically decoupling the handwheel from the roadwheels, steer-by-wire disrupts steering feel. Liu and Chang showed, using a simulator study, that this feel aids drivers in the driving task [47]. Furthermore, Gordon showed that after visual feedback, steering torque feedback was rated as the next highest source of input for drivers [28]. Much care is put into designing a good steering feel for modern vehicles. Particularly, elements of steering feel that drivers feel are important like the 'heaviness', the power assist effect, the 'stiffness' etc. are all carefully selected to create a good steering feel on production vehicles. Understanding how to design a good feel for steer-by-wire vehicles is important if these vehicles are going to be driven on the roads.

One way of creating steering feel on steer-by-wire vehicles is to feed back the steering motor torque directly to the driver. Shengbing et al. demonstrated using hardware-in-the-loop simulation that steering motor current can generate steering feedback [68]. Nguyen and Ryu used a similar approach and simulation to generate steering feel [55]. Asai et al. used a test bench setup to show that steering motor current coupled with a torque map can generate steering feel [8]. Though this technique generates a realistic steering feel, this feel is tied to the physical properties of the vehicle and cannot be varied easily in software.

Another way of creating steering feel is to use a steering model with some abstraction of the physical system. Low fidelity models, typically involving a spring

model based on steering angle, have been used on simulators by Segawa et al. [67] and Oh et al. [58]. Williams implemented a speed-varying spring model for steering feel on heavy trucks [76]. Husain et al. patented a simple pre-computed speed-varying steering feel model that depends solely on steering actuator load [35]. Low fidelity models, though simple to implement, cannot capture all the important elements of steering feel like power assist and 'heaviness' of steering. In order to capture more elements of steering feel than low fidelity models, higher fidelity models have been used in simulators by Salaani et al. [65] and Mandhata et al. [75]. Though higher fidelity models can capture more elements of steering feel, the increase in the number of model parameters makes tuning challenging. As a result, validation procedures such as the repeated subjective human evaluations used by Mandhata et al. [48] are required.

Currently, conventional vehicles have wide variation of steering feel. Steer-by-wire vehicles should be no different. Therefore, higher fidelity steering feel models, which can create a wide variation of steering feel, are necessary. However as model fidelity increases, the tuning of these models to obtain desired feel becomes more challenging. Therefore, finding the appropriate level of steering model fidelity is critical. The model must be complex enough to capture all the elements of steering feel that modern drivers care like 'heaviness', power assistance, 'stiffness' etc. However, it must remain simple enough to be tuned intuitively. This chapter analyzes objective steering feel performance measures used by industry as a means of understanding what elements of steering feel modern drivers think are important. This chapter then proposes using a steering feel model with the appropriate fidelity to capture these important elements while remaining intuitive to tune with a small set of parameters.

This chapter begins with a simple steering feel model which captures the effect of the moments acting on the tires, power assist, and the modification of the inherent inertia and damping of a steer-by-wire steering system. Objective steering feel performance measures used by industry are then introduced as a means of understanding and characterizing steering feel. These performance measures depend not only on the steering model but also on the vehicle dynamics. Using a simple dynamic vehicle simulation, a critical set of steering model parameters that tune these

measures are identified and a desired feel is designed. Experimental data then shows that the desired performance measures obtained via dynamic vehicle simulation can be replicated on an actual steer-by-wire vehicle. This work was first presented by Balachandran and Gerdes in [14].

2.1 Artificial Steering Feel

In conventional steering systems, the handwheel is mechanically connected to the roadwheels as illustrated in Figure 2.1. In steer-by-wire vehicles, the handwheel is mechanically decoupled from the roadwheels. The driver's steering commands are transferred electronically to motors that in turn actuate the roadwheels. This mechanical decoupling removes much of the steering feel that would normally be present in a conventional vehicle.

Steering feel can be artificially created in a steer-by-wire vehicle using a force feedback (FFB) steering system, illustrated in Figure 2.2. For this system, the handwheel torque felt by a driver (τ_{hw}) is determined by the motor torque (τ_{motor}) and the

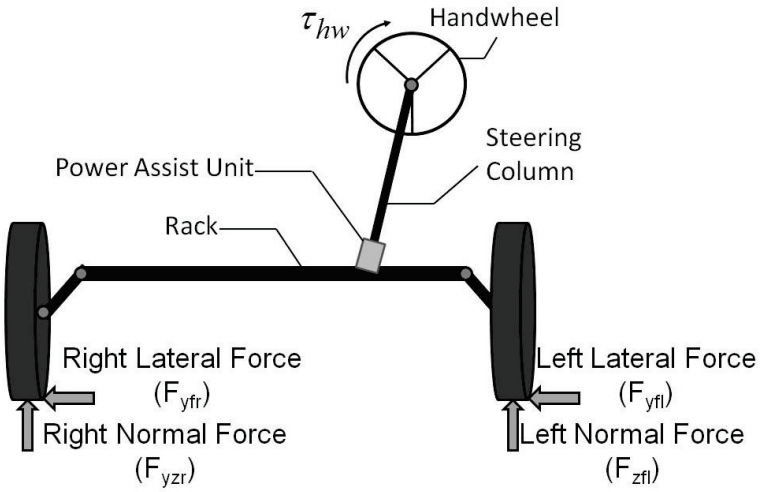

Figure 2.1: Conventional steering system

inherent steering system dynamics as follows:

$$\tau_{hw} = \tau_{motor} - J_{system}\ddot{\delta}_{hw} - b_{system}\dot{\delta}_{hw} \tag{2.1}$$

where the handwheel FFB motor torque (τ_{motor}) is commanded, the inherent system inertia (J_{system}) and system damping (b_{system}) are known from an identification of the mechanical system (see Appendix A.3), and the handwheel angle (δ_{hw}) is a driver input. Appendix A.3 also illustrates that the Coulomb friction term of the inherent steering system is small (about 1-2 [%] of the expected mean handwheel torque). This implies that, in general, the driver would not feel much of the friction in the system. Therefore, for the purposes of generating and analyzing artificial steering feel, the steering system model used omits the Coulomb friction effect.

2.1.1 Conventional Steering Feel

Developing an artificial steering feel for steer-by-wire vehicle involves having the FFB steering system feel like a conventional steering system. In conventional steering vehicles, there are three major torques that make up the steering feel. They are as follows:

(1) Tire moments

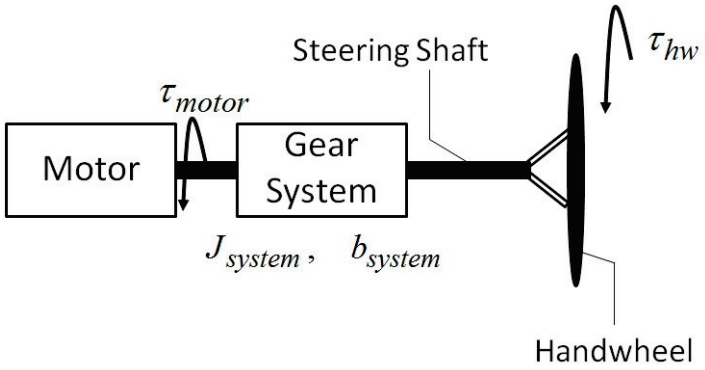

Figure 2.2: Force Feedback (FFB) steering system

(2) Torques due to inertia and damping

(3) Torque due to power assist

The weighted sum of these torques result in the steering feel felt by the driver.

Tire Moments

Figure 2.1 illustrates a conventional mechanical steering system with the right and left front lateral tire forces (F_{yfr}, F_{yfl}) and the right and left front normal tire forces (F_{zfr}, F_{zfl}) displayed. Figure 2.3 illustrates a typical suspension geometry of a conventional vehicle with the steer axis, mechanical trail (t_m), pneumatic trail (t_p), caster angle (θ_c), kingpin angle (θ_k) and scrub radius (d) indicated. The moments generated by the lateral and normal tire forces about the steer axis form a major component of steer feel.

The moment about the steer axis generated by the lateral tire forces is known as the aligning moment and is given by ([27]):

$$\tau_{alignMoment} = -\left(F_{yfl} + F_{yfr}\right)\left(t_m + t_p\right)\cos\sqrt{\theta_c^2 + \theta_k^2} \tag{2.2}$$

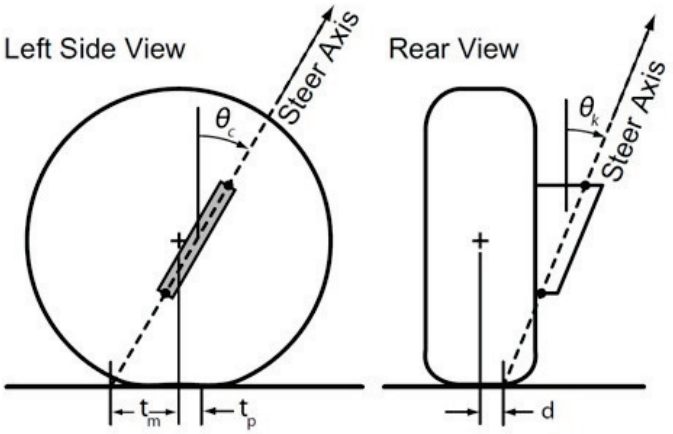

Figure 2.3: Typical suspension geometry on conventional vehicle

The aligning moment results in a strong self-centering torque at higher speeds.

The moment about the steer axis generated by the normal tire forces is known as the jacking torque and is given by ([27]):

$$\tau_{jackingTorque} = -(F_{zfl} + F_{zfr})\, d \sin\theta_k \sin\delta_{rw} + (F_{zfl} - F_{zfr})\, d \sin\theta_c \cos\delta_{rw} \quad (2.3)$$

where the δ_{rw} is the roadwheel angle. The jacking torque accounts for most of the self-centering effect of the steering feel at low speed when the effect of the aligning moment is small.

Transmission of the aligning moment and jacking torque via the steering linkages to the handwheel results in these two tire moments having a significant impact on the resultant steering feel.

Torques due to inertia and damping

Figure 2.1 illustrates that between the handwheel and the roadwheels there exists a set of mechanical connections including the steering column, power assist unit, rack and suspension which results in the steering system having some inherent damping and inertia. This inherent damping and inertia give rise to additional torques that are felt by the driver and form a part of the steering feel.

Torque due to Power Assist

In modern power steering systems, drivers receive an assistive torque counteracting the total front tire moment to aid them in turning the roadwheels [10]. The amount of this assistive torque depends on the difference in torque due to the total front tire moment and the driver's input torque as measured at the steering rack using a flexible torque-measuring element like a torsion bar. A greater difference in this torque results in a larger assistive torque. This assistive torque also features prominently in the steering feel.

2.1.2 Creating Artificial Steering Feel

Building a steering feel model with the appropriate fidelity allows the creation of artificial steering feel on steer-by-wire vehicles. The challenge is creating a model with the appropriate level of fidelity that balances the need for a realistic feel with the ease of tuning and real-time implementation. This results in a similar challenge found in implementing transparency in a teleoperated system [43]. Transparency implies that, in any bilateral teleoperator system design, the goal is to provide a faithful transmission of signals (positions, velocities, forces) between master and slave. This enables the coupling of the operator (in our case, the driver) as closely as possible to the remote task (in our case, the driving task). A natural question then becomes what level of transparency is possible (based on hardware and real-time implementation) and what is required (based on the tasks to be performed).

The model presented in this section builds upon the steering feel model developed by Mandhata et al. [75]. Mandhata's model incorporated tire moments, torques due to the steering system properties, static friction and a power assist model which assumed the use of a torsion bar. The model presented in this section, first proposed by Balachandran and Gerdes [13], [14], reduces the fidelity of Mandhata's model by incorporating tire moments and torques due to the steering system properties while omitting the static friction term. The model also proposes a tunable power assist model that does not require a torsion bar windup as an input. This is different from Mandhata's power assist model which required the torsion bar windup as an input and used a look-up table to determine the desired level of assist. Therefore this power assist model allows for more flexibility in designing a desired power assist effect. Furthermore, this power assist model enables the emulation of the power assist effect on steer-by-wire vehicles, like the one used in this work, which need not have a torsion bar. The model presented in this section has the appropriate level of fidelity to run in real-time on a steer-by-wire vehicle while being easy to tune intuitively. It also is able to capture the important elements of steering feel that drivers care about (as measured using objective steering feel metrics discussed in Section 2.2).

Based on this model, the motor torque (τ_{motor}) is given by:

$$\tau_{motor} = \tau_{damp} + \tau_{inertia} + K\tau_{assisted\ tire\ moment} \tag{2.4}$$

where the damping torque (τ_{damp}) and inertia torque ($\tau_{inertia}$) modify the inherent damping and inertia of the steering system and the assisted tire moment ($\tau_{assisted\ tire\ moment}$) represents the combined effect of the aligning moment, jacking torque and power assist. These are discussed in detail below. The tire moment gain (K) accounts for the transmission of moments from the tire to the handwheel and varies for different steering systems, suspension geometries and steering ratios. A larger K results in a great portion of the assisted tire moment being incorporated into the steering feel.

Damping Torque (τ_{damp})

Damping torque modifies the effect of the inherent system damping (b_{system}) on steering feel. Conventional vehicles have more inherent damping than steer-by-wire vehicles as they have a more mechanically complex steering system. Therefore, adding damping torque in a steer-by-wire system is usually necessary. In a conventional vehicle, modification of inherent damping is challenging as it involves actual hardware modification. However, using the model proposed in this section, modifying the system damping is much easier and can be done using software. The change in inherent damping is created using the following model:

$$\tau_{damp} = -\Delta b\dot{\delta}_{rw} \tag{2.5}$$

where the change in damping (Δb) to the system is a design parameter. A fairly clean signal for the derivative of the roadwheel angle ($\dot{\delta}_{rw}$) can be obtained using precise encoders and simple filtering.

Inertia Torque ($\tau_{inertia}$)

Inertia torque modifies the effect of the inherent system inertia (J_{system}) on steering feel. For the same reason as inherent damping, conventional vehicles have more

inherent inertia than steer-by-wire vehicles. Using the model proposed in this section, modifying the system inertia is much easier and can be done using software. The change in inherent inertia is created using the following model:

$$\tau_{inertia} = -\Delta J \ddot{\delta}_{rw} \tag{2.6}$$

where the change in inertia (ΔJ) to the system is a design parameter. Obtaining a clean signal for the second derivative of the roadwheel angle ($\ddot{\delta}_{rw}$) is challenging. Advanced filtering techniques can help with reducing the noise on this signal but typically, the resultant signal will still have some noise. To reduce the effect of this noise on the resultant steering feel, this work does not add an additional inertia via software (i.e. $\Delta J = 0$). Based on analysis of the objective steering feel measures presented later in this chapter, the effect of changing the inertia can be well captured using other design parameters that are less susceptible to noise.

Aligning Moment (τ_{align})

Front tire forces and their resulting moments have a large effect on steering feel. The effect that the front *lateral* tire forces (F_{yf}) have on steering feel is through the aligning moment. By assuming that the caster angle (θ_c) and kingpin angle (θ_k) are small in (2.2), the aligning moment can be approximated as the product of the front lateral tire forces and the total trail of the vehicle as shown:

$$\tau_{align} = -F_{yf}(t_m + t_p) \tag{2.7}$$

where t_m is the mechanical trail and t_p is the pneumatic trail of the vehicle. Taking the small angle assumption reduces the number of parameters needed for the model.

The brush tire model proposed by Fiala [24], and presented in the following form by Pacejka [59], gives a useful approximation of the nonlinear relationship between tire force and slip angle:

$$F_y = -C_\alpha \tan\alpha + \frac{C_\alpha^2}{3\mu F_z}\tan\alpha\,|\tan\alpha| - \frac{C_\alpha^3}{27\left(\mu F_z\right)^2}\tan^3\alpha \tag{2.8}$$

where the surface coefficient of friction (μ) and tire cornering stiffness (C_α) are design parameters. The normal load (F_z) can be obtained from the mass of the vehicle.

For simplicity, the mechanical trail (t_m) is assumed to be constant and the pneumatic trail (t_p) is modeled as a decreasing linear function of slip angle as introduced by Hsu et al. [34]:

$$t_p = t_{p0} - sgn(\alpha_f)\frac{t_{p0}C_{\alpha f}}{3\mu F_{zf}}\tan(\alpha_f) \tag{2.9}$$

where the pneumatic trail at zero front slip angle (t_{p0}), surface coefficient of friction (μ), front tire cornering stiffness ($C_{\alpha f}$) are design parameters. This simplification reduces the number of tuning parameters.

This aligning moment term reflects the current road condition to the driver via the steering feel. Real-time friction estimation approaches like that proposed by Hsu and Gerdes [33], can be used to obtain the surface coefficient of friction. This results in the appropriate front lateral tire force and pneumatic trail being used to generate an aligning moment term that corresponds to the current road condition.

Jacking Torque (τ_{jack})

The front *normal* tire forces (F_{zf}) affect the steering feel via the jacking torque. The jacking torque effect can be clearly seen when a driver turns the handwheel in a stationary vehicle. It causes the hood of the vehicle to 'jack up' (hence its name) and results in a self-returning torque on the handwheel. Its effect is much more pronounced at low speeds whereas the aligning moment effect is much more pronounced at higher speeds.

By making reasonable assumptions that the sum of the normal tire forces is much greater than their difference, i.e. $((F_{zfl} + F_{zfr}) >> (F_{zfl} - F_{zfr}))$, and that the road-wheel angle (δ_{rw}) is small, we can approximate (2.3) as a spring model. This spring model gives a useful approximation of jacking torque and captures the important centering effect in a simple model. A simple single spring model for jacking torque is given below:

$$\tau_{jack} = -K_{jack}\delta_{rw} \tag{2.10}$$

where the jacking torque stiffness (K_{jack}) is a design parameters.

Some production vehicles contain a steering deadband region where stiffness is lower than outside this region. To capture this effect, a two-spring-constant model can be used. The two-spring-constant model given below allows the deadband characteristics to be incorporated into the model.

$$\tau_{jack} = \begin{cases} -k_{db}\delta_{rw} & \text{if } |\delta_{rw}| \leq \delta_{db} \\ -k_{jack}\delta_{rw} - k_{db}\left(\text{sign}(\delta_{rw})\delta_{db}\right) & \text{if } |\delta_{rw}| > \delta_{db} \end{cases} \tag{2.11}$$

where the steering deadband (δ_{db}), deadband spring constant (k_{db}) and jacking torque spring constant (k_{jack}) are design parameters. The deadband region is typically very small (i.e. about 0.5 [%] of the entire steering range). Note that $k_{\text{db}} < k_{\text{jack}}$. However, k_{db} is chosen to be reasonably close to k_{jack} in value so as not to create an overly large change in gradient which would be uncomfortable for the driver. The resultant τ_{jack} given by this function is continuous. The two spring constants represent the different stiffnesses due to the steering deadband region.

Power Assist

In modern power steering systems, drivers receive an assistive torque counteracting the total front tire moment to aid them in turning the roadwheels. This torque factors into the steering feedback. Ryu and Kim demonstrated that the effect of this assistive torque on the resultant steering feedback is that a smaller fraction of the total front tire moment is included in the steering feedback [63]. Using the expressions for aligning moment and jacking torque obtained earlier, the total front tire moment can be approximated by:

$$\tau_{\text{tire moment}} \approx \tau_{\text{jack}} + \tau_{\text{align}} \tag{2.12}$$

The fraction of the total front tire moment felt by the driver is then modeled as

a weighting function (W_f) that depends on front slip angle. The resultant assisted total front tire moment is given as:

$$\tau_{\text{assisted tire moment}} = \tau_{\text{tire moment}} W_{\text{f}} \tag{2.13}$$

Building on the work of Ryu and Kim [63], this weighting function must have a unity value at zero front slip angle which decreases as the magnitude of front slip angle increases. This indicates that there is no assist at zero front tire force and the level of assist increases with the increasing magnitude of front tire force. The weighting function must also have a lower limit which translates to a saturation of the power assist effect when the magnitude of the front tire force exceeds a given threshold which is set based on the desired power assist characteristics. Modeling the weighting function (W_f) as a Gaussian function fulfills these critical requirements. The weighting function (W_f) is given by:

$$W_{\text{f}} = e^{\frac{-\alpha_{\text{f}}^2}{2\sigma_{\text{ps}}^2}} (W_{\text{f,max}} - W_{\text{f,min}}) + W_{\text{f,min}} \tag{2.14}$$

where the front slip angle (α_{f}) is known while the standard deviation (σ_{ps}), minimum weighting ($W_{\text{f,min}}$) and maximum weighting ($W_{\text{f,max}}$) are selected to create the desired power steering effect. A typical weighting function is illustrated in Figure 2.4. Note that $0 \leq W_{\text{f,min}} \leq W_{\text{f}} \leq W_{\text{f,max}} \leq 1$, $\forall \alpha_{\text{f}}$. A larger weight ($W_{\text{f}}$) results in a larger fraction of the total tire moment incorporated into the steering feel. Therefore, as slip angle increases and tire forces get larger, W_{f} decreases and a smaller fraction of the total tire forces is incorporated in the steering feel. This replicates the effect of power assist. A zero weight ($W_{\text{f}} = 0$) implies that none of the total tire moment and only the damping and inertia torques are included in the steering feel. $W_{\text{f,max}}$ is a design parameter which is typically set to 1. This represents that when there is no power assist effect, the steering feel incorporates the full tire moment effect similar to a vehicle with purely manual steering.

Based on the steering feel components listed above and using Equation (2.4), an artificial steering feel can be generated. Figure 2.5 illustrates the block diagram of the model and the resultant vehicle-driver system.

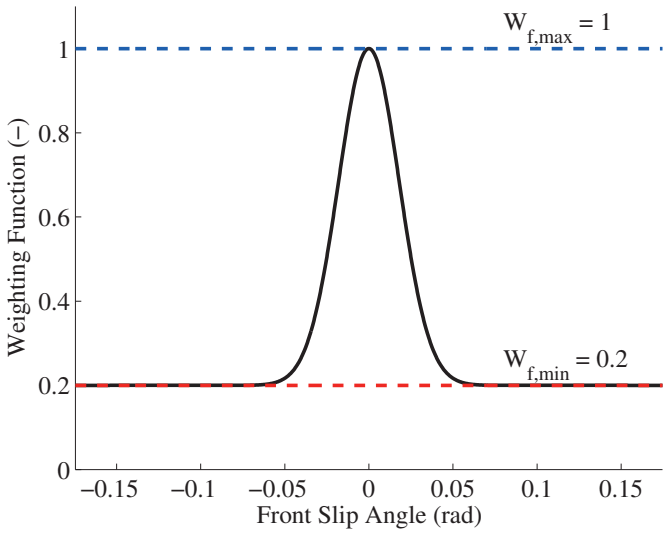

Figure 2.4: Power assist weighting function

2.2 Objective Steering Feel Performance Measures

Having a model to generate steering feel, as presented in the section above, is only one part of the solution to designing an artificial steering feel. In order to design a good steering feel, an effective way to characterize the steering feel must also be employed. One way to do this is to use surveys as a means of steering feel evaluation as demonstrated using a simulator by Mandhata et al. [48]. Though very useful in characterizing a given steering feel, surveys give a subjective evaluation of steering feel. This makes the iterative process of designing a good steering feel time-consuming as these experiments must be conducted repeatedly for each iteration.

In industry, objective performance measures for steering feel are used to give designers a means of characterizing steering feel. This characterization gives designers intuition into what aspects of the steering feel are important to drivers. These performance measures are used to evaluate on-center handling and are obtained by performing a weave test, in accordance with the ISO13674-1:2010 standard [37], as described by Norman [56] and Salaani et al. [64]. On-center handling describes the steering feel of a vehicle during nominal straight-line driving and in negotiating large

radius bends at high speed but low lateral acceleration. These performance measures depend not just on steering characteristics but on vehicle dynamics as well.

The performance measures introduced in this section are obtained from data of a vehicle performing a weave maneuver, which consists of a 0.2 [Hz] steering input such that a maximum lateral acceleration of 0.2 [g] is observed, at 60 [mph]. The weave is illustrated in Figure 2.6. Five different performance measures are obtained from this data:

(1) Returnability

(2) On-center feel

(3) Linearity

(4) Effective torque stiffness

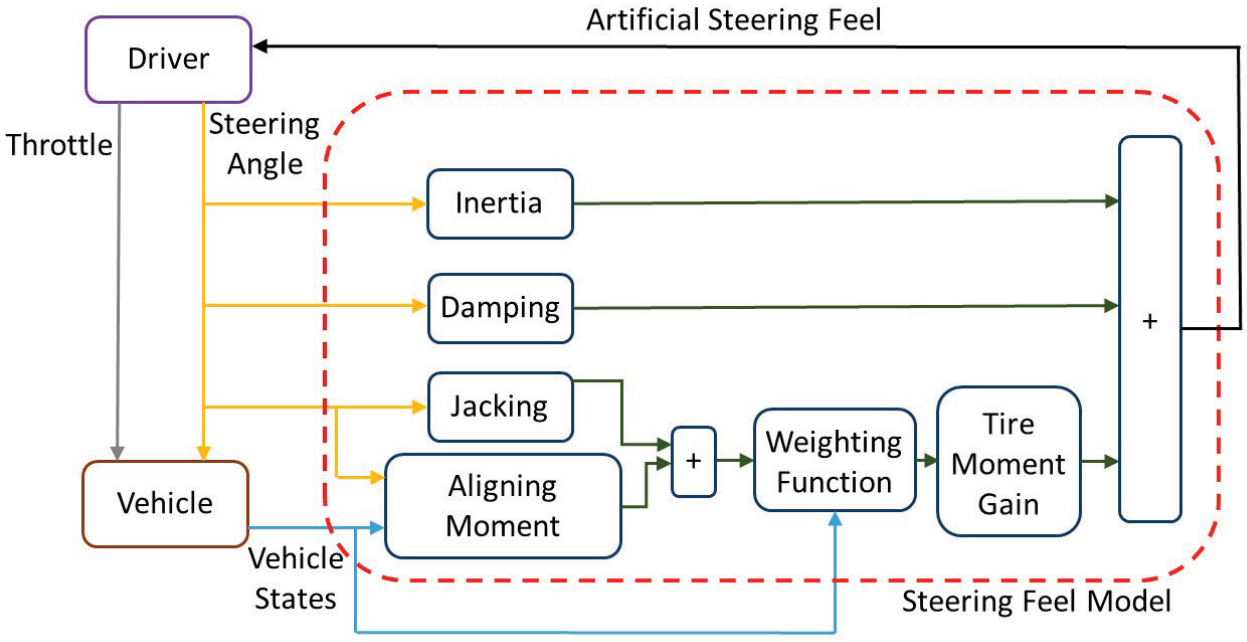

Figure 2.5: Block diagram of artificial steering feel model and resultant vehicle-driver system

(5) Steering sensitivity

These measures are obtained using three different cross plots:

(1) Handwheel torque versus driver steering input (Figure 2.8)

(2) Handwheel torque versus vehicle lateral acceleration (Figure 2.7)

(3) Vehicle lateral acceleration versus driver steering input (Figure 2.9)

Since a weave is a dynamic maneuver, the vehicle's handwheel torque and vehicle lateral acceleration depend on both the current driver steering input and the past state of the vehicle. Therefore, the cross plots listed above display hysteresis. The nonlinear nature of the dynamics also means that closed-form formulas for these plots cannot be obtained.

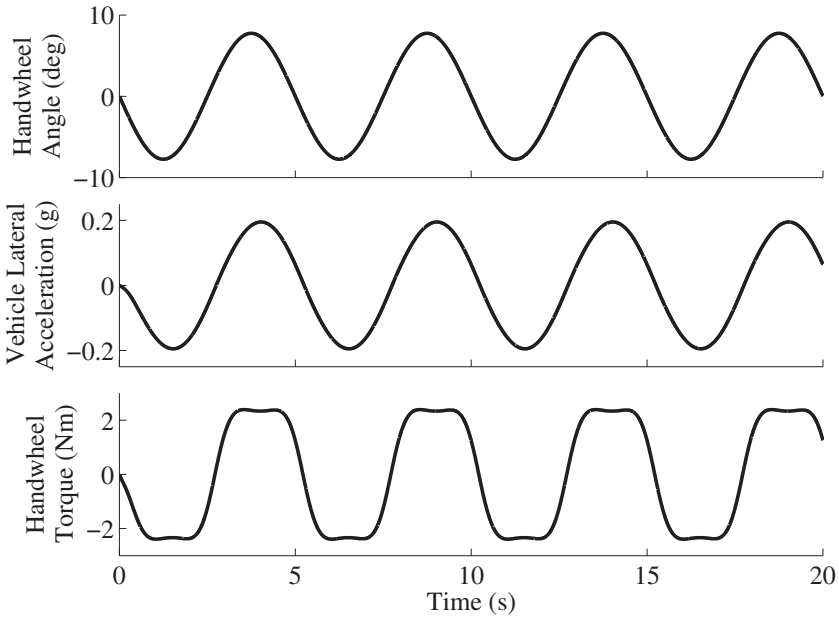

Figure 2.6: Weave at 60 [mph]

2.2.1 Measures from Handwheel Torque - Vehicle Lateral Acceleration Cross Plot

Figure 2.7 illustrates a typical handwheel torque versus vehicle lateral acceleration plot. *Returnability, on-center feel* and *steering torque linearity* are obtained from this plot.

Returnability

Returnability is the vehicle lateral acceleration at zero handwheel torque as illustrated in Figure 2.7 and represents the dynamic lag in the system. A high returnability indicates that the vehicle has persistent lateral acceleration while at zero handwheel torque and corresponds to a 'heavier' steering feel.

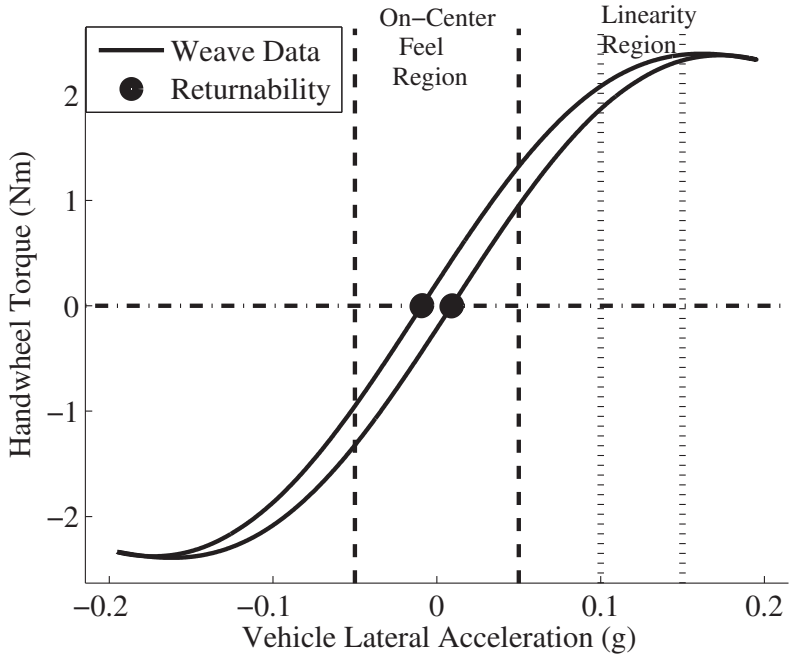

Figure 2.7: Handwheel torque - Vehicle lateral acceleration at 60 [mph]

On-Center Feel

On-center feel is the steering torque gradient between -0.05 [g] and +0.05 [g] in vehicle lateral acceleration as illustrated in Figure 2.7 and defined in the ISO13674-1:2010 standard [37]. It represents the handling of the vehicle during highway driving which includes nominally straight-line driving and the negotiation of large radius bends at high speeds but low lateral accelerations.

Steering Torque Linearity

Linearity is the ratio of the steering torque gradient between +0.1 [g] and +0.15 [g] (illustrated in Figure 2.7) and the on-center feel described above. Linearity represents the level of power assist with a larger linearity indicating a lower power assist effect and a clearer feel of tire dynamics and road properties for the driver.

2.2.2 Measures from Handwheel Torque - Driver Steering Input Cross Plot

Figure 2.8 illustrates a typical handwheel torque versus driver steering input plot. Data from this plot determines the *Effective torque stiffness*.

Effective Torque Stiffness

Effective torque stiffness is the steering torque gradient computed between -20 [%] and +20 [%] of the maximum steering input as illustrated in Figure 2.8, defined in the ISO13674-1:2010 standard [37] and, is the stiffness felt when turning. Drivers use the change in stiffness, which depends on the effective torque stiffness, as a means of detecting the center position of the handwheel. Increasing the stiffness will make the steering feel 'heavier' while also making the center position clearer to the driver.

2.2.3 Measures from Vehicle Lateral Acceleration versus Driver Steering Input Cross Plot

Figure 2.9 illustrates a typical vehicle lateral acceleration versus driver steering input plot. Data from this plot determines the *Steering sensitivity*.

Steering Sensitivity

Steering sensitivity is the handwheel angle gradient between -0.2 [g] and +0.2 [g] of lateral acceleration as defined in the ISO13674-1:2010 standard [37]. This lateral acceleration region captures the steering sensitivity during a typical on-center driving experience. A least squares linear fit of the data, as illustrated in Figure 2.9, gives this gradient. Increasing the sensitivity corresponds to a more 'crisp' and responsive feel. Since steering sensitivity depends solely on handwheel angle and lateral acceleration, it is independent of handwheel torque. Hence, the steering feel model presented in

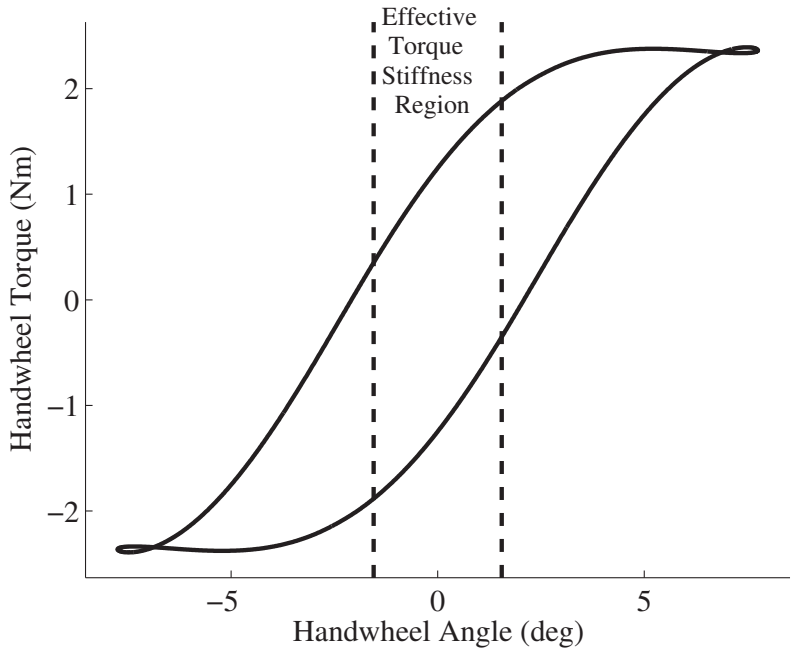

Figure 2.8: Handwheel torque - Driver steering input at 60 [mph]

Section 2.1 does not affect this measure. Decreasing the steering ratio or reducing the steering lag in a system will increase steering sensitivity.

2.3 Simulation Structure

The objective performance measures introduced in the prior section depend on both vehicle dynamics and the steering model. Therefore a dynamic vehicle simulation coupled with the steering model can be used to characterize and design a steering feel. Performing an ISO-standard weave in simulation with a particular set of vehicle and steering feel model parameters allows these performance measures to be obtained for a given set of model parameters. Using this simulation, different steering parameters, for any type of vehicle, can be rapidly evaluated and tuned objectively to obtain the desired steering feel.

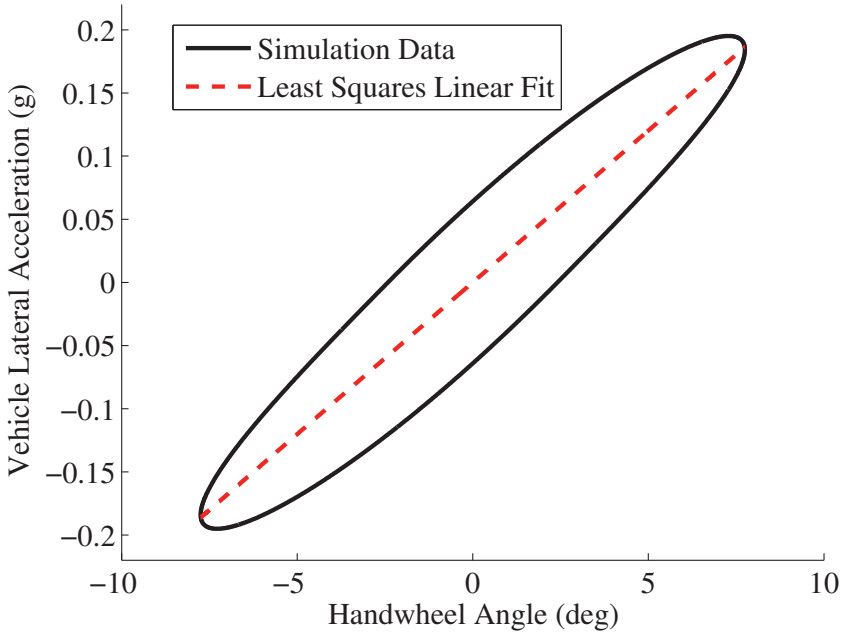

Figure 2.9: Vehicle lateral acceleration - Driver steering input at 60 [mph]

2.3.1 Vehicle Model

Since the weave maneuver is performed at a constant speed and with low lateral acceleration, a simple bicycle model, as illustrated in Figure 2.10, can be used for this simulation. The front and rear axles are lumped together and modeled as a single entity each. The dynamic states are sideslip (β) and yaw rate (r). The equations of motion are as follows:

$$\dot{\beta} = \frac{F_{yf} + F_{yr}}{mU_x} - r \tag{2.15}$$

$$\dot{r} = \frac{aF_{yf} - bF_{yr}}{I_{zz}} \tag{2.16}$$

where m is the vehicle mass, U_x is the longitudinal velocity in the body fixed frame, I_{zz} is the yaw inertia, and a and b are the distances from the center of gravity to the front and rear axles, respectively. Since this simulation represents the standard weave, U_x is constant. The tire slip angles are expressed as nonlinear functions of the

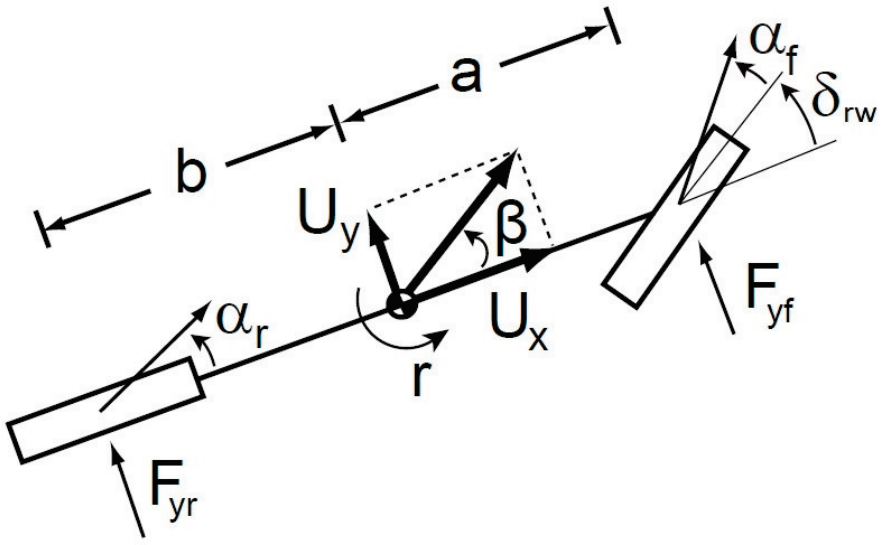

Figure 2.10: Bicycle model used for running vehicle simulation and for determining equations of motion

dynamic states and the front steer angle, δ_{rw}:

$$\alpha_f = \tan^{-1}\left(\beta + \frac{ar}{U_x}\right) - \delta_{rw} \quad (2.17)$$

$$\alpha_r = \tan^{-1}\left(\beta - \frac{br}{U_x}\right) \quad (2.18)$$

Lateral tire forces are obtained using the non-linear brush tire model (2.8).

2.3.2 Simulation Parameters

The vehicle parameters used in simulation are from an experimental steer-by-wire vehicle, X1, illustrated in Figure 2.11. The parameters are shown in Table 2.1. X1 is a true steer-by-wire vehicle with independent steering motors on each wheel and no steering rack or torsion bar. It also has a FFB steering system (see Appendix A) allowing artificial steering feel to be generated at the handwheel.

Table 2.1: X1 Parameters

Parameter	Value	Units
m	1973	kg
I_{zz}	2000	$\mathrm{kg \cdot m^2}$
a	1.53	m
b	1.23	m
$\mathrm{C}_{\alpha f}$	110	$\mathrm{kN \cdot rad^{-1}}$
$\mathrm{C}_{\alpha r}$	148	$\mathrm{kN \cdot rad^{-1}}$
J_{system}	0.0014	kgm^2
b_{system}	0.015	$Nm/rads^{-1}$

2.4 Steering Feel Design

Using the simulation structure described in Section 2.3, the effect of the steering feel model parameters and of varying speed on steering feel can be investigated. This knowledge is crucial to understanding and designing steering feel intuitively.

2.4.1 Effect of Parameters

Section 2.2 introduced four performance measures (*returnability, on-center feel, linearity, effective torque stiffness*) that can be changed by modifying the steering feel model parameters. The final performance measure (*steering sensitivity*) does not depend on handwheel torque and cannot be varied through changing the parameters of the steering feel model. It is simply a reflection of the mapping chosen from handwheel to roadwheel angle.

Section 2.1 introduced the following seven parameters that can be varied in the steering feel model to obtain different steering feel characteristics:

(1) Change in damping (Δb)

(2) Change in inertia (ΔJ)

Figure 2.11: X1 Steer-by-wire vehicle

(3) Deadband spring constant (k_{db})

(4) Jacking torque spring constant (k_{jack})

(5) Weighting function standard deviation (σ_{ps})

(6) Weighting function lower limit ($W_{\mathrm{f,min}}$)

(7) Tire moment gain (K)

By varying each of the parameters listed above in turn while the other parameters are held constant, the effect of each individual change can be investigated using the simulation described in Section 2.2. Table 2.2 documents the results of *increasing* each model parameter in turn while holding the other parameters constant. If the effect results in an *increase* in a particular performance measure, a up-arrow ($\uparrow$) is used. If the effect results in a *decrease* in that measure, a down-arrow ($\downarrow$) is used. If the effect results in the measure being held mostly *constant*, a dash ($-$) is used. For example, in the first row concerning the change in damping (Δb), increasing this parameter results in a increase in returnability while all other measures remaining approximately constant.

Critical Model Parameters

Table 2.2 shows that more than one model parameter can have the same effect on a given performance measure. Also, one model parameter can have an effect on multiple performance measures. Hence, a reduced set of critical model parameters can be tuned in order to to obtain any desired steering feel characteristics. This allows for a more intuitive tuning procedure. In order to control the four performance measures mentioned, four critical parameters are chosen. They are marked in bold in Table 2.2 and listed below:

(1) Change in damping (Δb)

(2) Jacking torque spring constant (k_{jack})

(3) Weighting function lower limit ($W_{\mathrm{f,min}}$)

(4) Tire moment gain (K)

The change in damping controls the returnability, the jacking torque spring constant controls the on-center feel, the weighting function lower limit controls the linearity and the tire moment gain controls the on-center feel and effective torque stiffness. These parameters have the additional benefit that their effect is limited mainly to the performance measures that they control resulting in a targeted tuning ability. Though the tire moment gain controls both the effective torque stiffness and the on-center feel, the jacking torque spring constant can be used to tune the on-center feel without affecting the effective torque stiffness. Note that the change in inertia and weighting function standard deviation can also be similarly used in tandem with another parameter to vary effective torque stiffness. However, the change in inertia requires a noisy twice differentiated handwheel angle signal for implementation and the weighting function standard deviation is a more abstract parameter as compared to the tire moment gain which has a physical basis. Therefore, using the tire moment gain as a means to vary effective torque stiffness results in better performance and a more intuitive tuning parameter.

The effect of each of these parameters on the steering feel crossplots and hence the performance measures, can be seen in Figure 2.12, Figure 2.13, Figure 2.14 and Figure 2.15 respectively, where the relevant regions for the performance measures are marked as in Figure 2.7 and Figure 2.8.

2.4.2 Effect of Speed

The performance measures described in Section 2.2 represent the steering feel characteristics of a vehicle performing a fixed speed weave maneuver. Since an ISO-standard weave can be performed at different speeds, this implies that the steering feel performance measures obtained depend on speed. Using the simulation described in Section 2.3, Figure 2.16 illustrates how the steering feel crossplots vary with speed given in meters per second [mps].

Effective torque stiffness and *steering sensitivity* both increase with increasing speed as seen in Figure 2.16. Though the relationship between these two performance

Increasing Parameter (↑)	Returnability	On-center Feel	Linearity	Effective Torque Stiffness
Change in damping (Δb)	**↑**	**-**	**-**	**-**
Change in inertia (ΔJ)	-	↓	-	↓
Deadband spring constant (k_{db})	↑	↑	-	↑
Jacking torque spring constant (k_{jack})	**-**	**↑**	**-**	**-**
Weighting function standard deviation (σ_{ps})	-	-	↑	↑
Weighting function lower limit ($W_{f,min}$)	**-**	**-**	**↑**	**-**
Tire moment gain (K)	**-**	**↑**	**-**	**↑**

Table 2.2: Steering Feel Algorithm Parameter Variation Table

measures and speed is mathematically complex, involving many different terms, it is approximately proportional ($\propto$) to speed when using typical steering parameters:

$$\text{Effective torque stiffness} \propto U_x \tag{2.19}$$

$$\text{Steering sensitivity} \propto U_x \tag{2.20}$$

Returnabilty of the feel decreases as speed increases resulting in the driver experiencing a 'lighter' feel. Again, though the relationship between returnability and speed is mathematically complex, it is approximately proportional to the reciprocal of speed when using typical steering parameters:

$$\text{Returnability} \propto \frac{1}{U_x} \tag{2.21}$$

On-center feel decreases with increasing speed, resulting in a less pronounced centering effect of the steering.

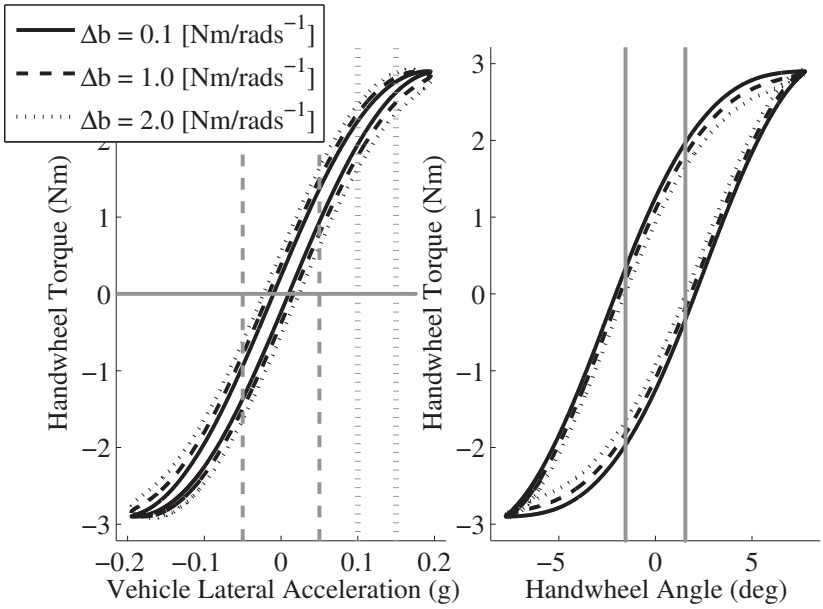

Figure 2.12: Steering feel crossplots when the change in damping is varied

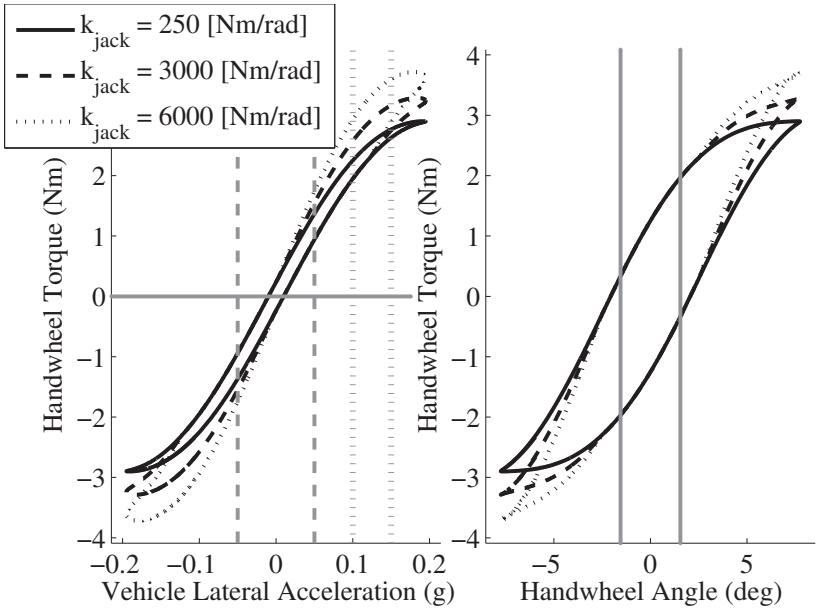

Figure 2.13: Steering feel crossplots when the jacking torque spring constant is varied

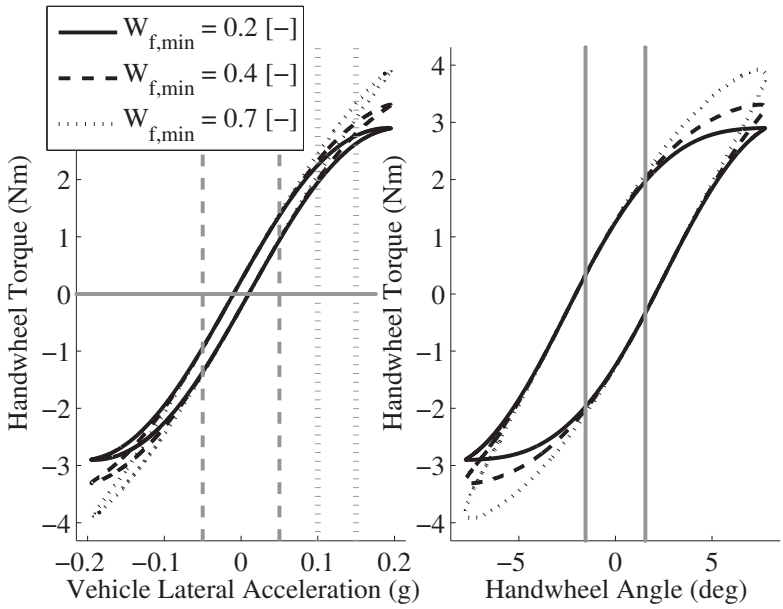

Figure 2.14: Steering feel crossplots when the weighting function lower limit is varied

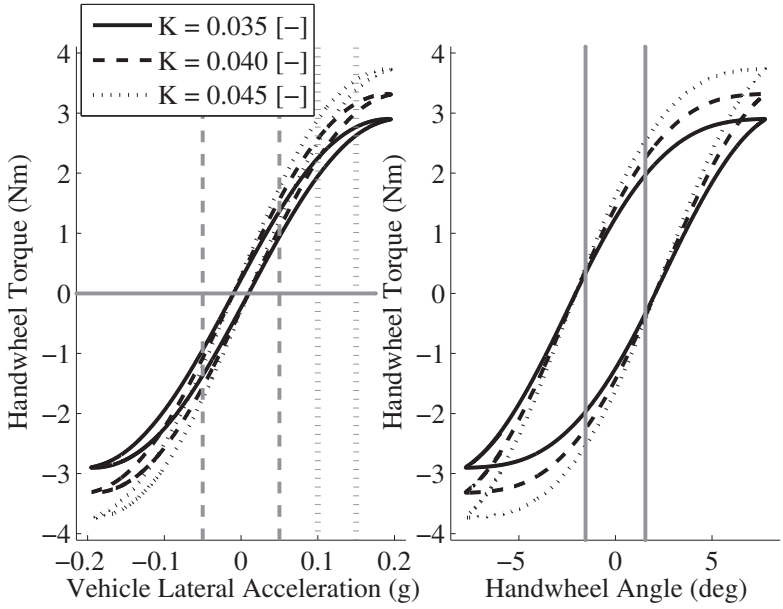

Figure 2.15: Steering feel crossplots when the tire moment gain is varied

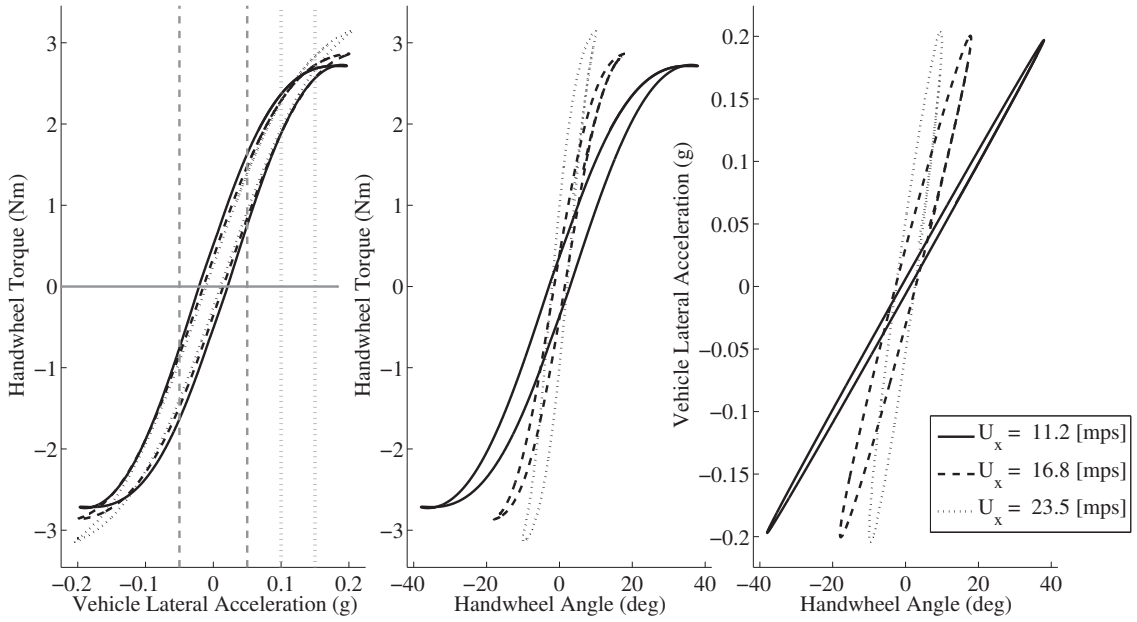

Figure 2.16: Steering feel crossplots when the speed is varied

Linearity increases with increasing speed, indicating that the power assist effect decreases as well.

The approximate scaling rules presented above, give the designer a means of predicting how a particular artificial steering feel's objective measures will vary with speed. Therefore, a designer can create a feel based on a fixed speed weave and still have intuition about how that feel will vary as the vehicle speed varies during the driving task. Practically, a designer can then design a feel using a standard ISO weave maneuver at 60 [mph] (which is the speed at which a realistic range of objective measures is documented, see Table 2.3). The designer can create a feel at this speed that has the desired objective measures while still understanding how these measures vary with speed.

2.4.3 Design of Steering Feel

Using the simulation described in the Section 2.3, any given set of parameters for the model can, through simulation at a given speed, be mapped to the five performance measures described. This allows steering feel to be designed objectively. Realistic ranges for the performance measures can be obtained from surveys of a variety of different vehicle models performing an ISO-standard weave at a fixed speed [64]. A steering feel can then be designed in simulation to obtain the desired performance measures using these ranges as a guide. This desired set of performance measures will then reflect the steering feel effects that individual designers deem important.

With this in mind, a realistic steering feel was designed for use in the steer-by-wire vehicle, X1. Low *returnability* and *linearity* helped to emulate the familiar 'lighter' and highly assisted steering feel of modern power steering vehicles. A middle of the range *on-center feel* ensured comfortable centering properties during nominal highway driving while the appropriate *stiffness* ensured comfortable centering properties at low speeds. Lastly, a higher *steering sensitivity* than the given range exploited the inherent benefit of a steer-by-wire system in reducing conventional steering lag, resulting in a highly responsive driving experience. The realistic performance measure ranges for a weave at 60 [mph] as well as the measures selected for X1 at 60 [mph]

and the corresponding measures for X1 at 25 [mph] are shown in Table 2.3.

Table 2.3: Steering Feel Design

Measure	Realistic Range (60 [mph]) [64]	X1 (60 [mph])	X1 (25 [mph])
On-Center Feel (Nm/g)	7 - 33	17	22
Stiffness (Nm/deg)	NR	0.37	0.12
Sensitivity (g/100deg)	0.27 - 1.42	2.33	0.52
Linearity (%)	6 - 121	25	22.7
Returnability (g)	0.01 - 0.13	0.01	0.01

2.5 Artificial Steering Feel on a Steer-by-wire Vehicle

2.5.1 Implementation on a Steer-by-wire Vehicle

The model described in Section 2.1.2 can also be programmed directly on a steer-by-wire vehicle. The model uses the driver's steering angle (δ_{hw}), roadwheel angle (δ_{rw}) and front slip angle (α_f) as inputs while generating the handwheel FFB motor torque (τ_{motor}) in (2.1).

On the steer-by-wire vehicle X1, encoders obtain the handwheel angle and roadwheel angle. The roadwheel angle derivative is approximated by differencing the encoder signal. A low-pass filter with cutoff frequency 10 [Hz] removes high frequency sensor noise on this derivative. Since a change in inertia is not necessary with this vehicle, the second derivative of the roadwheel angle is not calculated.

X1 uses an integrated Global Positioning System (GPS) and Inertia Measurement System (INS) to obtain the yawrate (r), sideslip (β) and longitudinal speed (U_x) of the vehicle. Based on (2.17), the front slip angle (α_f) can be calculated from this information. The motor torque (τ_{motor}) is then fed to the motor that is part of the FFB steering system on the vehicle. A dSPACE MicroAutoBox II (DS1401) performs all computation at a rate of 500 [Hz].

2.5.2 Experimental Validation of Simulation Design Technique

Since the performance measures are dependent not just on the steering feel model but also vehicle dynamics, experiments validate the simulation based design technique. A manual weave test was conducted on the X1 test vehicle, introduced in Section 2.3.1, at a speed of 24 - 26 [mph]. The experimental test was run at a lower speed due to test track and vehicle acceleration limitations.

2.5.3 Experimental Results

Figure 2.17, Figure 2.18 and Figure 2.19 illustrate the crossplots obtained from data of the artificial steering feel emulation on X1. Since the experiment was conducted at a lower speed than the design simulation, the steering angle required in the weave to get the maximum vehicle lateral acceleration of 0.2 [g] is larger in the experiment than in the design simulation. This results in Figure 2.18 and Figure 2.19 having a smaller

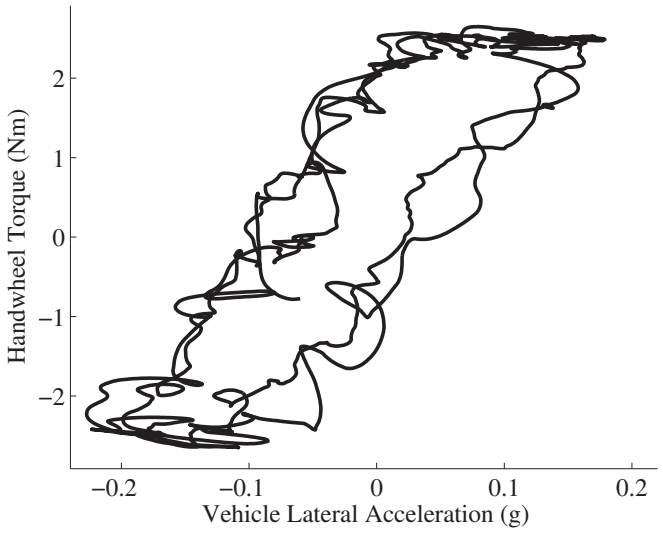

Figure 2.17: Experiment: Commanded Handwheel torque - Measured Vehicle lateral acceleration at 25 [mph]

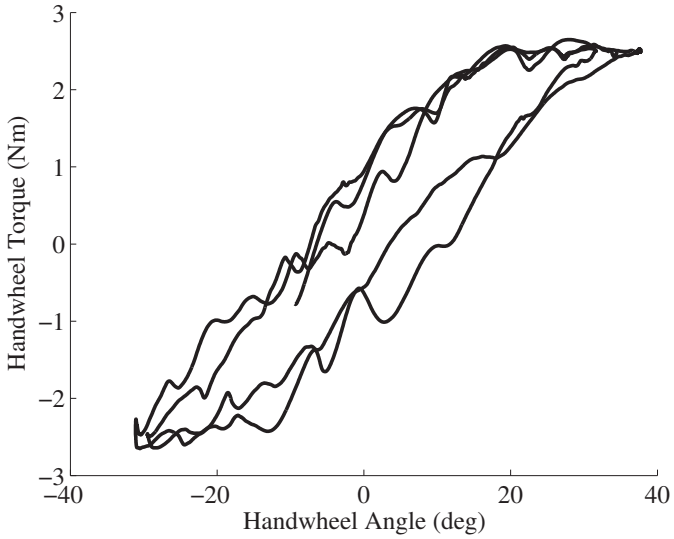

Figure 2.18: Experiment: Commanded Handwheel torque - Measured Driver steering input at 25 [mph]

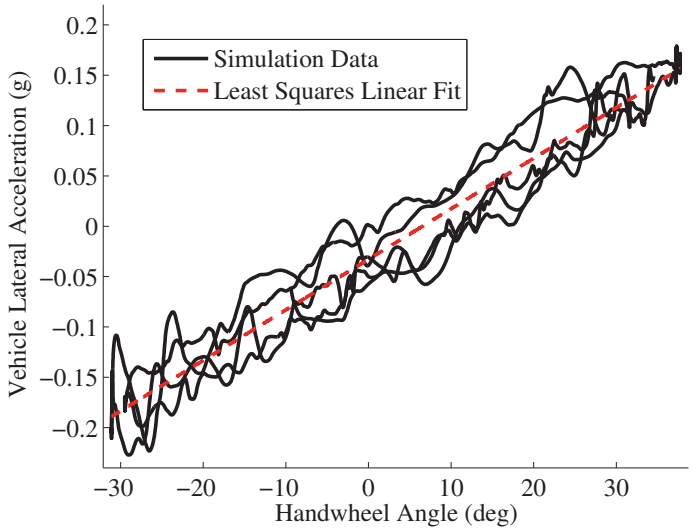

Figure 2.19: Experiment: Measured Vehicle lateral acceleration - Measured Driver steering input at 25 [mph]

range of steering input than Figure 2.8 and Figure 2.9. Also, since returnability increases with decreasing speed, the experimental crossplot in Figure 2.17 is wider than the design simulation crossplot given in Figure 2.7.

To compare the experimental data with simulation, a new simulation is performed to account for the change in speed and steering input. Table 2.4 compares the performance measures obtained using this simple vehicle simulation and the experimental weave performed by X1. The first four performance measures obtained through simulation match well with the measures obtained through experimental data as evidenced in absolute terms and in the percentage errors. Note that even though the error in the returnability metric seems large, in absolute terms, the error is on the order of 0.01 [g] which is extremely small and indeed within measurement error of the accelerometer. Therefore, the design technique based on this simulation could be used to incorporate a desired set of objective performance measures into an actual vehicle's steering feel.

Table 2.4: Experimental Comparison (25 [mph])

Measure	X1 (Experimental)	X1 (Simulation)	Error [%]
On-Center Feel (Nm/g)	23	22	4.5
Stiffness (Nm/deg)	0.11	0.12	-8.3
Sensitivity (g/100deg)	0.50	0.52	-3.8
Linearity (%)	23	22.7	1.3
Returnability (g)	0.02	0.01	100

2.6 Summary

This chapter proposes a steering feel model of appropriate fidelity to capture the elements of steering feel used for objective evaluation. The fidelity of this model is such that while capturing all these effects, it remains intuitive to tune objectively with a small set of parameters. Using a simple dynamic vehicle simulation, coupled with the steering feel model, steering feel can be designed for an individual vehicle. Tuning a critical set of parameters of the steering feel model in simulation allows the

design of a steering feel which has a desired set of performance measures. This desired steering feel can be implemented as the baseline steering feel on a steer-by-wire vehicle. Additional haptic information can then be overlaid on this feel to communicate vital information (e.g., lane boundaries, oncoming obstacles, vehicle handling limits) to the driver, aiding in the development of new driver assistance systems.

Chapter 3

Artificial Steering Feel Stability

The steering feel model presented in the previous chapter contains a few nonlinearities resulting from tire saturation and power assist effects which pose a major challenge to stability analysis. Prior approaches to analyzing the stability of power assisted steering systems have sought to enforce a linear structure on the problem so as to be able to use linear stability analysis techniques. For example, to overcome the issues due to the power assist nonlinearities, Odenthal et al. analyzed stability of the manual steering component of steering feel, leaving out the nonlinear power assist components [57]. Avoiding the tire model nonlinearities, Canudas-de-Wit et al. analyzed stability by modeling road torque with a time-varying spring model, to enforce a linear structure on the tire forces [19]. Similarly, Zaremba and Davis modeled the tie rod force as a speed dependent linear spring also enforcing a linear structure on the tire forces [79]. To provide stability guarantees for a steering feel up to the limits of tire saturation and including power assist, nonlinear stability techniques must be used.

This chapter begins by briefly illustrating the canonical example for Lyapunov stability analysis: the mass spring damper system. This example is used to give the reader intuitive insight into the nature of Lyapunov functions. Then the models used in analyzing the stability of the system are introduced. Bounding techniques are used to bound the nonlinearities due to the tire model, total trail (see Section 2.1.2) and power assist weighting function. This chapter then uses Lyapunov stability analysis

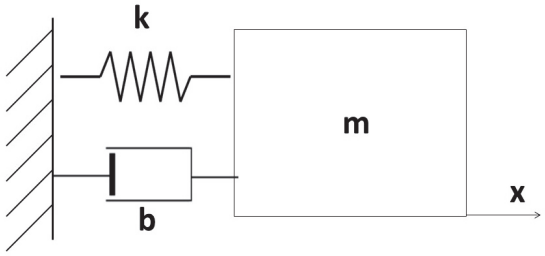

Figure 3.1: Mass spring damper system

to obtain four conditions on the steering feel model parameters that, when met, guarantee system stability. These stability guarantees account for tire saturation effects. Finally, bounds on the amount of power assist allowable for stability are investigated, providing guidance on how to design the power assistance effect.

3.1 Understanding Lyapunov Functions

In order to demonstrate the intuition behind using Lyapunov functions to prove stability, it is illustrative to look at the canonical example of a linear mass spring damper system (see Figure 3.1). Lyapunov stability analysis first requires a model of the system to be created. In the case of a mass spring damper system, using Newton's Laws of motion result in the following equation of motion:

$$m\ddot{x} = -b\dot{x} - kx \tag{3.1}$$

where x is the displacement of the mass from rest, m is the mass, b is the damping constant and k is the spring constant. Next a candidate Lyapunov function ($V(x)$) must be obtained. A candidate function which fulfills the following requirements implies that the system is globally asymptotically stable (G.A.S.) at the origin.:

(1) $V(x)$ is positive definite

(2) $\frac{dV(x)}{dt}$ is negative definite

(3) $V(x) \to \infty$ as $||x|| \to \infty$

$V(x)$ can be thought of as an energy-like function. This being the case, the first and third condition imply that system energy is positive and grows with the states of the system. The second conditions implies that, in a stable system, the energy of that system dissipates over time. Using this analogy, a logical choice for a candidate Lyapunov function for the mass spring damper system is the total energy of the system:

$$V(x) = \frac{1}{2}kx^2 + \frac{1}{2}m\dot{x}^2 \tag{3.2}$$

where the first term is the potential energy of the system and the second term is the kinetic energy of the system. This function clearly fulfills conditions 1 and 3. By taking the derivative of the Lyapunov function with respect to time:

$$\begin{aligned} \dot{V}(x) &= kx\dot{x} + m\dot{x}\ddot{x} \\ &= kx\dot{x} + \dot{x}\left(-b\dot{x} - kx\right) \\ &= -b\dot{x}^2 \end{aligned} \tag{3.3}$$

However, $\dot{V}(x)$ is clearly negative semi-definite rather than negative definite (as required by condition 2), indicating that this function does not fulfill the requirements for the system to be G.A.S. The fundamental challenge with using the chosen energy based Lyapunov function is that its time derivative does not dissipate energy when $\dot{x}$ is zero. To solve this issue, Chang et al. proposed adding a cross-term to the energy based function given in Equation (3.2) [20]. Arimoto et al. also introduced a cross-term to prove exponential asymptotic stability of proportional-derivative (PD) feedback in robot control [7]. The new candidate Lyapunov function is then:

$$V(x) = \frac{1}{2}kx^2 + \frac{1}{2}m\dot{x}^2 + \epsilon x\dot{x} \tag{3.4}$$

where ϵ is bounded to be between $\left(0, \sqrt{km}\right)$ for $V(x) > 0 \; \forall x$ (i.e. fulfilling condition 1). Now, $\dot{V}(x)$ becomes:

$$\dot{V}(x) \;\; = \;\; (\epsilon - b)\dot{x}^2 - \frac{\epsilon}{m} bx\dot{x} - \frac{\epsilon}{m} kx^2$$

Using Sylvester's criterion to find conditions such that $-\dot{V}(x) > 0 \; \forall x$, bounds on ϵ are obtained. Therefore, if $0 < \epsilon < \frac{4kbm}{b^2+4km}$, then $\dot{V}(x)$ is negative definite and condition 2 is fulfilled. This new candidate Lyapunov function then fulfills all conditions to prove that the system is G.A.S. Including the $\epsilon x\dot{x}$ cross-term modifies the purely energy-based Lyapunov function so that it can fulfill the conditions required for G.A.S.

3.2 Component Models for Analyzing Stability

As seen in the Section 3.1, Lyapunov stability analysis requires models of the system in question. In this section, the three main models used for the stability analysis are presented. The first model restates the artificial steering feel model proposed in the previous chapter in a form that makes it conducive to Lyapunov stability analysis. The second model presents a slightly more complex vehicle model that incorporates the longitudinal dynamics of the vehicle. The last model illustrates a tire model which captures the full scope of the tire force curves for different surfaces and includes the tire saturation effect. Using these three models, stability guarantees provided for the artificial steering feel account for nonlinearities due to tire saturation and power assist.

3.2.1 Artificial Steering Feel Model

The model proposed in the previous chapter (see Equation 2.4) can be restated as:

$$\tau_{\text{motor}} = -\Delta b\dot{\delta} - \Delta J\ddot{\delta} + W_{\text{f}} K \left(-K_{\text{jack}}\delta - F_{\text{yf}}\hat{t}\right) \tag{3.5}$$

where K_{jack} is the jacking torque stiffness (see Equation (2.10)), Δb is the additional damping (see Equation (2.5)) and ΔJ is the additional inertia (see Equation (2.6)).

The weighting function W_{f} and total trail $\hat{t}$ are bounded as follows:

$$0 \leq \hat{t} \leq \hat{t}_{\max} \tag{3.6}$$

$$0 \leq W_{\mathrm{f,min}} \leq W_{\mathrm{f}} \leq W_{\mathrm{f,max}} \leq 1 \tag{3.7}$$

where the maximum total trail ($\hat{t}_{\max}$), minimum weighting ($W_{\mathrm{f,min}}$) and maximum weighting ($W_{\mathrm{f,max}}$) are chosen.

One challenge of analyzing system stability is that, if he or she so chooses, a driver can put in an unbounded steering input to create an unbounded system response. However, if the underlying system (i.e. without the driver) is shown to be stable, then prior work shows us that, when coupled with a driver, the driver tends to have a stabilizing effect on the resultant system [73]. Therefore, in this analysis, the driver is assumed to apply zero torque to the handwheel resulting in its motion being purely determined by the steering system dynamics. If stability of this system can be proven, then the underlying system is inherently stable. This approach of assuming zero driver torque input to analyze the stability of the system is similar to prior approaches in literature. For example, Switkes used it to prove the stability of a lanekeeping system with force feedback steering [73]. Using this assumption, $\tau_{\mathrm{hw}} = 0$, Equation (2.1) becomes:

$$J_{\mathrm{system}}\ddot{\delta}_{\mathrm{hw}} + b_{\mathrm{system}}\dot{\delta}_{\mathrm{hw}} = -\Delta b\dot{\delta} - \Delta J\ddot{\delta} + W_{\mathrm{f}}K\left(-K_{\mathrm{jack}}\delta - F_{\mathrm{yf}}\hat{t}\right) \tag{3.8}$$

One assumption made for this analysis is that the steer-by-wire system has sufficient bandwidth and tracking capability such that the roadwheel simply tracks the handwheel command when there is no active steering intervention. The steering controller used on X1 is certainly fast enough for this assumption to hold and the resultant model then becomes:

$$J_{\mathrm{hw}}\ddot{\delta} = -b_{\mathrm{hw}}\dot{\delta} + W_{\mathrm{f}}K\left(-K_{\mathrm{jack}}\delta - F_{\mathrm{yf}}\hat{t}\right) \tag{3.9}$$

where overall system inertia and damping are given by:

$$J_{\text{hw}} = \eta_{\text{SR}} J_{\text{system}} + \Delta J \tag{3.10}$$

$$b_{\text{hw}} = \eta_{\text{SR}} b_{\text{system}} + \Delta b \tag{3.11}$$

and η_{SR} is the steering ratio of the vehicle and accounts for the fact that the FFB system inertia and damping are found based on the handwheel angle.

Production steer-by-wire systems (like that found on the Infiniti 2014 Q50) are created to be fast as well. However, it is important to note that the steering controller dynamics may not be negligible for production systems and may need to be incorporated into the model during stability analysis.

Figure 3.2 illustrates the artificial steering model and the resultant vehicle-driver system used for the stability analysis. The block labeled 'Steering System Dynamics' has replaced the 'Driver' block from the block diagram in Figure 2.5.

3.2.2 Vehicle Model

Since the energy of the vehicle depends on the lateral velocity (U_{y}), yaw rate (r) *and* longitudinal velocity (U_{x}), the two-state vehicle model presented in Section 2.3.1 which assumes a constant longitudinal speed is insufficient. Rather, a slightly more complex model including the longitudinal dynamics of the vehicle is required. Using small angle assumptions, the new equations of motion for lateral velocity (U_{y}), yaw rate (r) and longitudinal velocity (U_{x}) are as follows:

$$\dot{U}_{\text{x}} = rU_{\text{y}} - \frac{F_{\text{yf}}}{m}\delta \tag{3.12}$$

$$\dot{U}_{\text{y}} = \frac{F_{\text{yf}}}{m} + \frac{F_{\text{yr}}}{m} - rU_{\text{x}} \tag{3.13}$$

$$\dot{r} = \frac{\text{a}F_{\text{yf}}}{I_{\text{zz}}} - \frac{\text{b}F_{\text{yr}}}{I_{\text{zz}}} \tag{3.14}$$

where $F_{\text{y[f,r]}}$ is the lateral tire force of the [front, rear] axle, m is the vehicle mass, I_{zz} is the yaw inertia, δ is the steer angle and a and b are the distances from the center of gravity to the front and rear axles, respectively.

3.2.3 Tire Force Model

To capture tire saturation the tire model presented by Talvala et al., with time-varying tire saturation parameters ν_{f} and ν_{r}, is used [74]:

$$F_{\mathrm{yf}} = -\nu_{\mathrm{f}} C_{\alpha\mathrm{f}} \alpha_{\mathrm{f}} \tag{3.15}$$

$$F_{\mathrm{yr}} = -\nu_{\mathrm{r}} C_{\alpha\mathrm{r}} \alpha_{\mathrm{r}} \tag{3.16}$$

where ν_{f} and ν_{r} are bounded such that $\nu_{\mathrm{f}} \in (0, 1]$ and $\nu_{\mathrm{r}} \in (0, 1]$. Figure 3.3 illustrates this model by showing typical tire force curves for various surfaces and the bounds created using the model with tire saturation parameters $\nu = 0$ and $\nu = 1$. As ν varies between $(0, 1]$, the slope of the line representing $F_{\mathrm{yf}} = -\nu_{\mathrm{f}} C_{\alpha\mathrm{f}} \alpha_{\mathrm{f}}$ varies between the

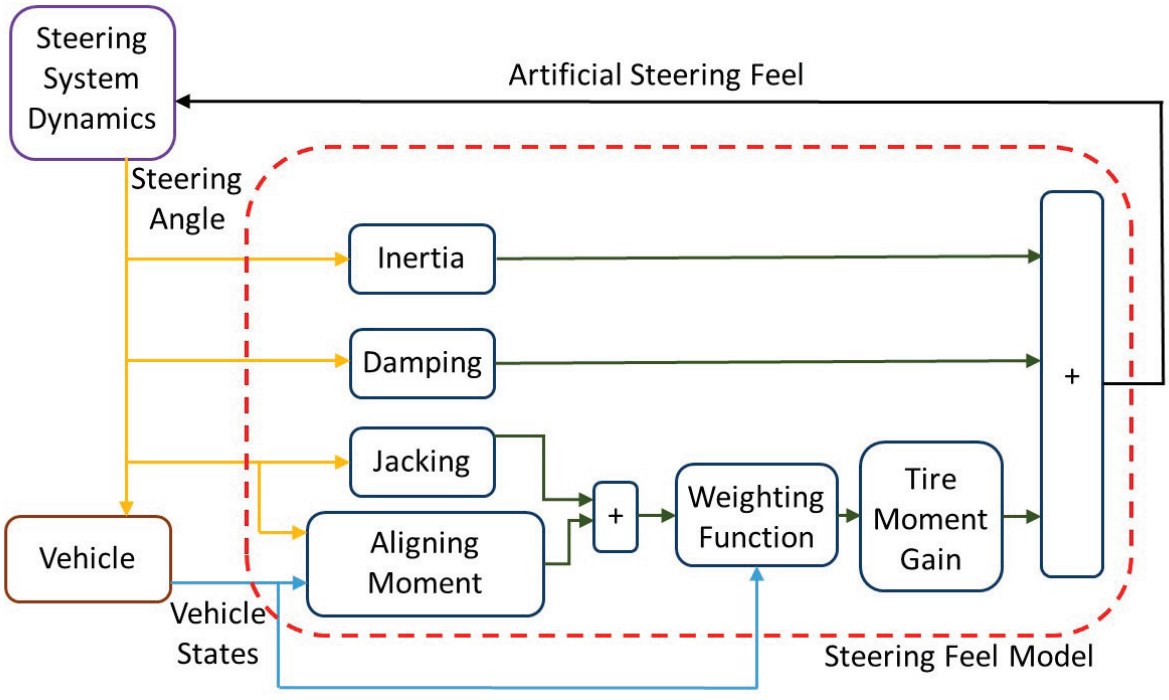

Figure 3.2: Block diagram of artificial steering feel model and resultant vehicle-driver system for stability analysis

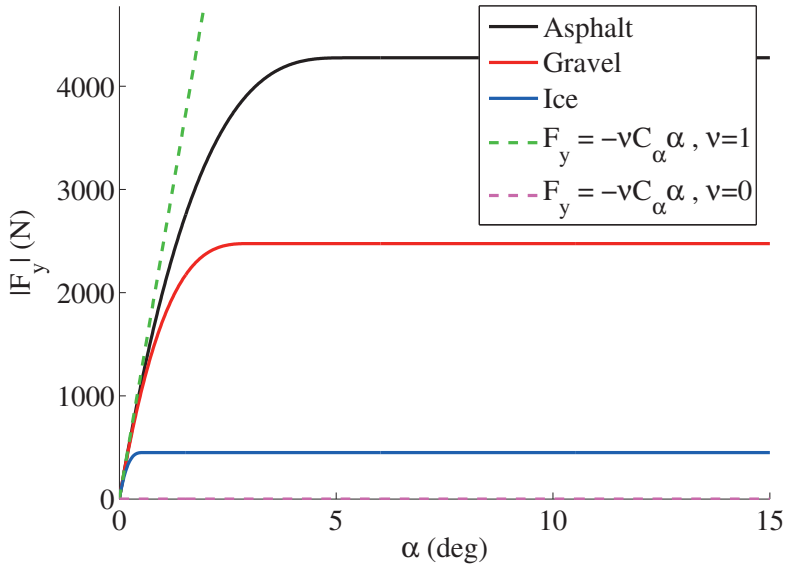

Figure 3.3: Typical tire force curves for various surfaces

slopes given by the lines for $\nu = 0$ and $\nu = 1$. Therefore, this model sweeps through the region between the lines for $\nu = 0$ and $\nu = 1$ and captures every point between those two lines. It can consequently capture tire forces encompassing different surface conditions up to and including tire saturation.

3.3 Lyapunov Stability Analysis

Figure 3.2 illustrates the artificial steering model and the resultant vehicle-driver system used for the stability analysis. The states in this model are the vehicle's longitudinal velocity, lateral velocity, yaw rate and steering angle. The first three states are obtained from the vehicle's dynamics and the steering angle is obtained from the steering system's dynamics.

3.3.1 Candidate Lyapunov Function

As illustrated in Section 3.1, looking at energy-like functions that represent the total energy of the system is useful in determining a candidate Lyapunov function. In this case, the sum of the energies of the vehicle and the steering system determines the candidate Lyapunov function (V). A cross-term based on steering angle and steering angle velocity ensured that the function always dissipates energy even when the steering angle velocity is zero (see Section 3.1 for a better understanding behind the addition of the cross-term). The candidate Lyapunov function is as follows:

$$V = \frac{1}{2}I_{\mathrm{zz}}r^2 + \frac{1}{2}mU_{\mathrm{x}}^2 + \frac{1}{2}mU_{\mathrm{y}}^2 + \frac{1}{2}(b_{\mathrm{hw}} + KK_{\mathrm{jack}})\delta^2 + \frac{1}{2}J_{\mathrm{hw}}\dot{\delta}^2 + J_{\mathrm{hw}}\dot{\delta}\delta \quad (3.17)$$

where the first three terms represent the total kinetic energy of the vehicle, the next two terms represent the kinetic and potential energy of the steering system and the last term is the cross-term. This Lyapunov function can be converted to a quadratic form:

$$V = \frac{1}{2}x_V^T A_V x_V \quad (3.18)$$

where

$$x_V = \begin{bmatrix} r & U_{\mathrm{x}} & U_{\mathrm{y}} & \delta & \dot{\delta} \end{bmatrix}^T$$

$$A_V = \begin{bmatrix} I_{\mathrm{zz}} & 0 & 0 & 0 & 0 \\ 0 & m & 0 & 0 & 0 \\ 0 & 0 & m & 0 & 0 \\ 0 & 0 & 0 & b_{\mathrm{hw}} + KK_{\mathrm{jack}} & J_{\mathrm{hw}} \\ 0 & 0 & 0 & J_{\mathrm{hw}} & J_{\mathrm{hw}} \end{bmatrix}$$

Since the cross-term exists, conditions for which V is positive definite must be found. This can be done using Sylvester's Criterion to find conditions such that

$V > 0 \ \forall x_V$ resulting in:

$$b_{\mathrm{hw}} + KK_{\mathrm{jack}} > J_{\mathrm{hw}} \tag{3.19}$$

3.3.2 Candidate Lyapunov Function Derivative

Differentiating V with respect to time and substituting Equations (3.12), (3.13) and (3.14) results in:

$$\dot{V} = F_{\mathrm{yf}}(\alpha_{\mathrm{f}}U_{\mathrm{x}} - KW_{\mathrm{f}}\hat{t}(\delta+\dot{\delta})) + F_{\mathrm{yr}}(\alpha_{\mathrm{r}}U_{\mathrm{x}}) + (J_{\mathrm{hw}} - b_{\mathrm{hw}})\dot{\delta}^2 - W_{\mathrm{f}}KK_{\mathrm{jack}}\delta^2 + KK_{\mathrm{jack}}(1-W_{\mathrm{f}})\delta\dot{\delta} \tag{3.20}$$

Using the tire force model proposed above, Equation (3.20) then becomes:

$$\begin{aligned}\dot{V} = &-\nu_{\mathrm{f}}C_{\alpha\mathrm{f}}\alpha_{\mathrm{f}}(\alpha_{\mathrm{f}}U_{\mathrm{x}} - KW_{\mathrm{f}}\hat{t}(\delta+\dot{\delta})) - \nu_{\mathrm{r}}C_{\alpha\mathrm{r}}\alpha_{\mathrm{r}}(\alpha_{\mathrm{r}}U_{\mathrm{x}}) \\ &+ (J_{\mathrm{hw}} - b_{\mathrm{hw}})\dot{\delta}^2 - W_{\mathrm{f}}KK_{\mathrm{jack}}\delta^2 + KK_{\mathrm{jack}}(1-W_{\mathrm{f}})\delta\dot{\delta}\end{aligned} \tag{3.21}$$

Deriving conditions such that $\dot{V} < 0$ from Sylvester's Criterion requires restating $\dot{V}$ as a quadratic form. To do this, longitudinal speed (U_{x}) is treated separately. The resulting conditions obtained hold for the original state vector over the feasible range of speeds a vehicle can attain (see Table 3.1). Treating longitudinal speed (U_{x}) separately, results in the following quadratic form for $\dot{V}$:

$$\dot{V} = x_{\dot{V}}^T A_{\dot{V}} x_{\dot{V}} \tag{3.22}$$

where

$$x_{\dot{V}} = \begin{bmatrix} \alpha_{\mathrm{f}} & \alpha_{\mathrm{r}} & \delta & \dot{\delta} \end{bmatrix}^T$$

$$A_{\dot{V}} = \begin{bmatrix} -\nu_{\mathrm{f}} C_{\alpha\mathrm{f}} U_{\mathrm{x}} & 0 & a_1 & a_1 \\ 0 & -\nu_{\mathrm{r}} C_{\alpha\mathrm{r}} U_{\mathrm{x}} & 0 & 0 \\ a_1 & 0 & -K K_{\mathrm{jack}} W_{\mathrm{f}} & a_2 \\ a_1 & 0 & a_2 & J_{\mathrm{hw}} - b_{\mathrm{hw}} \end{bmatrix}$$

and

$$a_1 = \frac{\nu_{\mathrm{f}} C_{\alpha\mathrm{f}} K W_{\mathrm{f}} \hat{t}}{2}$$
$$a_2 = -\frac{\left(K K_{\mathrm{jack}} (W_{\mathrm{f}} - 1)\right)}{2}$$

Using Sylvester's Criterion to find conditions such that $-\dot{V} > 0 \ \forall x_{\dot{V}}$ results in following 4 conditions:

1. $\nu_{\mathrm{f}} C_{\alpha\mathrm{f}} U_{\mathrm{x}} > 0$
2. $\nu_f \nu_{\mathrm{r}} C_{\alpha\mathrm{r}} C_{\alpha\mathrm{f}} U_{\mathrm{x}}^2 > 0$
3. $K_{\mathrm{jack}} > \frac{\nu_{\mathrm{f}} C_{\alpha\mathrm{f}} K W_{\mathrm{f}} \hat{t}^2}{4 U_{\mathrm{x}}}$
4. $-K \left(K_{\mathrm{jack}}^2 U_{\mathrm{x}} + \nu_{\mathrm{f}} C_{\alpha\mathrm{f}} \hat{t}^2 \left(b_{\mathrm{hw}} + K K_{\mathrm{jack}} - J_{\mathrm{hw}}\right)\right) W_{\mathrm{f}}^2$
   $2 K_{\mathrm{jack}} U_{\mathrm{x}} \left(2 b_{\mathrm{hw}} - 2 J_{\mathrm{hw}} + K K_{\mathrm{jack}}\right) W_f$
   $- K K_{\mathrm{jack}}^2 U_{\mathrm{x}} > 0$

If U_{x} is assumed to be strictly positive (i.e. the vehicle is moving forward) conditions 1 and 2 are immediately satisfied as cornering stiffnesses and tire saturation parameters are strictly positive.

Condition 3 contains the terms W_{f}, $\hat{t}$ and ν_{f} which are time-varying and bounded (see Equations (3.7) and (3.6)). A conservative bound on jacking torque stiffness can be obtained by using the largest possible W_{f} ($W_{\mathrm{f,max}} = 1$), $\hat{t}$ ($\hat{t} = \hat{t}_{\mathrm{max}}$) and ν_{f} ($\nu_{\mathrm{f}} = 1$):

$$K_{\text{jack}} > \frac{C_{\alpha\text{f}} K \hat{t}_{\text{max}}^2}{4U_{\text{x}}} \tag{3.23}$$

Condition 4 is a quadratic function in W_{f} and can be solved to obtain both a upper and lower bound on W_{f} (i.e. $W_{\text{f,max}}$ and $W_{\text{f,min}}$). These bounds translate to limits on the power assist effect in a steering feel to guarantee stability. The following section deals with this limit on the power assist effect as different parameters in the feel are varied.

3.4 Effect of Parameter Variation on the Limits of Power Assist

To investigate the effect of parameter variation on the limits of power assist, condition 4 must be solved for a variety of different parameter values. Reasonable ranges for the design parameters used in the steering feel model provide a range over which condition 4 can be evaluated to determine bounds on the weighting function. The front tire cornering stiffness from test vehicle, X1, provides a nominal cornering stiffness value used to evaluate condition 4.

Table 3.1: X1 Parameters Ranges for Stability Analysis

Parameter	Value/Range	Units
$C_{\alpha\text{f}}$	140	$\text{kN} \cdot \text{rad}^{-1}$
b_{hw}	0.01 - 10	$\frac{\text{Nm}}{\text{rad}\cdot\text{s}^{-1}}$
J_{hw}	0.001 - 0.1	$\text{kg} \cdot \text{m}^2$
U_{x}	1 - 50	m/s
ν_{f}	0 - 1	–
$\hat{t}$	0 - 0.035	m
K	0.01 - 0.1	–
K_{jack}	0 - 250	Nm/rad

Table 3.1 shows the nominal cornering stiffness as well as the ranges of the steering feel model parameters that were investigated. By varying each of the parameters

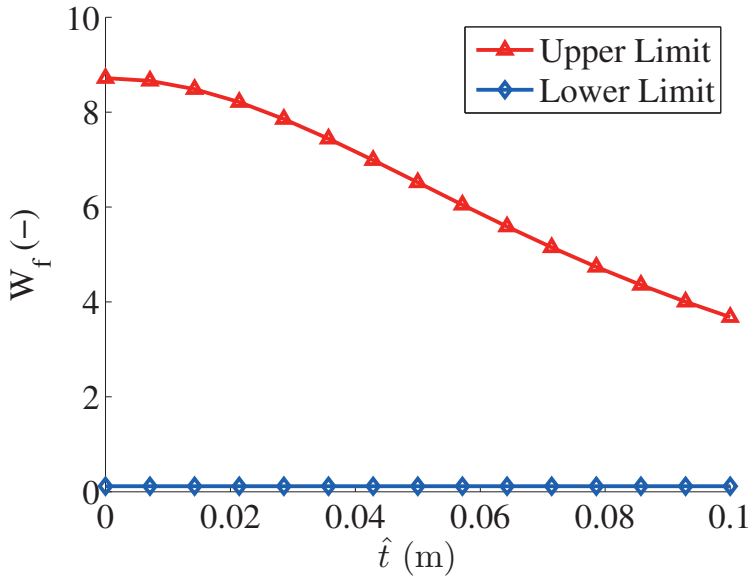

Figure 3.4: Weighting function bounds with varying total trail ($\hat{t}$)

present in this condition in turn while the other parameters are held constant, the effect of each individual change can be investigated. For example, Figure 3.4 shows how the bounds for the power assist vary with increasing total trail. As the total trail increases, the weighting function lower limit ($W_{\text{f,min}}$) stays fairly constant while the upper limit ($W_{\text{f,max}}$) decreases. Despite this decrease, the upper limit is always greater that 1 for the reasonable range considered. Since $W_{\text{f,max}} \leq 1$ (see Equation 3.7), this implies that changing the total trail does not have any meaningful impact on the limits of the power assist.

Figures 3.5, 3.6, 3.7, 3.8, 3.9 and 3.10 show similar plots illustrating the limits of the maximum and minimum values of the weighting function for varying speeds (U_x), front tire saturation parameters (ν_f), jacking torque stiffnesses (K_{jack}), system damping values (b_{hw}), tire moment gains (K) and system inertia values (J_{hw}) respectively.

Table 3.2 documents the results of *increasing* each model parameter in turn while holding the other parameters constant. If the effect results in an *increase* in the value or bound, a up-arrow (↑) is used. If the effect results in a *decrease* then a down-arrow

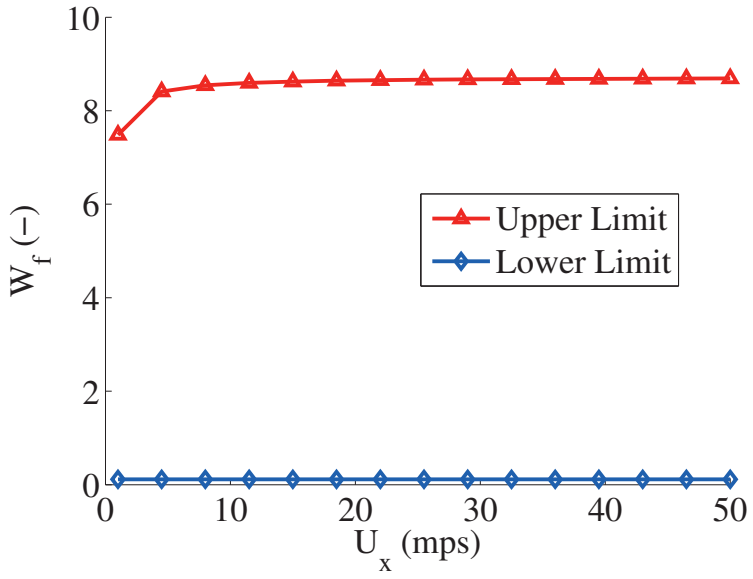

Figure 3.5: Weighting function bounds with varying speed (U_x)

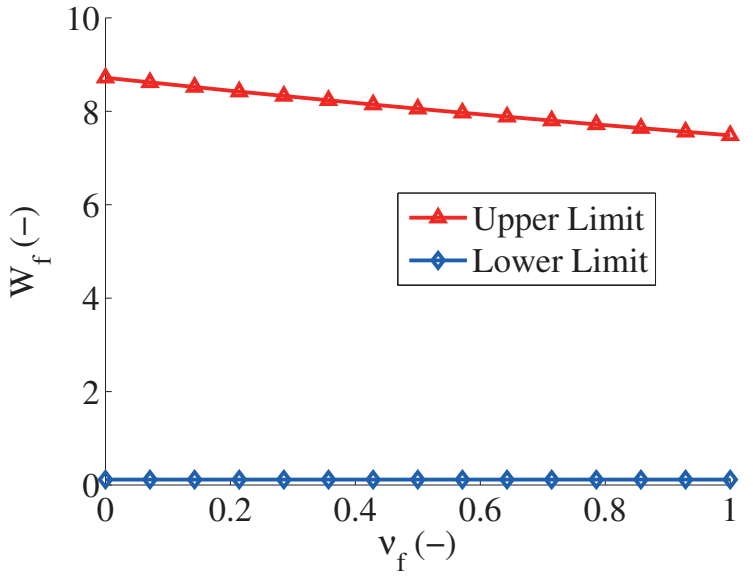

Figure 3.6: Weighting function bounds with varying front tire saturation parameter (ν_{f})

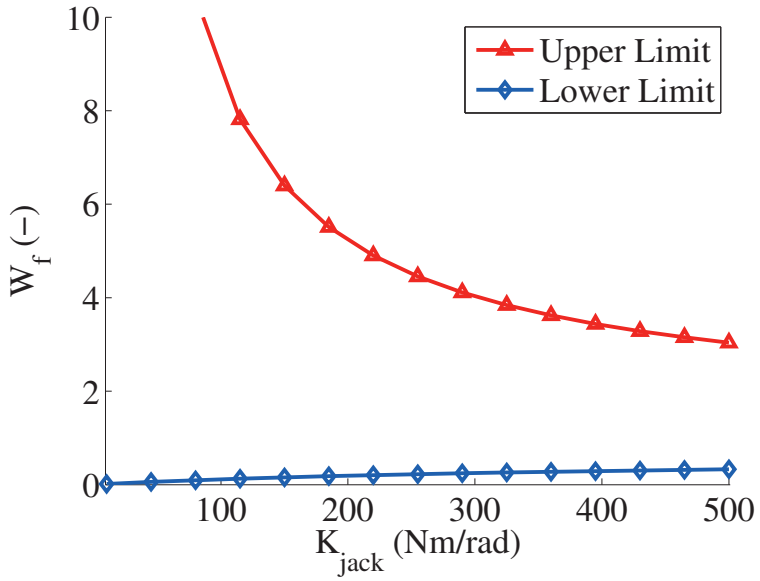

Figure 3.7: Weighting function bounds with varying jacking torque stiffness (K_{jack})

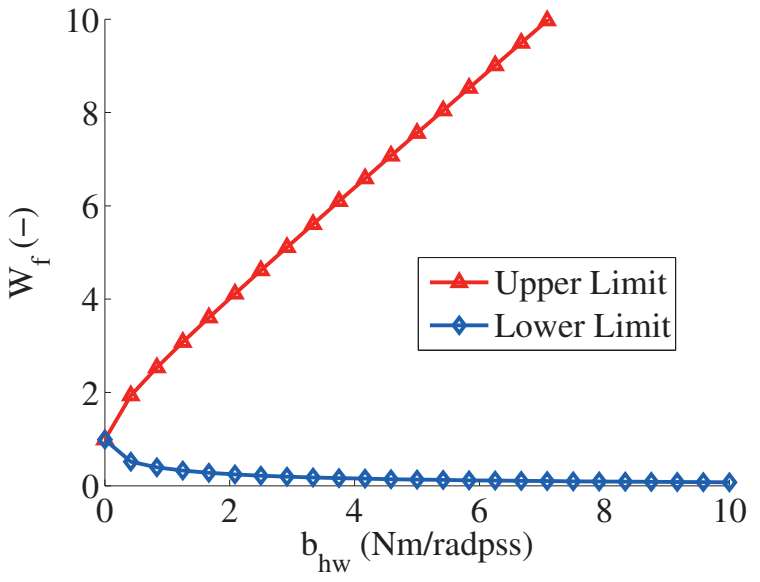

Figure 3.8: Weighting function bounds with varying system damping (b_{hw})

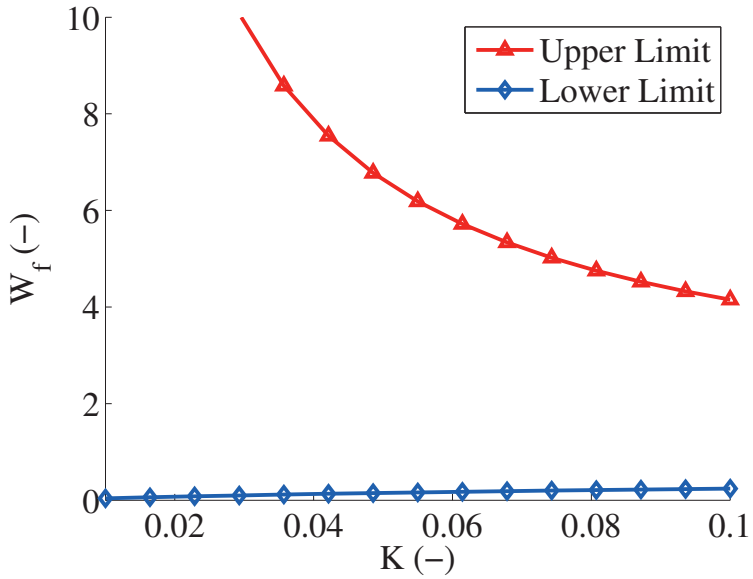

Figure 3.9: Weighting function bounds with varying tire moment gain (K)

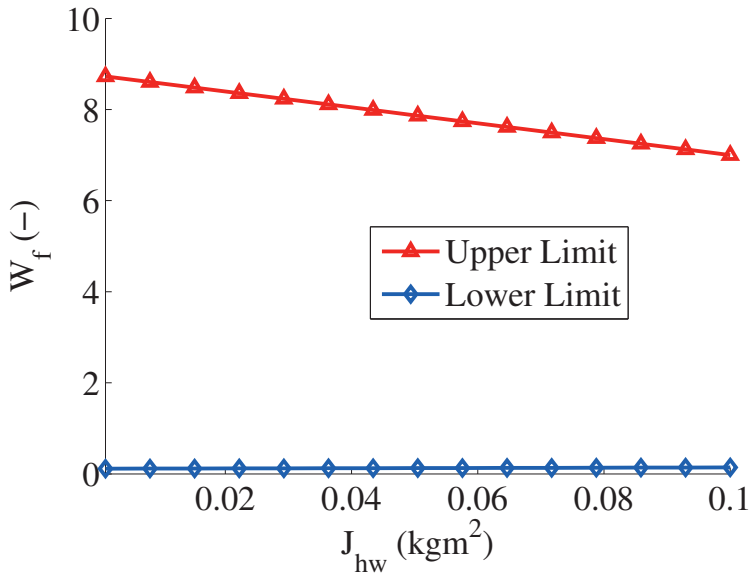

Figure 3.10: Weighting function bounds with varying system inertia (J_{hw}))

Increasing Parameter (↑)	$W_{\mathrm{f,min}}$	$W_{\mathrm{f,max}}$	**Overall Bound**
Speed (U_{x})	-	↑	↑
Total trail ($\hat{t}$)	-	↓	↓
Front tire saturation parameter (ν_{f})	-	↓	↓
Jacking torque stiffness (K_{jack})	↑	↓	↓
Change in damping (b_{hw})	↓	↑	↑
Change in inertia (J_{hw})	-	↓	↓
Tire moment gain (K)	↑	↓	↓

Table 3.2: Steering Feel Stability Parameter Variation Table

(↓) is used. If the effect results in a mostly *constant* response, a dash (−) is used. For example, in the first row concerning speed (U_{x}), increasing speed results in a relatively constant lower limit but an increasing upper limit leading to a increasing overall bound on W_{f}.

Based on Table 3.2, a conservative bound for W_{f} can be found by solving condition 4 for $W_{\mathrm{f,max}}$ and $W_{\mathrm{f,min}}$ while taking the extreme values of all the parameters so as to create the smallest overall bound. Note that for all parameters investigated, the upper limit ($W_{\mathrm{f,max}}$) despite decreasing for some parameters, never decreased to below one. Since $W_{\mathrm{f,min}} \leq 1$ (see Equation 3.7), this implies that it was not the limiting factor and that one can have no assist effect in a steering feel without compromising stability.

However, the lower limit of the weighting function ($W_{\mathrm{f,min}}$) was consistently found to be greater than zero. Since $0 \leq W_{\mathrm{f,min}}$ (see Equation 3.7), this implies that the lower limit is the limiting factor as it can never be zero. Intuitively, this means that a fully assisted vehicle (i.e. $W_{\mathrm{f,min}} = 0$) may not be stable. Essentially, this points to the fact that a perfectly decoupled system between the steering feel and the moments acting on the tires can lead to potential instability. This makes sense as the tires form the main dissipative element in the system and removing the connection between the steering feel and the tires (i.e. with a fully assisted feel) can result in potential instability. Therefore to ensure stability, some coupling between the moments acting at the tire and the steering feel is required.

3.5 Summary

This chapter illustrates a Lyapunov stability analysis of the artificial steering feel introduced in Chapter 2 by providing a means for bounding the various nonlinearities present. The four conditions obtained allow a designer to select model parameters such that system stability is guaranteed up till and including the tire saturation region. This chapter also discusses the impact of power assist on stability and provides a means of creating a conservative bound on the power assist maximum and minimum bounds. This technique concludes that some coupling between the steering feel and the tire moments is required to ensure system stability.

Chapter 4

Supportive Steering Feel for Active Steering

Active steering augments the driver's steering command either through roadwheel steering corrections. This means that the roadwheels do not reflect the actual driver command. By contrast, power steering conveys the driver's steering command faithfully to the roadwheels but the steering torque that the driver uses to actuate the roadwheels is dependent on the power assistance characteristics of that particular system [69]. Active steering can be used to improve stability and safety by modifying the lateral dynamics of the vehicle. ZF Lenksysteme and BMW AG developed such an active steering system without the loss of mechanical connection from the handwheel to the roadwheel [42]. Steer-by-wire systems also provide a means of creating these active steering interventions. By mechanically decoupling the handwheel from the roadwheel, steer-by-wire systems allow for the actuation of the roadwheels independently from the driver's steering command.

During scenarios without active steering interventions, a supportive steering feel must convey accurate information about the forces acting on the roadwheels, replicate effects common to modern vehicles like power assisted steering and provide stability guarantees on performance. Mandhata et al. [48] and Williams and Sherwin [77] among others have developed steering feel models of various complexity to create artificial steering feel. In particular, Balachandran and Gerdes proposed a steering feel

model, which is described in Chapter 2, of sufficient complexity to capture common steering feel effects while being simple enough to run in real-time on an actual steer-by-wire vehicle [14].

During an active steering intervention, the driver's intended steering command via the handwheel and the roadwheel angle differs. Therefore, the driver's command and the vehicle's motion are no longer in sync and this can prove confusing to the driver. A supportive steering feel should act to aid the driver to turn with the intervention, thereby reducing the discrepancy between the driver's command and the vehicle's motion. Basing the steering feel on the tire moments acting on the actual roadwheels for steering feedback results in handwheel torque that acts in opposition to the intervention. Finding an approach that results in a supportive steering feel for scenarios with and without active steering is important and this chapter introduces the concept of the virtual wheel to address this issue.

This chapter investigates a steering feel model for steer-by-wire vehicles based on the virtual wheel concept. It shows that using the virtual wheel concept creates supportive steering feel during scenarios with and without active steering interventions. The chapter begins by describing the vehicle model with positional states that is used for the simulation and, when linearized, is used for the active steering controller. This model builds on the one presented in Section 2.3.1 by incorporating positional states for the vehicle as well. This chapter expands the artificial steering feel model presented in Section 2.1.2 to incorporate the virtual wheel concept. To investigate the interaction between this model and active steering interventions, interventions are created using the obstacle avoidance controller proposed by Erlien et al. [22]. The chapter then demonstrates, through simulation and experiments, that using the virtual wheel creates supportive handwheel torque that reduces the discrepancy between the driver command and the active steering system.

4.1 Vehicle Model with Positional States

The vehicle model used is a constant speed, planar bicycle model differing from that presented in Section 2.3.1 only in its inclusion of positional states. The vehicle's

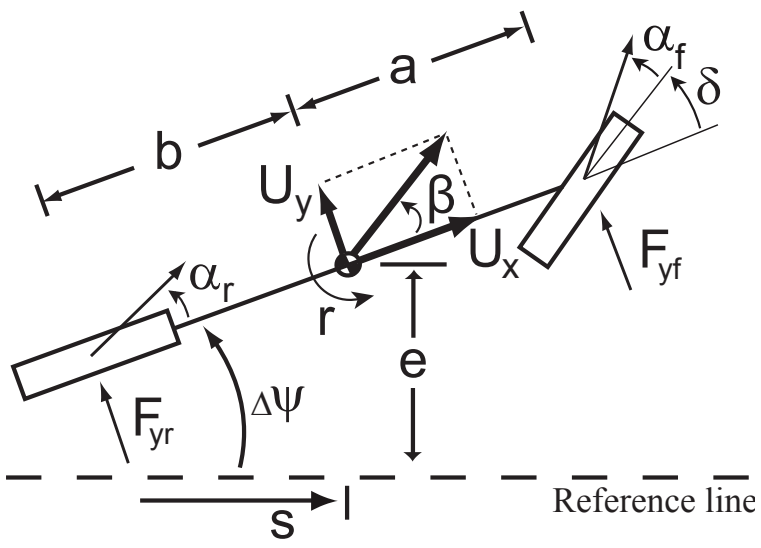

Figure 4.1: Bicycle model with positional states

motion is described by two states: sideslip β and yaw rate r. These are defined in Figure 4.1 and have the equations of motion given by Equations (2.15) and (2.16) respectively.

The vehicle's position is specified relative to a reference line using three states: heading deviation $\Delta\psi$, lateral deviation e, and distance along the path s as defined in Figure 4.1. The equations of motion of these states are then:

$$\dot{\Delta\psi} = r \tag{4.1}$$

$$\dot{e} = U_{\mathrm{x}} \sin(\Delta\psi) + U_{\mathrm{y}} \cos(\Delta\psi) \tag{4.2}$$

$$\dot{s} = U_{\mathrm{x}} \cos(\Delta\psi) - U_{\mathrm{y}} \sin(\Delta\psi) \tag{4.3}$$

4.2 Incorporating the Virtual Wheel

The virtual wheel refers to using the driver's intended steering command rather than the actual roadwheel angle. When there is no active steering intervention, the virtual wheel and the actual roadwheel are the same. During an active steering intervention, the roadwheel angle differs from the desired steering command obtained from the

handwheel. The steering feedback can now be based on either the moments acting on the actual roadwheels or the moments that would act on roadwheels had they followed the driver's intended steering command. The second option is known as the virtual wheel concept and is described below. This section illustrates how to include the virtual wheel concept into the proposed steering feel model.

If feedback is based on the moments acting on the actual roadwheels then, the steer angle used in Equations (2.17), (2.5), (2.6), and (2.11) to obtain front slip angle, damping torque, inertia torque and jacking torque respectively would be the actual roadwheel angle (δ_{rw}):

$$\delta = \delta_{\mathrm{rw}} \tag{4.4}$$

If the virtual wheel concept is implemented, then the steer angle used in these equations is the driver's intended steer angle based on the handwheel angle:

$$\delta = \frac{\delta_{\mathrm{hw}}}{\eta_{\mathrm{SR}}} \tag{4.5}$$

where η_{SR} is the steering ratio. Note that if there is no active steering intervention, both of these approaches yield the same result.

Basing feedback on the virtual wheel is similar to the concept of a proxy from haptic teleoperation literature [52], [62]. In haptic teleoperation, a proxy is a representation of the master device (in this case the handwheel) in the environment (in this case the road surface). It can be used to generate useful haptic feedback to the operator of the teleoperated system. The virtual wheel concept introduced in this chapter represents a proxy of the handwheel. This chapter will show that feeding back the actual tire moments results in a steering feedback torque that does not support the active steering intervention. Rather the concept of the virtual wheel can be used to generate supportive steering feedback torque in scenarios with and without active steering interventions.

4.3 Obstacle Avoidance Controller

Investigating the interaction between active steering interventions and the steering feedback torque requires large interventions to be generated. Large interventions result in a bigger difference between the feedback using the virtual wheel and the feedback using the actual roadwheel position. Since obstacle avoidance controllers generally result in large active steering interventions, this chapter uses the obstacle avoidance controller developed by Erlien and Gerdes [22].

This controller shares control with a human driver using safe driving envelopes. Vehicle handling limits define the stable handling envelope while obstacles and road boundaries in the environment define the environmental envelope. A Model Predictive Control (MPC) scheme determines if the driver's current steering command allows for a safe vehicle trajectory within these two safe driving envelopes, intervening when such a trajectory does not exist. This controller is briefly described in this section.

4.3.1 MPC Vehicle Model

The vehicle model used in the online MPC controller is a linearization of the vehicle model presented in Section 4.1. Although this model assumes constant speed, in practice, the measured vehicle speed is used at each execution of the MPC controller and only assumed constant over the prediction horizon. The input to this vehicle model is F_{yf}; therefore, the controller computes an optimal front tire force which is then mapped to δ_{rw} using (2.8) and (2.17):

$$\delta_{\text{rw}} \;=\; \beta + \frac{ar}{U_{\text{x}}} - f_{\text{tire}}^{-1}\left(F_{\text{yf}}\right) \tag{4.6}$$

where f_{tire}^{-1} is computed numerically.

Use of F_{yf} as the model input enables explicit consideration of the nonlinear dynamics of the front tires. For the rear tires, which cannot be steered, a linearization of the nonlinear tire model (2.8) at a nominal rear tire slip angle, $\bar{\alpha}_{\text{r}}$, models rear tire

force, F_{yr}, as an affine function of α_{r}:

$$F_{\mathrm{yr}} = \bar{F}_{\mathrm{yr}} - \bar{C}_{\bar{\alpha}_{\mathrm{r}}}(\alpha_{\mathrm{r}} - \bar{\alpha}_{\mathrm{r}}) \tag{4.7}$$

where $\bar{F}_{\mathrm{yr}} = f_{\mathrm{tire}}(\bar{\alpha}_{\mathrm{r}})$ and $\bar{C}_{\bar{\alpha}_{\mathrm{r}}}$ is the equivalent cornering stiffness at $\bar{\alpha}_{\mathrm{r}}$. In the near term of the prediction horizon, this rear tire model is linearized around the measured rear tire slip angle, α_{r} (see Beal and Gerdes [16]), which enables accurate prediction of vehicle state propagation in the near term. In the remainder of the horizon, a linear tire model with $\bar{\alpha}_{\mathrm{r}} = 0$ is used.

Small angle approximations give linear expressions for non-linear tire slip equations (2.17) and (2.18). Equations (4.2) and (4.3) for the positional states of the vehicle can be similarly simplified as:

$$\dot{e} \approx U_{\mathrm{x}}\Delta\psi + U_{\mathrm{x}}\beta \tag{4.8}$$

$$\dot{s} \approx U_{\mathrm{x}} - U_{\mathrm{x}}\beta\Delta\psi \approx U_{\mathrm{x}} \tag{4.9}$$

using small angle assumptions for $\Delta\psi$ and β. With these simplifying assumptions, a discrete, time-varying vehicle model can be expressed as:

$$x^{(k+1)} = A^{(k)}_{\bar{\alpha}_{\mathrm{r}},t_{\mathrm{s}}} x^{(k)} + B^{(k)}_{\bar{\alpha}_r,t_s} {F_{\mathrm{yf}}}^{(k)} + d^{(k)}_{\bar{\alpha}_r,t_s} \tag{4.10}$$

where $x = [\beta \quad r \quad \Delta\psi \quad s \quad e]^T$, k is a time step index, subscript $\bar{\alpha}_{\mathrm{r}}$ denotes linearization of the rear tire model around rear slip angle $\bar{\alpha}_{\mathrm{r}}$, and subscript t_{s} denotes discretization of the vehicle model using time step length t_{s}.

4.3.2 Stable Handling Envelope

Understanding vehicle stability in terms of the β - $\dot{\beta}$ phase plane was original presented by Inagaki et al. [36] and Hoffman et al. [32]. In this work the stable handling envelope, developed by Beal and Gerdes [16], which defines limits on the states describing the vehicle's motion as illustrated in Figure 4.2 is used. This envelope reflects the maximum capabilities of the vehicle's tires so at any point within this envelope, there

exists a steering command to safely remain inside, ensuring stability.

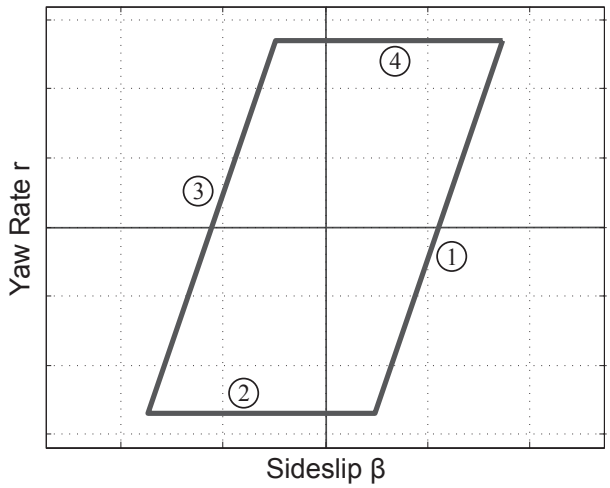

Figure 4.2: Stable handling envelope

The maximum steady-state yaw rate defines bounds (2) and (4) in Figure 4.2, while the rear slip angle at which lateral force saturates serves as the basis for bounds (1) and (3). The desire to restrain the vehicle states within the stable handling envelope is compactly expressed as the inequality:

$$\left|H_{\text{sh}}x^{(k)}\right| \leq G_{\text{sh}} \tag{4.11}$$

where subscript sh indicates the stable handling envelope.

4.3.3 Environmental Envelope

The environmental envelope consists of a set of collision free tubes along the reference line like the two illustrated in Figure 4.3. To avoid collision with the environment, the vehicle's trajectory must be fully contained within any one of these tubes. Each tube defines time-varying constraints on the lateral deviation of the vehicle from the

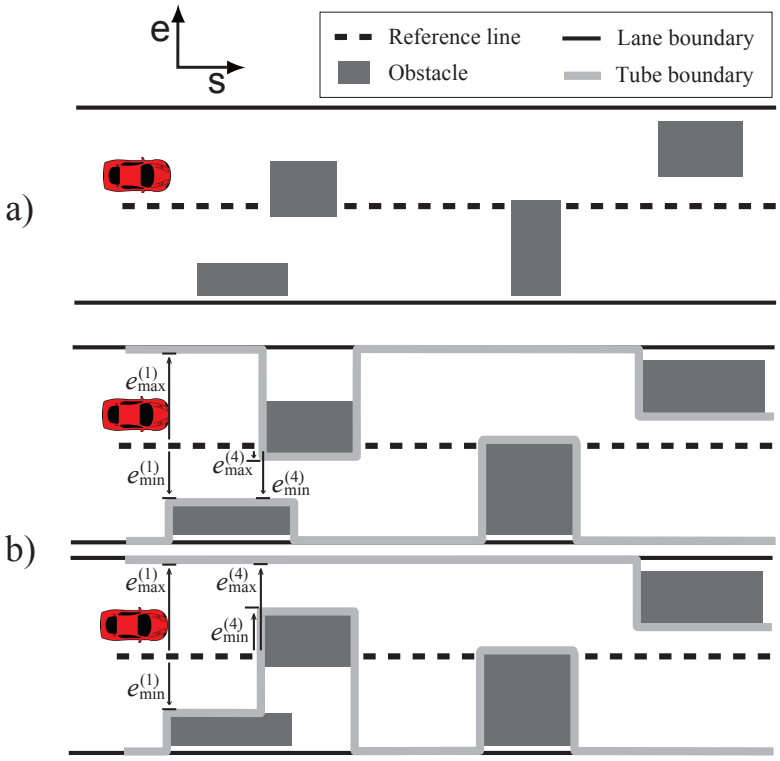

Figure 4.3: The environmental envelope is a representation of a) a collection of obstacles along the reference line using b) tubes (two of them in this example) which define a maximum ($e^{(k)}_{\max}$) and minimum ($e^{(k)}_{\min}$) lateral deviation from the reference line at each time step, k.

reference line:

$$e^{(k)} \leq e^{(k)}_{\max} - \frac{1}{2}d - d_{\text{buffer}} \tag{4.12}$$

$$e^{(k)} \geq e^{(k)}_{\min} + \frac{1}{2}d + d_{\text{buffer}} \tag{4.13}$$

where $e^{(k)}_{\max}$ and $e^{(k)}_{\min}$ indicate the lateral deviation bounds for time step k, d is the vehicle's width, and d_{buffer} specifies a preferred minimum distance between obstacles and the vehicle to ensure driver comfort.

Inequalities (4.12) and (4.13) can be compactly expressed as:

$$H_{\text{env}} x^{(k)} \leq G_{\text{env}}^{(k)} \tag{4.14}$$

where subscript env indicates the environmental envelope. A vehicle trajectory is collision free throughout the prediction horizon if and only if it satisfies inequality (4.14) for all k for any *one* tube in the environmental envelope. In this dissertation, the environments that are considered can be represented using only one tube; however, Erlien et al. previously published a method for handling multi-tube environments and generating these tubes in real-time [22].

4.3.4 MPC Formulation

The controller's objectives can be expressed as an optimization problem to be evaluated over a finite prediction horizon:

$$\begin{aligned}
\text{minimize} \quad & \sum_{k=0}^{10} \left| F_{\text{yf,driver}}^{(k)} - F_{\text{yf,opt}}^{(k)} \right| && \text{(4.15a)} \\
& + \sum_{k} \gamma^{(k)} \left| \left| F_{\text{yf,opt}}^{(k)} - F_{\text{yf,opt}}^{(k-1)} \right| \right|_2 && \text{(4.15b)} \\
\text{subject to} \quad & x^{(k+1)} = A_{\bar{\alpha}_{\text{r}},t_{\text{s}}}^{(k)} x^{(k)} + B_{\bar{\alpha}_{\text{r}},t_{\text{s}}}^{(k)} F_{\text{yf,opt}}^{(k)} + d_{\bar{\alpha}_{\text{r}},t_{\text{s}}}^{(k)} && \text{(4.15c)} \\
& \left| F_{\text{yf,opt}}^{(k)} \right| \leq F_{\text{yf,max}} && \text{(4.15d)} \\
& \left| H_{\text{sh}} x^{(k+1)} \right| \leq G_{\text{sh}} && \text{(4.15e)} \\
& H_{\text{env}} x^{(k+1)} \leq G_{\text{env}}^{(k+1)} && \text{(4.15f)} \\
& \left| F_{\text{yf,opt}}^{(k)} - F_{\text{yf,opt}}^{(k-1)} \right| \leq F_{\text{yf,max slew}}^{(k)} && \text{(4.15g)}
\end{aligned}$$

where $k = 0 \ldots 29$ and the variables to be optimized are the optimal input trajectory ($F_{\text{yf,opt}}$). As is typical in receding horizon control, only the calculated optimal force at the first time step, $F_{\text{yf,opt}}^{(0)}$, is applied to the vehicle, and the optimization problem (4.15) is re-solved at the next time step.

A tunable weight in this optimization is γ, which trades off between generating smooth steering inputs and matching driver intent. Constraint (4.15d) reflects the maximum force capabilities of the front tires and (4.15g) reflects the slew rate limits of a physical steering system. Constraints (4.15e) and (4.15f) enforce the stable handling and environmental envelopes, respectively. In practice, slack variables are used on these constraints to ensure optimization problem (4.15) is always feasible.

The prediction horizon used in optimization problem (4.15) uses time steps of different length in the near and long terms of the horizon to consider obstacles in the long term without compromising the prediction of vehicle states in the near term. CVXGEN [50] is used to leverage the significantly sparse structure of convex optimization problem (4.15) to produce an efficient solver for real-time implementation [51]. Table 4.1 shows the parameters used for both the short and long term prediction horizons.

4.3.5 Identically Matching The Driver

The controller balances the two objectives of following the driver's command and maintaining a feasible trajectory by trying to identically match the driver. Cost term (4.15a) uses the l_1 norm as a convex approximation to the objective of *identically matching* the driver's command where $F_{\text{yf,driver}}^{(k)}$ is the front tire force corresponding to the driver's handwheel angle, $\delta_{\text{hw}}^{(k)}$ at prediction index k. This 'identically matching' cost is used for the first 10 prediction indices (i.e. $1 \leq k \leq 10$) as shown in the summation of cost term (4.15a). The driver's handwheel angle at prediction index

Table 4.1: Prediction Horizon Parameters

Parameter	**Near Term Horizon**	**Long Term Horizon**
k	0...9	10...29
t_{s}	0.01 [s]	0.2 [s]
γ	30	1.5
$F_{\text{yf,max slew}}$	0.2 [kN]	5 [kN]
$\bar{\alpha}_{\text{r}}$	α_{r}	0
Total horizon length	100 [ms]	4 [s]

k is linearly extrapolated from the driver's current steering angle and steering rate. The previously described tire model (2.8) maps from $\delta_{\text{hw}}^{(k)}$ to $F_{\text{yf,driver}}^{(k)}$:

$$F_{\text{yf,driver}}^{(k)} = f_{\text{tire}}\left(\beta + \frac{ar}{U_x} - \delta_{\text{hw}}^{(k)}\right) \tag{4.16}$$

These first 10 prediction indices translate to a prediction horizon of 100 [ms]. Since a driver's maximum steering frequency is about 4 [Hz], in the first 100 [ms] of the prediction horizon, a linear extrapolation assumption can reasonably be used to model a driver's future steering command. The controller biases the early prediction indices to the driver (i.e. $k = 0...9$). Since this controller executes in real-time every 10 [ms], an updated extrapolation of the driver intent is obtained regularly. In this way, the controller only intervenes if it determines that, based on the driver's current steering input, no trajectories exist without vehicle instability or collision with the environment.

4.4 Interaction Between Steering Torque Feedback and Active Steering

When the controller's steering solution and the driver's steering input deviates from the first timestep of the solution, then the steering command used to actuate the roadwheels will differ from the driver's steering command. This is an active steering intervention. During such an intervention, the driver's steering command via the handwheel differs from the actual roadwheel position. The driver's steering command is now no longer in sync with the vehicle's motion. This can be disorientating to the driver as the vehicle is moving differently from the driver's projected motion for the vehicle based on his steering command. Providing a supportive steering feel during these situations that will aid the driver to turn with the intervention, will reduce the discrepancy between the driver's command and the vehicle's motion. This section investigates using the tire moment feedback from the actual roadwheels and the tire moment feedback using the virtual wheel to generate steering feel. It considers the

effect of steering interventions on the resultant feel generated by both approaches.

4.4.1 Simulation

The effect of both these feedback approaches with an active steering intervention for obstacle avoidance can be studied using a simple non-linear vehicle simulation based on the vehicle model presented in Section 4.1. The simulation scenario used in this chapter illustrates an inattentive driver who veers toward an obstacle at the side of the road. The driver is initially modeled as slowly increasing the steering angle so that he veers into the obstacle. Once the active steering intervention begins, the steering torque varies quickly and, sometimes, drastically. Suzuki [72] showed that different drivers react differently to steering torque feedback with some acting exactly

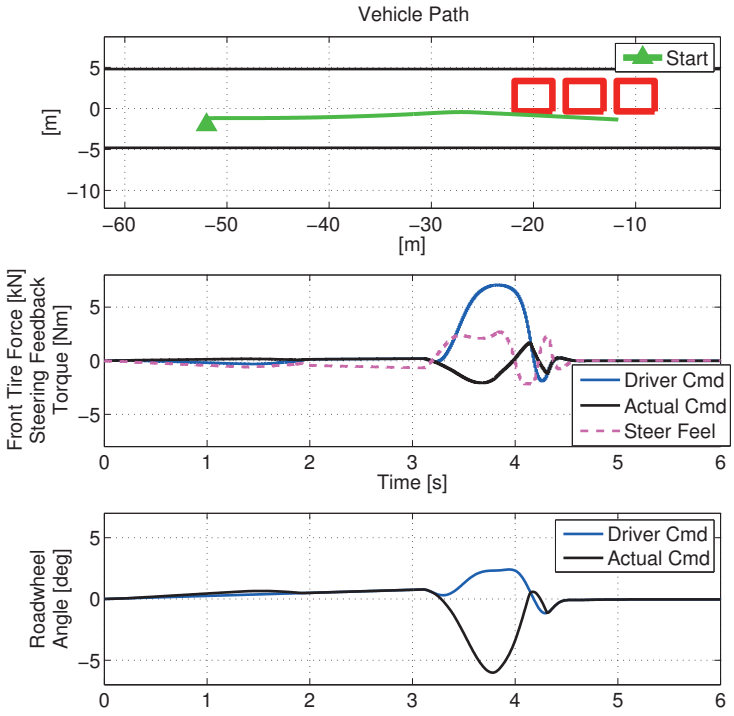

Figure 4.4: Simulation: Feedback without the virtual wheel

the opposite as others making a high fidelity model of the human reaction not very feasible. In order to model the driver during the intervention, this simulation uses a simple spring damper model of the passive arm and steering dynamics developed by Pick and Cole [60]:

$$J_{\text{driver}}\ddot{\delta}_{\text{hw}} + b_{\text{driver}}\dot{\delta}_{\text{hw}} + k_{\text{driver}}\delta_{\text{hw}} = \tau_{\text{hw}} \tag{4.17}$$

where the driver's arm and steering inertia (J_{driver}), damping (b_{driver}) and spring constant (k_{driver}) are determined through averaging measurements taken over eight test subjects. This model acts as a simple abstraction for a driver who simply allows his arm and steering system dynamics to dictate his handwheel angle (i.e. a passive driver).

Simulation Results

Figure 4.4 illustrates the simulation scenario of an passive, inattentive driver who veers into an obstacle (the red boxes) at the side of the road. When the active steering intervention occurs (i.e. 3.1 - 4.1 [s]), the steering torque acts in opposition to the intervention. The passive driver then turns the handwheel left while the vehicle's active steering intervention moves the vehicle to the right. This increases the discrepancy between the driver's command and the vehicle's motion resulting in the active steering system deviating further from the driver's command. These effects enhance the disconnection between the driver's command and the vehicle's motion.

Figure 4.5 illustrates the same simulation scenario as Figure 4.4 but with the virtual wheel concept implemented. The steering feedback now has the same sign as the actual roadwheel command during the intervention (i.e. 3.1 - 4.3 [s]). This steering torque acts to support the intervention. The passive driver's steering command now indeed moves in the same direction as the actual roadwheel angle. Therefore, the driver's actions have a smaller deviation from the active steering system. This reduces the disconnect between the driver's command and the vehicle's motion.

Discussion

The reason that the virtual wheel results in supportive steering torque feedback is that this feedback contains a large tire moment component. During an active steering intervention, the controller either increases or decreases the actual front lateral tire force (F_{yf}) beyond the driver's intended command using the roadwheel steer angle (δ_{rw}). Based on Equation (2.7), the actual roadwheel aligning moment has the opposite sign to the front lateral tire force. This causes the active steering intervention to always act in a manner that results in the actual aligning moment opposing it. Similarly, the jacking torque component has the opposite sign to the actual steer angle (see Equation (2.11). Therefore, during an active steering intervention, the jacking torque component will also act in a manner to oppose the steering intervention.

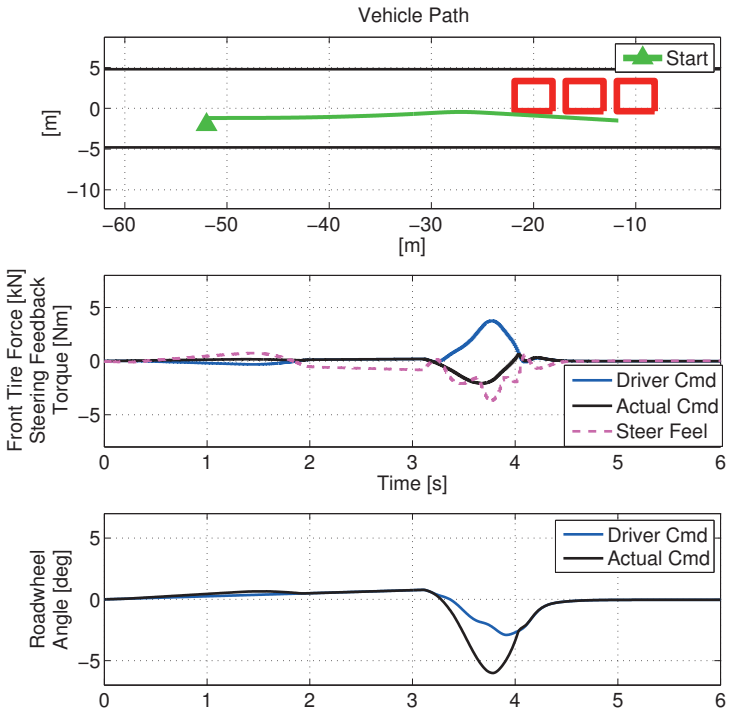

Figure 4.5: Simulation: Feedback with virtual wheel

For example, if the intervention commands a more positive tire force than the driver's command which also results in the intervention corresponding to a larger roadwheel angle, the aligning moment based on the actual roadwheel position would be more negative than the aligning moment based on the driver's intended roadwheel angle (i.e. the virtual wheel). The jacking torque would also be more negative. Using feedback based on the actual roadwheel position results in the driver getting a more negative steering feedback torque which tends to cause the driver to reduce his commanded tire force in opposition to the intent of the steering intervention.

Using the virtual wheel to generate the feedback overcomes these problems. The feedback now is based on the driver commanded tire force and steer angle. If the intervention results in a larger tire force than the driver command, the feedback will now not result in a more negative steering torque feedback that causes the driver to act against the intervention. In this way, using the virtual wheel to create feedback results in the driver obtaining supportive steering feedback during active steering interventions.

Griffin et al. found a similar result for tele-manipulated shared control systems [29]. There, the authors found that feeding back the operator's *commanded* force rather than the *actual* force resulted in lower force application by the operator and fewer task failures. Using the commanded force in that work is analogous to using the forces from the virtual wheel presented in this dissertation.

4.5 Experimental Validation

Experiments run on the steer-by-wire vehicle, X1 (illustrated in Figure 2.11) confirmed these simulations. The model predictive active steering controller was implemented on a single core of an Intel i7 processor utilizing MATLAB's real-time xPC toolbox at a rate of 100 [Hz]. Two experimental scenarios were created: a lanekeeping scenario and an obstacle avoidance scenario.

4.5.1 Test Scenario 1: Lanekeeping

The experiment involves the vehicle being intentionally driven towards the left road boundary. Based on the controller described in Section 4.3, when the vehicle's future trajectory violates the road boundary, the active steering engages to prevent the violation. After each time the driver drives towards the road boundary and the active steering intervention engages, the driver drives away from the boundary and repeats the process a few meters later. Three collision with the road boundary were performed in each data set. The experiment was performed on an asphalt road with friction coefficient (μ) of about 0.85.

Figure 4.6 shows the data from the test without the virtual wheel. The driver

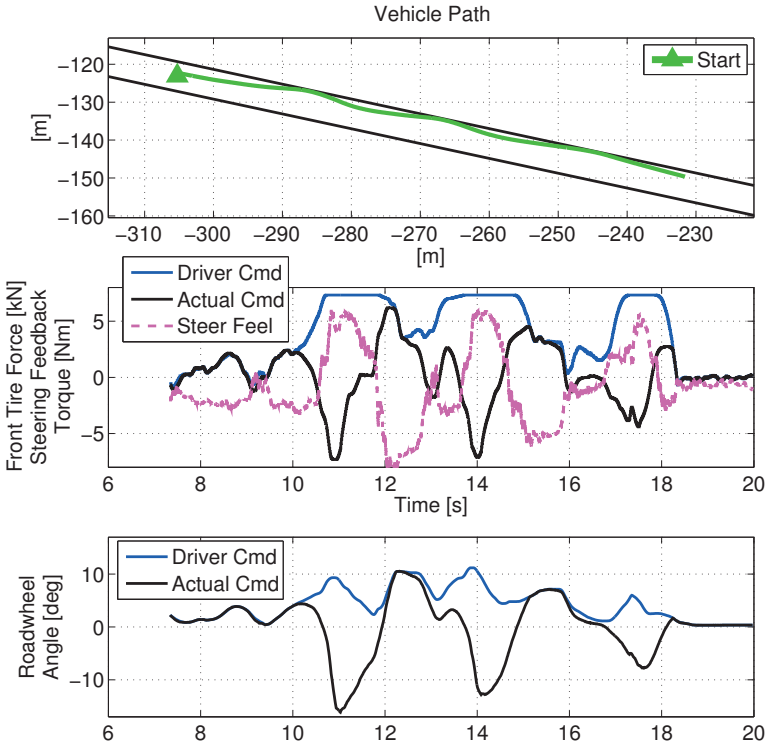

Figure 4.6: Experiment (lanekeeping): Feedback without virtual wheel

drives into the left road edge three times at around 11 [s], 14 [s] and 17.5 [s]. At each of these times, the steering feedback acts in the opposite direction to the actual roadwheel command. Therefore, the feedback opposes the intervention. This results in the handwheel being pulled in such a manner as to cause the vehicle to steer into the road boundary rather than away from it. This increases the discrepancy between the driver's command and the active steering system. There is a disconnect between the driver's actions and the vehicle's motion.

Figure 4.7 illustrates a similar test but with the virtual wheel concept implemented. Once again the driver drives into the left road edge three times at around 7.5 [s], 10 [s] and 12.5 [s]. At each of these times, the steering feedback acts in the same direction as the actual roadwheel command. The feedback now supports the

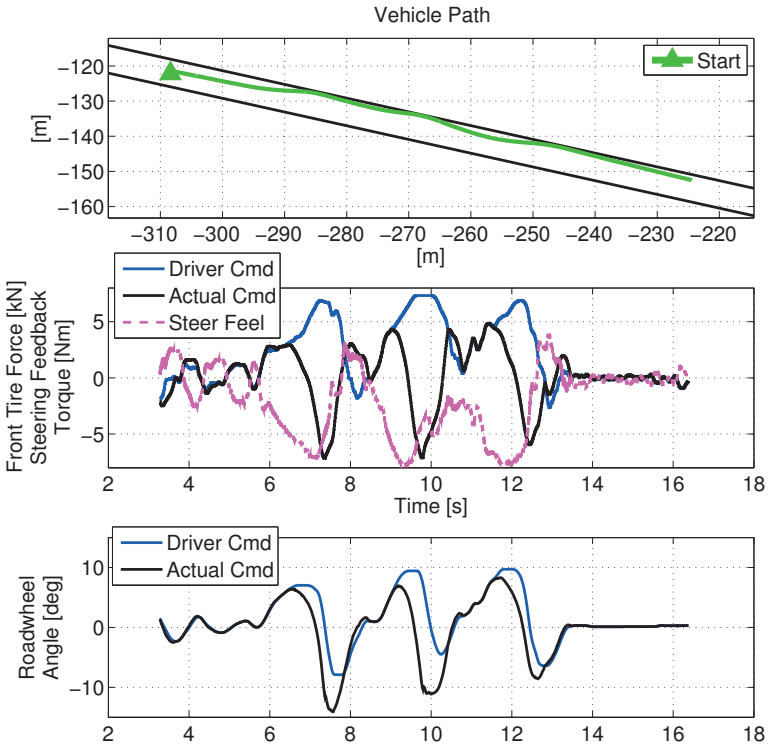

Figure 4.7: Experiment (lanekeeping): Feedback with virtual wheel

intervention. Instead of the handwheel being pulled in such a manner as to cause the vehicle to steer into the road boundary as before, the steering feedback acts to push the driver away from the boundary and maintain a safe trajectory. This reduces the discrepancy between the driver's command and the active steering system (as seen in the bottom plot).

4.5.2 Test Scenario 2: Obstacle Avoidance

The experiment involves the vehicle being intentionally driven towards a traffic cone used to simulate an obstacle. Based on the controller described in Section 4.3, an active steering intervention occurs to prevent the vehicle's future trajectory from violating either the road boundary or obstacle. The experiment was performed on an asphalt road with friction coefficient (μ) of about 0.85.

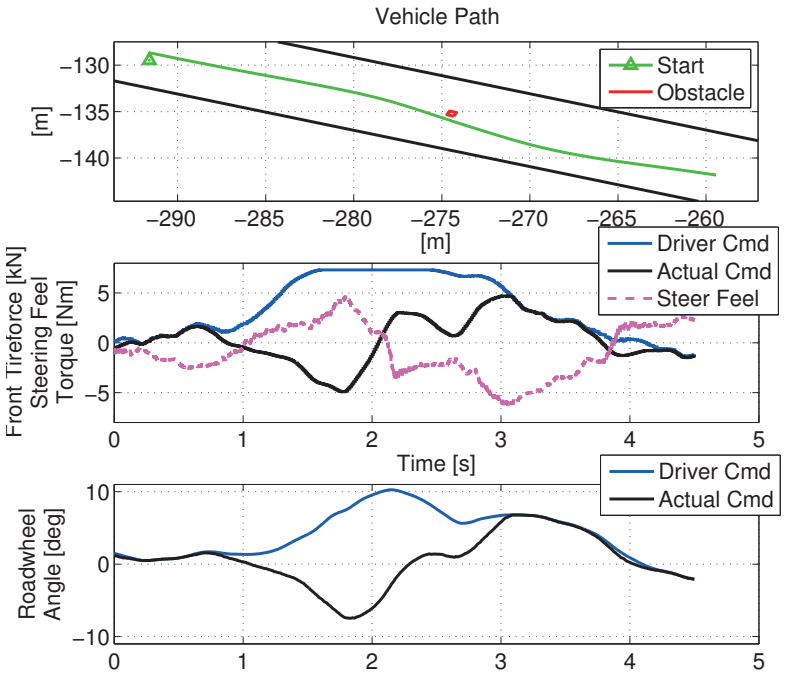

Figure 4.8: Experiment (obstacle avoidance): Feedback without virtual wheel

Figure 4.8 shows the data from the test without the virtual wheel. The experimenter drives towards the obstacle marked in red. When the active steering intervenes to steer the vehicle away from the obstacle, the steering feedback acts in the opposite direction to the actual roadwheel command. Therefore, the feedback opposes the intervention.

Figure 4.9 illustrates a similar test but with the virtual wheel concept implemented. Once again the experimenter drives towards the obstacle marked in red. Now, the steering feedback acts in the same direction to the actual roadwheel command. The feedback now supports the intervention. This reduces the discrepancy between the driver's command and the active steering system (as seen in the bottom plot). These experiments show that the virtual wheel concept provides supportive steering feel during both obstacle avoidance and lanekeeping scenarios.

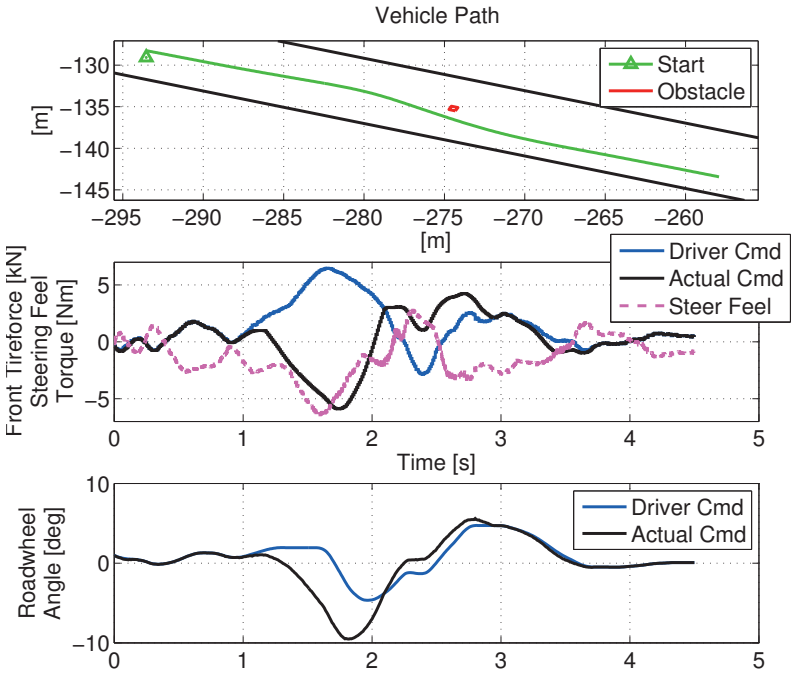

Figure 4.9: Experiment (obstacle avoidance): Feedback with virtual wheel

4.6 Summary

This chapter proposes a single steering feel model that provides supportive steering feel for both scenarios with and without active steering interventions. This model incorporates the concept of the virtual wheel which uses the driver's commanded steer angle and tire forces to generate the steering feedback torque felt at the handwheel. During scenarios without active steering interventions, the model produces steering feel that reflects the moment acting on the actual roadwheels while also including important effects like power assist (i.e. the same model as seen in Section 2). During active steering interventions, steering feedback that is based on the actual roadwheel position results in handwheel torque that opposes the intervention. This leads to a large discrepancy between the driver's command and the active steering controller. By implementing the virtual wheel concept, the driver's intended tire moment command rather than the actual tire moments generate the steering torque feedback. This technique allows for a realistic steering feedback when there is no active steering intervention as the driver's intended tire moments is the same as the actual tire moments. During a large active steering intervention, this technique results in steering feedback that supports the intervention. Simulation demonstrate that this reduces the discrepancy between the driver's command and the active steering system. Experiments further show how using the virtual wheel results in supportive steering feedback torque during the lanekeeping and obstacle avoidance tasks.

Chapter 5

Predictive Haptic Feedback

New perception technologies enable modern vehicles to have knowledge of the environment around them [44], [45], [9]. Sensing systems like radar, cameras and laser systems provide rich information about the environment in real-time even when human visual perception is limited due to distraction, poor lighting and/or fog. Coupled with steer-by-wire systems that enable active steering capabilities, predictive controllers can share control with the driver and enhance the safety of modern vehicles. Kawabe et al. presented a receding horizon control framework that uses information about the surrounding environment to generate optimal paths to guide a human driver [41]. These controllers allow drivers to have full control of the vehicle unless the controller detects that the vehicle is going to interact negatively with the environment (i.e. lane departure, collision). During these scenarios, the controller will then intervene, using active steering as a means of augmenting the driver's command to ensure the safety of the vehicle.

One challenge in designing shared control systems is how to incorporate the driver in these systems. One approach involves the controller determining an optimal trajectory which does not explicitly incorporate the driver's input. Rather, the driver's input is blended with the controller's optimal solution and the resultant command is sent to the roadwheels. Katzourakis et al. used this approach when they introduced a shared control regime for road departure prevention [39]. Anderson et al. blended the driver's command with the solution of a Model Predictive Control (MPC) obstacle

avoidance controller to create a shared control framework [5]. By not explicitly incorporating the driver's input in formulating the optimal trajectory, it is challenging for these controllers to formulate solutions that incorporate the driver's intent. Another approach involves explicitly incorporating the driver's input as a reference signal in the formulation of the optimal solution. Erlien et al. proposed such a shared control framework for maintaining a safe trajectory that explicitly considers the driver's command in its MPC solution [22]. Doing this enables the controller to better track the driver's intent when creating optimal trajectories.

Shared control regimes constantly balance the sometimes competing objectives of following the driver's command and maintaining a feasible trajectory for the vehicle. Biasing the controller heavily to the latter objective results in conservative active steering interventions where the controller deviates early and frequently to cause the vehicle to follow its desired path. This can possibly reduce the driver's control authority. Heavily biasing the controller to follow the driver results in the controller deviating from the driver very late and only as a last resort to maintain a feasible path. This leaves control authority with the driver for longer but results in more aggressive and uncomfortable maneuvers. Anderson et al. state that these interventions should not alter the driver's command 'too much', 'too often' or 'too soon' while still guaranteeing that the vehicle maintains a safe trajectory [6]. Communicating the tension between these two objectives to the driver and having him modify his behavior early to reduce this tension could then be very useful in addressing this issue. Controllers could then be biased to have later interventions while still communicating to the driver early of the need to modify his command.

Haptic steering feedback can effectively be used to communicate current information between a vehicle or controller to the driver. This information may then aid the driver in the driving task. Katzourakis et al. used haptic steering feedback to effectively communicate the tires' cornering limits to the driver and improve his ability to handle the vehicle at its limits [40] . Mulder et al. used haptic feedback to improve driver's curve negotiation behavior in a simulator [54]. Switkes et al. performed a simulator study that used the lanekeeping potential field force acting on a vehicle as haptic steering feedback [73]. Steele and Gillespie generated haptic feedback on

a simulator using the difference between the driver's current steering angle and the desired steering angle as determined by a autonomous path-tracking controller and a pre-defined static path [71]. Brandt et al. used a similar approach to generate haptic feedback on a simulator except, instead of static paths, a potential field technique was used to generate dynamic paths [18]. Predictive controllers enable haptic feedback based on the future tension between the objectives of following the driver or maintaining a feasible path. This feedback could guide the driver to modify his actions early.

This chapter proposes a novel method of generating haptic steering feedback based on the future tension between the potentially competing objectives of following the driver and maintaining a feasible path. This chapter begins by using simulation to show how to obtain predictive haptic feedback from this shared controller, developed by Erlien et al. for obstacle avoidance [22]. This feedback mirrors the tension between the two shared controller objectives. This feedback is based on future differences between the predictive controller and the driver. The simulation also shows the inherent trade-off between getting earlier haptic feedback by using information further in the prediction horizon and the greater uncertainty in those predictions injecting variability in the feedback. An experimental driver study shows that this feedback, with statistical significance, causes participants to react earlier and turn out of the path of an obstacle. This is accomplished with reduced driver steering inputs and results in a less aggressive maneuver. This work was first discussed by Balachandran et al. [11].

5.1 Generating Predictive Haptic Feedback

Figure 5.1 shows a simulation of a vehicle using the controller described in Section 4.3 as it avoids an obstacle. This simulation is used to help the reader understand the tension between the controller objectives of following the driver's command and maintaining a feasible trajectory. Furthermore, this section presents a method of generating feedback that reflects this tension.

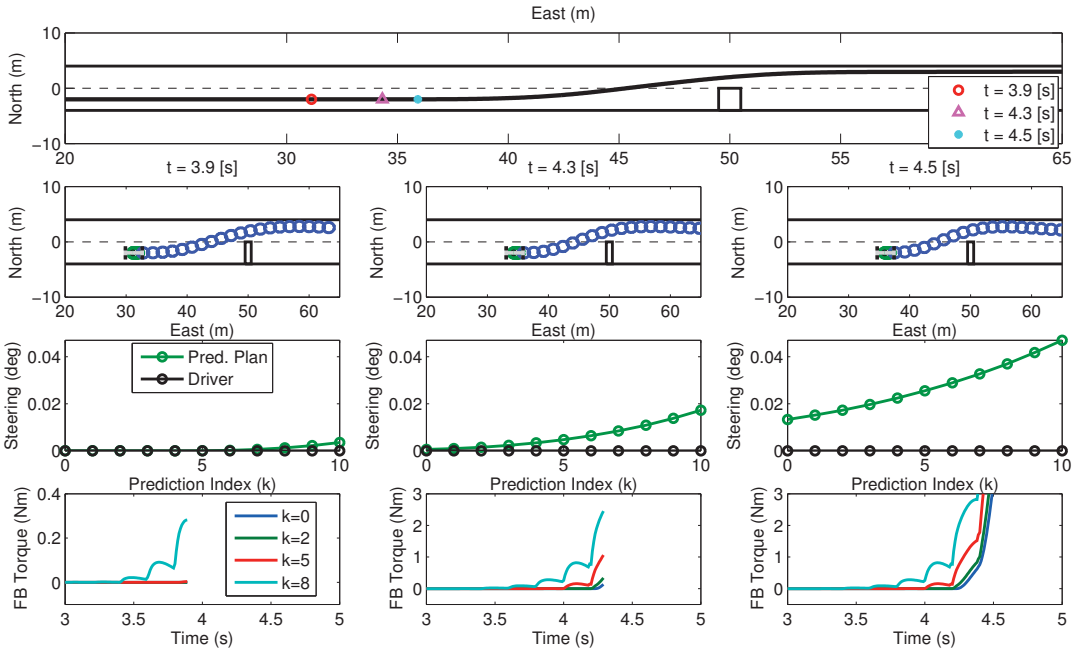

Figure 5.1: Simulation results showing the generation of the feedback torque over time as the tension between the controller's objectives of following the driver's command and maintaining a feasible trajectory increases

5.1.1 Tension Between Controller Objectives

Figure 5.1 shows a simulation demonstrating the tension between controller objectives. The scenario used for generating this simulation involves a vehicle starting on the right lane of a two-lane road and traveling at a constant speed towards an obstacle blocking the right lane. The driver is modeled as holding a constant zero steering angle throughout the simulation. The uppermost plot of Figure 5.1 represents the trajectory of the vehicle over the simulation. This plot shows that as the driver approaches the obstacle and continues holding a zero steering angle, the controller will eventually use an active steering intervention to affect a lane change maneuver so as not to collide.

The columns of the 3 vertical plots below the uppermost plot provide a visualization of the MPC solution at simulation execution time steps $t = 3.9[s]$, $t = 4.3[s]$ and $t = 4.5[s]$. These execution time steps correspond to the vehicle having a time to collision (TTC) with the center of the obstacle of 2.36 [s], 1.96 [s] and 1.76 [s] respectively. The first row of these columns shows, spatially, the optimal trajectory solution of the MPC optimization. The second row of these columns shows the driver's steering input (in this case always zero) and the MPC solution's optimal desired steering action for the first 10 prediction indices, k.

Tension between the objectives of following the driver's command and maintaining a feasible trajectory builds as the steering action required to maintain a feasible trajectory starts differing greatly from the driver's input. This tension begins far out in the prediction horizon and propagates to smaller prediction indices if the driver continues to not modify his steering input. This can been seen in the second row of steering plots. The difference between the driver's input and the controller's desired steering action is the largest at the end of the horizon and propagates to smaller prediction indices as the execution time step increases (i.e. going from left to right). In the steering plot for the execution time step at $t = 4.5[s]$, the driver's input and the controller's desired steering angle no longer agree on the first prediction index, $k = 0$, indicating that an active steering intervention is occurring to maintain a collision-free trajectory. Intuitively, this shows the tension growing as the driver continues without changing his steering input and travels towards the obstacle. By correlating these

steering plots with the trajectory plots in the row above, notice that this tension grows as the required trajectory to avoid the obstacle becomes more aggressive.

5.1.2 Generating Predictive Haptic Steering Feedback

Since the tension begins far out in the prediction horizon and propagates to smaller prediction indices, haptic feedback can be generated using the predicted future tension in the controller. This predictive haptic feedback then mirrors the amount of future tension between the two objectives. To make the haptic feedback reflect this future tension, it is given to be proportional to the difference between the driver's steering input and the controller's desired steering action at a predetermined future prediction index. The haptic torque is generated as follows:

$$\tau_{\text{haptic}} = K_{\text{haptic}} \left(\delta_{\text{opt}}^{(k)} - \delta_{\text{driver}}^{(k)} \right) \tag{5.1}$$

where τ_{haptic} is the predictive haptic feedback torque, K_{haptic} is the gain for the haptic feedback, $\delta_{\text{opt}}^{(k)}$ is the optimal steering angle at a pre-determined prediction index k, obtained from the optimization, and $\delta_{\text{driver}}^{(k)}$ is the driver's steering input at that same prediction index. This section investigates the generation of this feedback and the impact of using different prediction indices, k.

The last row of the columns in Figure 5.1, shows the haptic feedback torque calculated by using Equation (5.1) at different prediction indices (k), up to and including that particular column's execution time step. The haptic feedback gain K_{haptic} was set at 150 [Nm/rad]. The larger the prediction index used to generate the feedback, the earlier this feedback is felt by the driver. This makes sense as the tension propagates down from further out in the prediction horizon to smaller prediction indices over time. Therefore, using a larger prediction index to generate the feedback results in the feedback kicking in earlier and indicating to the driver that the tension between the competing objectives is growing. In this way, predictive feedback can be given to the driver to guide him in modifying his actions early to reduce this tension. This feedback mirrors the tension between the competing objectives of following the driver's command versus maintaining a feasible path. If there is no environmental

danger detected, there is no tension as the driver's input will result in a feasible path. Therefore, the driver's input and the controller's desired steering action will be the same and there will be no feedback. However, as this tension grows so will the difference between the driver's input and controller's desired steering angle, resulting in a feedback torque.

Since these objectives vary with different situations, the tension between balancing them is also highly situation dependent. Therefore, unlike other obstacle avoidance haptic warnings, the haptic feedback using this technique is not based on a fixed time to collision (TTC). Rather the magnitude of the feedback is based on the level of conflict between the shared controller's objectives of following the driver's command and maintaining a feasible trajectory.

However, there is a trade-off in using the larger prediction indices. As with any prediction, the longer into the prediction horizon that one looks at, the more uncertainty there will be. This uncertainty finds its way into the haptic feedback torque generated if large prediction indices are used. This can been seen in the feedback torque plot of execution time step $t = 4.5[s]$ where the larger the prediction index, k, used to generate the feedback, the more variability in that feedback torque. Therefore, as the prediction index, k, increases the feedback kicks in earlier but has more variability. Much of this variability can be damped out by the inherent dissipative dynamics of the steering system and the driver's arms. The authors have found that using prediction indices between 4 and 10 result in early feedback with smaller variability.

5.2 Experimental Results

Experiments run on the steer-by-wire vehicle, X1 (illustrated in Figure 2.11) verified the efficacy of this predictive haptic feedback on the obstacle avoidance task. A nominal steering feel, similar to that of a production vehicle, is generated on X1 to ensure that the participants feel comfortable driving. The steering feel model based on tire moments and steering system dynamics proposed in Chapter 2 is used to create this feel.

5.2.1 Test Scenario

The efficacy of this predictive haptic feedback can be characterized by seeing if drivers are able to interpret what it means and react to it quickly and easily. To do this, the visual indication of an upcoming obstacle must be decoupled from the predictive haptic feedback. This ensures that recorded driver reactions are due to the predictive haptic feedback rather than the visual cue of an upcoming obstacle. This decoupling models scenarios in which vehicles with enhanced perception technologies have better information about the environment than the driver, particularly during poor lighting or foggy conditions. Jensen et al. decoupled haptic and visual cues during an obstacle task to show, using a simulator, the efficacy of using sinusoidal haptic feedback to alert the driver to upcoming obstacles [38]. Griffiths and Gillespie used visual occlusion techniques, on a simulator, to investigate the lower visual demand needed due to haptic feedback assistance for the obstacle avoidance task [30].

Decoupling the visual and haptic cues of an obstacle in a simulator setting is reasonably straight-forward as the experiment designer has direct control over when the obstacle appears on screen for the driver. On an on-road experimental setup, decoupling the visual and haptic cues of the obstacle is more challenging. Solutions are few and tend to be expensive and difficult to set up. Multiple obstacle experiments quickly then become cost and time prohibitive.

To enable the decoupling capability in the on-car experiments presented in this dissertation, a novel 'popup' obstacle solution was created. This obstacle fulfilled the requirements of being low cost, easy to set up and non-damaging to the vehicle/participant in the event of collision. Figure 5.2 illustrates the 'popup' obstacle. Essentially, the obstacle is an air-filled tube that can be inflated to act as a lane blockage. Before inflation the obstacle does not block the lane. The obstacle inflates in 0.3 [s] and is controlled wirelessly from the vehicle.

Figure 5.3 illustrates the two-lane test scenario and 'popup' obstacles setup used for this experiment. The vehicle has information about the upcoming obstacle before deployment so the driver receives predictive haptic feedback before the actual deployment of the obstacle. Before the deployment of the obstacle, drivers started by driving on the right lane as illustrated in Figure 5.3(a). Cruise control was used

to maintain a constant speed (7 [mps]) so that drivers avoided the obstacle through only the use of steering. During each trial, either one or none of the three 'popup' obstacles (indicated in Figure 5.3 as the red dotted circles) would randomly deploy at a TTC of about 2.5 [s]. If an obstacle deployed, it would block the rightmost lane as indicated in Figure 5.3(b) causing drivers to perform a lane change to the left lane. Figure 5.4 shows the course from the driver's perspective before the deployment of the obstacle and Figure 5.5 shows the course from the same perspective after deployment of the obstacle.

Drivers drove with both treatments, with and without predictive haptic feedback, where the future index used to obtain the feedback was 10 (i.e. $k = 10$). Since the experimental conditions were repeatable for each participant, this setup resulted in the haptic feedback occurring at about a TTC of 3.5 [s] for all participants.

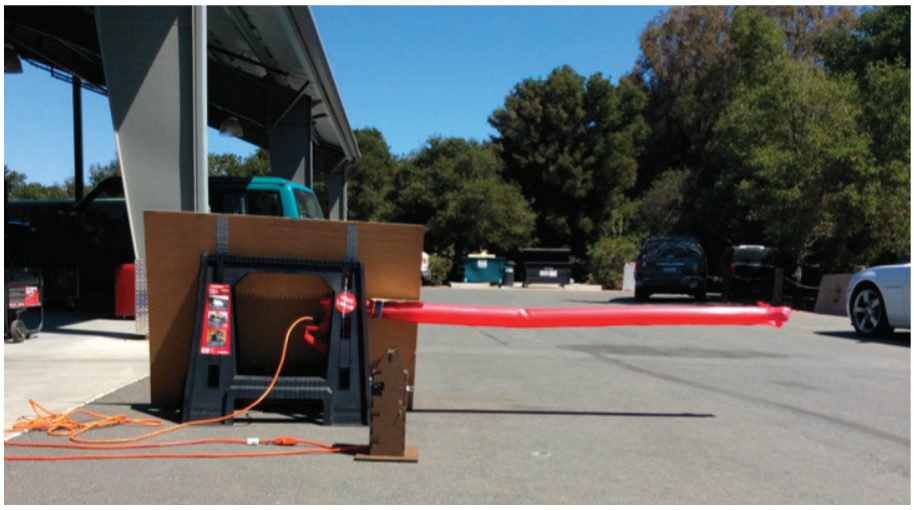

Figure 5.2: 'Popup' obstacle

Ensuring that the participants feel comfortable driving the test vehicle means having a steering feel based on the actual tire moments similar to that of a production vehicle. Therefore, the steering feel model proposed in Chapter 2 was implemented on X1. Due to the shared control regime being used, there exists a possibility that an active steering intervention may occur. However, since the obstacle was only ever deployed at a time to collision (TTC) of 2.5 [s], drivers needed to perform a fairly

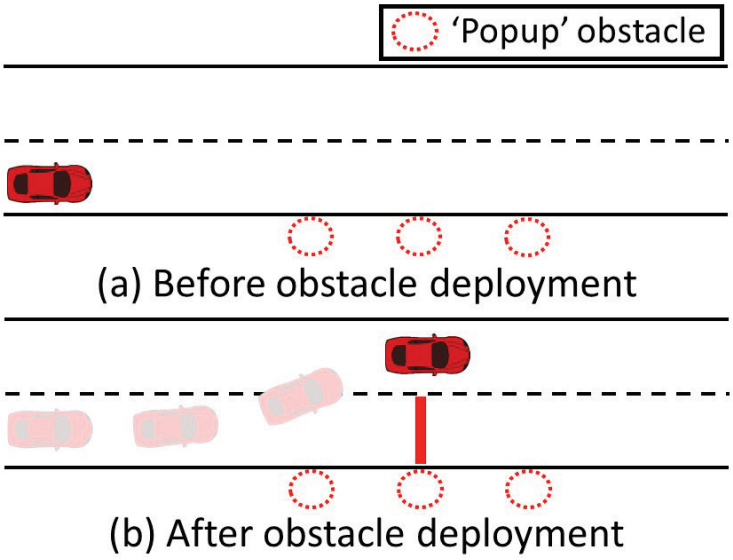

Figure 5.3: Experimental setup

benign lane change maneuver to avoid them. Drivers performed these maneuvers without any need for an active steering intervention. The intervention capability was left as a means of ensuring safety so that drivers did not veer of the course and collide with the actual environment (i.e. walls). If a large steering intervention did occur, Balachandran et al. showed that a steering feel based on actual tire moments would cause the driver to act against the intervention resulting in unsafe behavior [12]. Therefore, as a safety feature if a large intervention did occur, the virtual wheel concept proposed by Balachandran et al. was used to generate a steering feel that would cause the driver to follow the intervention [12]. Since no emergency scenarios occurred during the experiments presented here, no active steering interventions occurred.

5.2.2 Test Procedure

A total of 11 participants (2 females, 9 male, age mean: 26.6 years, age STD: 3.3 years) participated in the experiment. Before the start of the experiment, each participant

Figure 5.4: Driver's perspective: Before obstacle deployment

was told to stay in the right lane unless an obstacle deployed. Each participant then performed a drive through the course to ensure familiarity with the test setup and vehicle. The order of treatment for participants varied, 6 started without feedback and 5 started with feedback. All participants performed the experiment with both treatments. Each treatment involved drivers performing 5 trials where either no obstacle deployed or one of the three obstacles deployed. The choice of if and which obstacle would deploy was determined pseudo-randomly *a priori*. Before the 'with feedback' treatment, drivers also had 2 training trials where they were told which obstacle would deploy before the trial. This allowed drivers to get used to the haptic feedack and minimized learning effects. The training trials were not used for the analysis. Each non-training trial for which an obstacle deployed was recorded as a single independent event. In total, 34 individual events were obtained for the 'with feedback' treatment and 42 individual events were obtained for the 'without feedback' treatment.

Figure 5.5: Driver's perspective: After obstacle deployment

5.2.3 Discussion: Single Driver

Figure 5.6 illustrates experimental data from a single driver. A single trial with predictive feedback (red-dotted) and one without (blue) is shown. The large plot on the left shows the trajectory of the vehicle and indicates that with the predictive feedback, the driver modifies his trajectory to avoid the obstacle earlier. This is clearly seen in the handwheel angle plot on the top right where the red line indicates an earlier turn than the blue line. The peak steering input required is also smaller. The handwheel angle derivative (second plot from the top) also indicates that fewer steering corrections are required with the feedback. The bottom two plots indicate vehicle yaw rate and lateral acceleration respectively and show that these quantities are generally smaller as well, indicating a smoother motion of the vehicle. Overall, the predictive feedback results in the driver reacting and turning earlier in response to an upcoming obstacle. This in turn results in a smaller required steering input, fewer required steering corrections and a smoother vehicle motion.

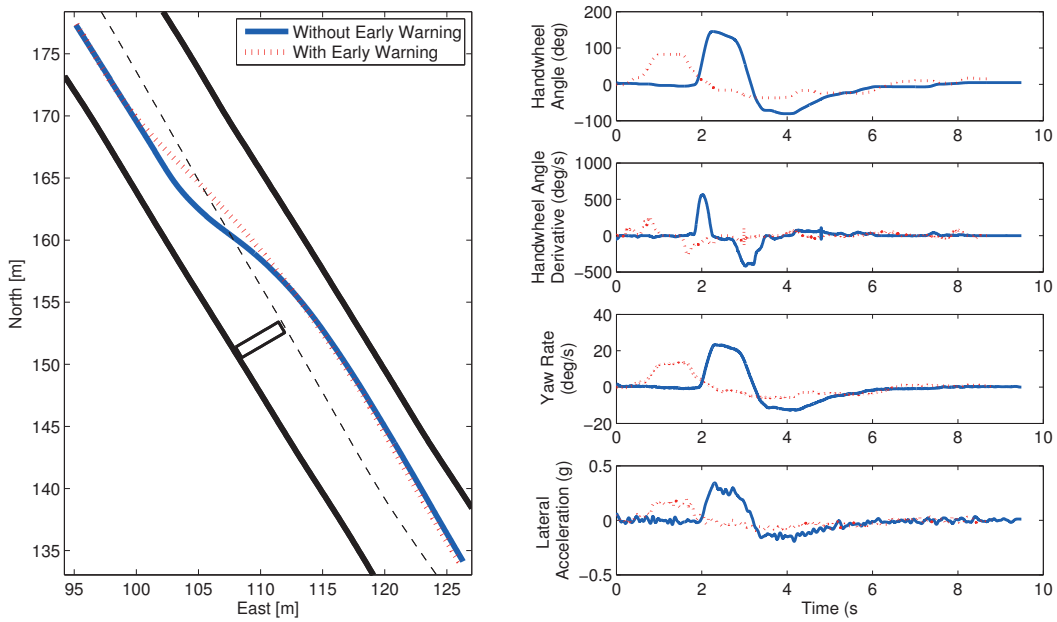

Figure 5.6: Experimental data: single driver

5.2.4 Discussion: Driver Study

The section above describes the qualitative impact of the feedback on a single driver. In order to make a quantitative statement, data from the full driver study was analyzed. Five performance measures were analyzed to interpret the results. They are minimum TTC, peak handwheel angle, peak handwheel steering rate, peak yaw rate and peak lateral acceleration. Since there are only two treatments (i.e. with and without feedback), significant differences between treatments for each measure were analyzed using independent t-tests. These act as a conservative means of analyzing differences.

Figure 5.7 shows the minimum time to collision (TTC) with both treatments. A higher TTC implies that the driver reacted earlier to move out of the path of the obstacle. The minimum mean TTC is significantly higher for the 'with feedback' treatment, indicating that drivers do indeed turn earlier with the predictive feedback. This backs up the analysis obtained from a single driver.

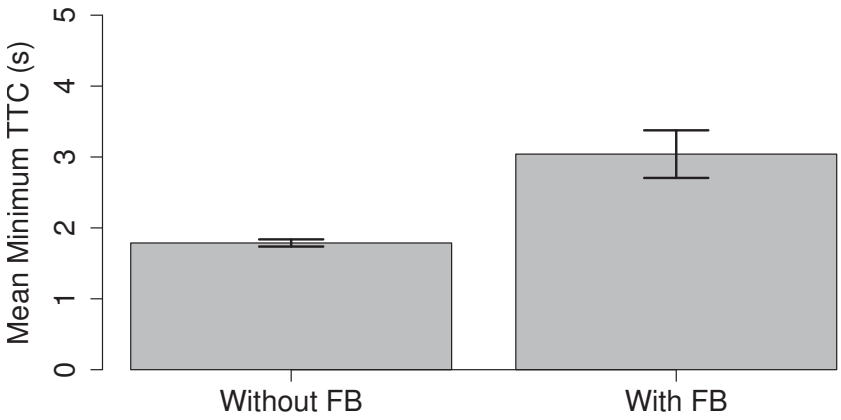

Figure 5.7: Mean minimum time to collision for both treatments with 95% confidence bounds marked

This increase in minimum TTC is not unexpected as the haptic feedback does kick in 1 [s] before the visual feedback of the obstacle. Looking at the difference in time between minimum TTC and the actual feedback signal (i.e. 2.5 [s] for visual feedback and 3.5 [s] for haptic feedback of the obstacle), a simple measure for the drivers mean reaction time to those feedback modalities is obtained. Using this metric, the reaction time for a driver reacting to the purely visual feedback is found to be 0.7 [s] but with the haptic feedback, the reaction time reduces to 0.5 [s]. Therefore, based on this metric, reaction times of drivers are also lower with the haptic feedback indicating that drivers react sooner to that form of feedback. The 95% confidence bounds on this data are also very tight. This indicates that the variation in mean minimum TTC across the entire study is small and that the feedback resulted in similar mean minimum TTCs between different participants and trials.

The peak handwheel angle and peak handwheel steering rate illustrate the driver inputs during the maneuver. Figure 5.8 shows the means for these two measures for both treatments with their 95% confidence bounds. The 95% confidence on these measures are very tight demonstrating that there is little variation between different

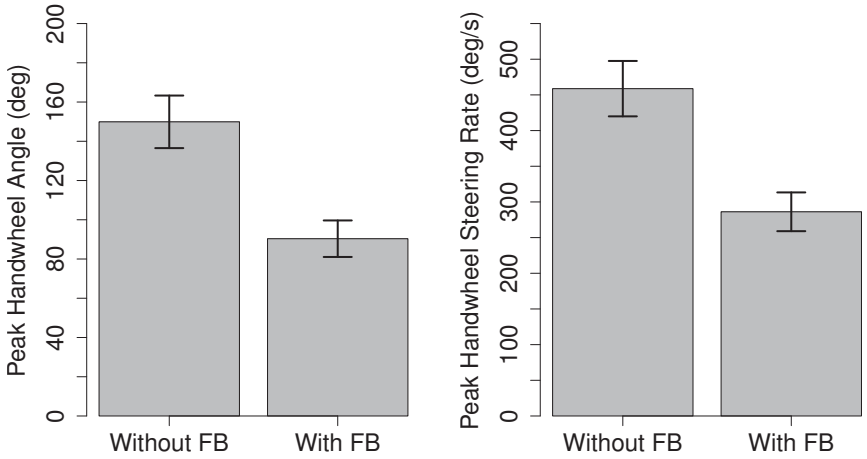

Figure 5.8: Experimental performance measures (driver inputs) for both treatments with 95% confidence bounds marked

participants and trials. Table 5.1 shows the means and standard deviations of these two measures and the minimum TTC for all the trials broken down by treatment. The last row of the table reflects the p values for independent t-tests that were conducted for each measure between the 2 treatments and shows that all t-tests were significant with $p < 0.01$. This table shows that the minimum TTC, peak handwheel angle and peak handwheel steering rate are also statistically lower for the treatment with feedback. This indicates that drivers not only turned earlier with the predictive feedback, but they also turned less aggressively.

	TTC [s]		**Peak Handwheel Angle [deg]**		**Peak Handwheel Steering Rate [degs^{-1}]**	
	Mean	STD	Mean	STD	Mean	STD
Without Feedback	1.79	0.17	149.9	44.3	458.8	128.4
With Feedback	3.04	1	90.4	27.7	286.2	80.8
P Value	$p < 0.01$		$p < 0.01$		$p < 0.01$	

Table 5.1: Driver Study Data: Driver Inputs

The peak yaw rate and peal lateral acceleration measures illustrate the vehicle's

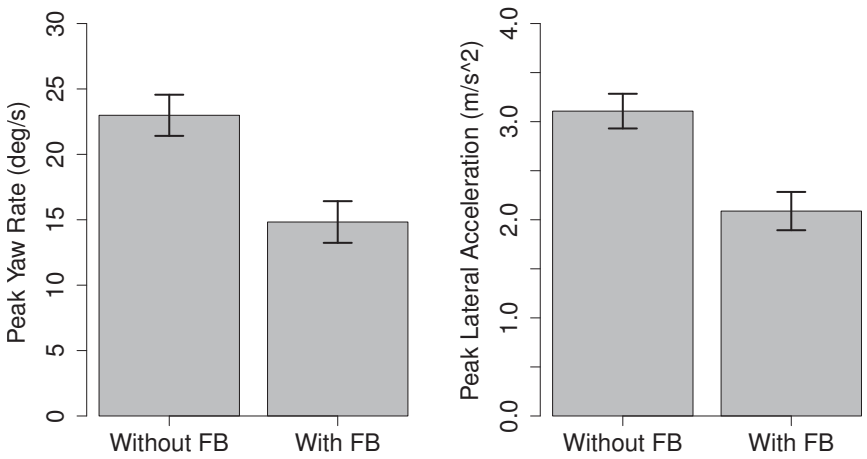

Figure 5.9: Experimental performance measures (vehicle response) for both treatments with 95% confidence bounds marked

response. Figure 5.9 shows the means for these two measures for both treatments with their 95% confidence bounds. Table 5.2 shows the means and standard deviations of these two measures for all the trials broken down by treatment (same format to Table 5.1). This table shows that the peak yaw rate and lateral acceleration are also statistically lower for the 'with feedback' treatment. This indicates that the obstacle avoidance maneuvers performed with feedback are less aggressive. These two measures also correlate with driver comfort indicating that the maneuvers are also more comfortable for the driver. The 95% confidence bounds on these measures are very tight demonstrating that there is little variation between different participants and trials.

To summarize:

(1) Drivers have a higher minimum TTC with haptic feedback

(2) Drivers react faster to haptic feedback than purely visual feedback

(3) Drivers use less aggressive inputs with the haptic feedback

	Peak Yaw rate [degs^{-1}]		**Peak Lateral Acceleration [ms^{-2}]**	
	Mean	STD	Mean	STD
Without Feedback	23	5.2	3.1	0.58
With Feedback	14.8	4.7	2.1	0.6
P Value	$p < 0.01$		$p < 0.01$	

Table 5.2: Driver Study Data: Vehicle Response

(4) Corresponding vehicle motion is less aggressive and more comfortable with haptic feedback.

It is important to note that this experiment is meant as a proof-of-concept. More experiments and surveys are required to show that drivers understand this form of haptic feedback and are able to interpret what to do about that feedback more easily than other forms of feedback. Also, different metrics can be used to more accurately measure driver reaction time to the different feedback modalities.

5.3 Summary

This chapter proposes a novel method of generating predictive haptic feedback using a Model Predictive shared control framework. The feedback is proportional to the difference between the driver's steering input and the controller's desired steering action at a predetermined future prediction index. This reflects the future tension between a shared controller's potentially competing objectives of following the driver and maintaining a feasible path. This feedback can then guide a driver to modify his actions early so as to reduce this tension. The chapter shows that using information from further in the prediction horizon (i.e. larger prediction index) creates earlier feedback for the driver. However, there exists an inherent trade-off between getting earlier haptic feedback by using information further in the prediction horizon and the greater uncertainty in those predictions injecting variability in the feedback. An experimental driver study showed that using predictive feedback can, with statistical significance, cause participants to react earlier and turn out of the path of an obstacle. This also resulted in reduced driver steering inputs and a less aggressive vehicle

maneuver with minimal variation per treatment between different participants and trials.

Chapter 6

Conclusion

Steer-by-wire technology enables a variety of capabilities that can make vehicles safer and change the way that driver's interact with their vehicles. In particular, the mechanical decoupling of the handwheel from the roadwheels in steer-by-wire systems, enables a flexible active steering capability. This capability can be used to improve vehicle safety and stability, prevent collisions and share control with the driver to ensure feasible vehicle trajectories. However, this same mechanical decoupling also results in the handwheel no longer having any useful steering feedback torque. Fortunately, Force Feedback (FFB) steering systems can be designed and built that allow a designer to artificially create arbitrary torque on the handwheel for the driver to feel. This dissertation investigates how to create these torques.

The first contribution presented is the creation of an artificial steering feel on a steer-by-wire vehicle that mimics the feel found in conventional steering vehicles. Chapter 2 proposes a steering feel model that is based on reflecting the actual tire moments to the driver. This model has sufficient complexity to capture the elements of steering feel that are important as determined by objective steering feel metrics used by industry. This includes the power assist effect which is very important in modern vehicles. Simulations and experiments demonstrate that this model is simple enough to be tuned intuitively and run in real-time on an actual steer-by-wire vehicle.

Before this feel can be implemented for on-road use, showing that it is stable is important. Chapter 3 discusses stability guarantees for the proposed steering feel

model which accounts for the nonlinear tire saturation and power assist effects. This chapter analyzes the stability of this artificial steering feel model using Lyapunov stability analysis techniques. This ensures that stability guarantees encompassing both tire saturation and power assist effects can be obtained. Together, chapters 2 and 3 provide the reader a means of creating a realistic artificial steering feel with stability guarantees for steer-by-wire vehicles during conventional driving scenarios (i.e. without active steering interventions).

Chapter 4 investigates the interaction between steering feel and active steering and proposes the virtual wheel concept as a means of creating supportive steering feel. Active steering is a major benefit of using steer-by-wire systems and its effect on steering feel is not well documented. Reflecting the actual tire moments to the driver via the steering feel results in supportive steering feel when there is no active steering intervention. However, simulation and experiment show that, when there is an active steering intervention, this feel results in steering torque that causes the driver to turn against the intervention. This increases the disconnect between the driver and the active steering controller. Instead of using the tire moments acting on the actual roadwheel, the steering feel model should reflect the tire moments that act on the virtual wheel. The virtual wheel reflects where the roadwheels would be if they followed the driver's command during an active steering intervention. By definition, when there is no active steering intervention, this model boils down to the the steering feel model presented in Chapter 2. However, during an active steering intervention, it results in a supportive steering feel that encourages the driver to turn with the intervention rather than fight it. This reduces the disconnect between the driver and the controller. This result is borne out through simulation and experiment.

With the knowledge from Chapters 2, 3 and 4, an artificial steering feel that supports scenarios with and without active steering can be implemented on steer-by-wire vehicles. Chapter 5 builds on this by investigating overlaying this supportive steering feel with predictive haptic cues to aid in the obstacle avoidance task. This technique to create predictive haptic feedback to warn a driver of an upcoming obstacle is based on using a Model Predictive shared control framework. This technique mirrors the future tension between the shared controller's objectives of following the driver and

maintaining a feasible trajectory in its prediction horizon. This future tension provides current haptic feedback to the driver to cause him to modify his behavior early to maintain a safe trajectory. To test the efficacy of this feedback a proof-of-concept on-road experiment is conducted. This experiment decouples the visual and haptic cues of an obstacle during the obstacle avoidance task allowing the experimenter to test the efficacy of the predictive haptic feedback. This experimental setup was used in conjunction with a 11 participant driver study to show that the predictive feedback caused participants to react earlier and turn out of the path of an obstacle. This also resulted in reduced driver steering inputs and a less aggressive vehicle maneuver with minimal variation per treatment between different participants and trials.

6.1 Future Work

This dissertation lays the foundation for future research into using the capabilities of FFB steering to enhance the driver experience. A solution to create a realistic, supportive steering feel for drivers and the on-road obstacle avoidance experiment design proposed in this dissertation enable future work to focus on creating and studying haptic steering cues that could enhance vehicle safety and driver comfort.

Future work can focus on the human element of haptic feedback. In particular, driver acceptance of the predictive haptic feedback can be investigated for different demographic groups. Anecdotal evidence suggests that highly skilled performance drivers may be less accepting of the feedback than the average driver. Surveys can be used to determine the level of driver acceptance. The level of haptic assistance (LoHA as defined by Mulder et al. [53] and Abbink et al. [1]) can also be investigated to see if driver acceptance varies with the strength of haptic feedback.

Furthermore, going beyond the current FFB steering system, different and new haptic modalities can be used to communicate with the driver. In particular, skin stretch technology, which has proven effective in other scenarios with robotics [66], [15], [31], can be used either alone or in tandem with FFB, to provide haptic information to drivers. These experiments can shed light on which kinds of feedback are more effective than others.

Beyond surveys, physiological data can be used to investigate drivers' acceptance of the haptic feedback. In particular, an electroencephalogram (EEG) and/or a functional near infrared (fNIRS) system can be used to provide information about a driver's neurological reactions to haptic feedback. This reaction can be used to gauge a driver's acceptance of a particular form and level of feedback. This would build upon conflict monitoring work from the neuroscience field as discussed by Matsumoto and Tanaka. [49] and Botvinick et al. [17].

Though the 'popup' obstacle will still prove useful in decoupling the visual and haptic cues of the obstacle, different experiments may have to be designed to test the various new experimental questions objectively. For example, driver detection time of skin stretch versus force feedback must be taken into account when designing an experiment to test the efficacy of both these modalities. Also new experiment designs may have to incorporate directionality of the lane change as well. This will allow experimenters to test the efficacy of certain kinds of feedback like sinusoidal haptic feedback, which contain no directional information, against skin stretch and/or haptic steering, which do contain directional cues. Lastly, obtaining a larger and more diverse pool of drivers for the study would enable researchers to obtain findings related to driver demographics like age, driving experience and driving behavior.

Appendix A

X1 Force Feedback Steering System

The X1 experimental test vehicle is an electric vehicle designed and constructed by students at Stanford University. This vehicle is a true steer-by-wire vehicle with no mechanical connection between the handwheel and roadwheel. In order to create the torques on the handwheel which are needed for the work presented in this dissertation, a Force Feedback (FFB) steering system was designed and built. Based on the maximum torque required for artificial steering feel and haptic steering communication from prior work, this FFB steering system was designed to output up to 8 [Nm] of torque at the handwheel [46], [3], [57], [77]. Table A.1 illustrates the desired system specifications for the FFB system on X1. Figure A.1 shows the final FFB steering system that is currently mounted on X1 and is used for all the work presented in this dissertation. This appendix briefly illustrates the key features of the FFB steering system mounted on X1.

A.1 Mechanical Design

The FFB steering system is designed to give it as much of the functionality of a production steering system as possible. As a result, a fully telescoping steering system is desired. This gives the driver the ability to customize the position of the handwheel

making it comparable to a production system. This capability is also useful during driver studies in which drivers may have different preferences for their handwheel location. The driver then has the ability to move the steering system longitudinally (i.e. towards or away from the driver) and also change the angle of the handwheel column. Figure A.2 shows the front and side views of the CAD visualization of the FFB steering system. The longitudinal telescoping property is created by having the steering system slide on 80-20 rails. The ability to change the angle of the handwheel is implemented by having discrete mounting points drilled into quarter-circle plates (seen clearly in Figure A.2(b)). The driver can then use different mounting points to

Table A.1: FFB System Specifications

Parameter	Specification	Units
Maximum input frequency at handwheel	3	Hz
Average input frequency at handwheel	1.5	Hz
Maximum torque applied at handwheel	8	Nm
Average torque applied at handwheel	4	Nm
Maximum axial load at handwheel	500	N
Maximum radial load at handwheel	2000	N

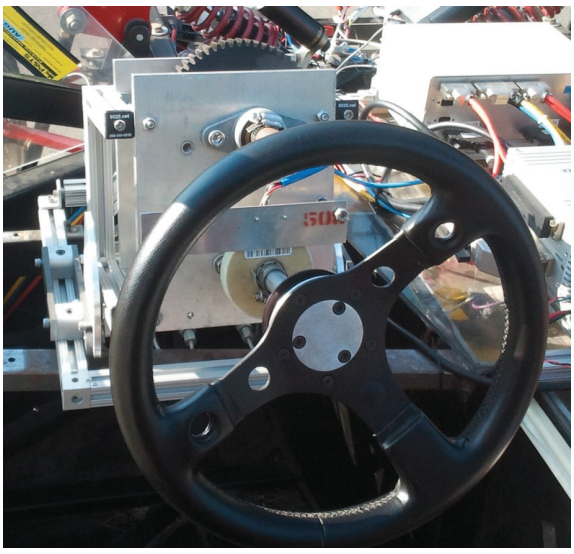

Figure A.1: FFB steering system mounted on X1

obtain different angles of the handwheel column.

A.2 Electrical Design

Figure A.3 illustrates the electrical schematic for the FFB steering system. A dSpace computer reads all inputs, performs all computation and sends all actuator commands on X1 at 500 [Hz]. It acts as a central node. A combination of a potentiometer and encoder sends information to the dSpace computer which can then compute the handwheel angle electronically. The dSpace computer communicates, using a CANopen bus, with the FFB motor amplifier. The FFB motor is coupled with a 30:1 harmonic drive which gears the torque up. This torque is then applied to the handwheel. Failure of the CANopen bus results in the dSpace computer reinitializing the bus within 1-2 execution timesteps ensuring effectively continuously operation.

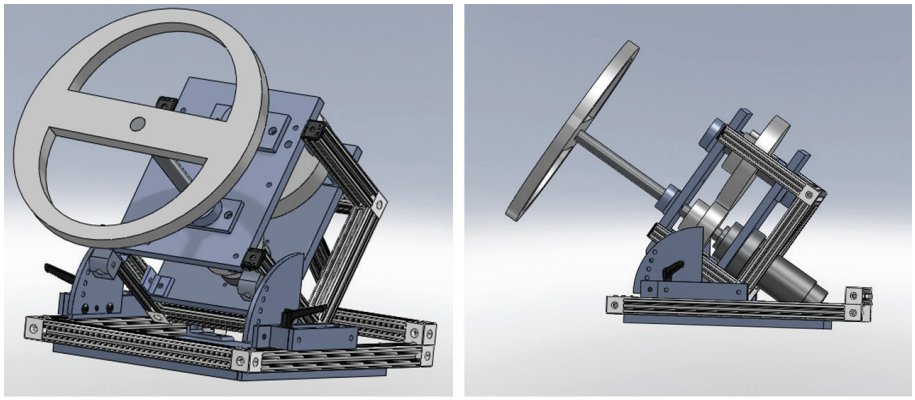

Figure A.2: CAD visualization of FFB steering system

A.3 System Identification

Performing system identification on the FFB steering system characterizes the system to obtain the inherent system inertia, damping and friction. The following model of the steering system is used for the system identification:

$$J_{system}\ddot{\delta_{hw}} + b_{system}\dot{\delta_{hw}} + F_s sign(\dot{\delta_{hw}}) = \tau_{input} \tag{A.1}$$

where δ_{hw} is the handwheel angle, J_{system} is the inherent system inertia, b_{system} is the inherent system damping and F_s is the coulomb friction present in the system. τ_{input} is the input torque on this system. Based on the motor and harmonic drive specifications, a direct relationship is obtained between current commanded to the system and the input torque, τ_{input} on the system.

To characterize the steering system, an input signal which excites the system in the frequency range of interest must be generated. For this system, since a typical driver's steering input frequency range is no more than 5 [Hz], a chirp current input signal

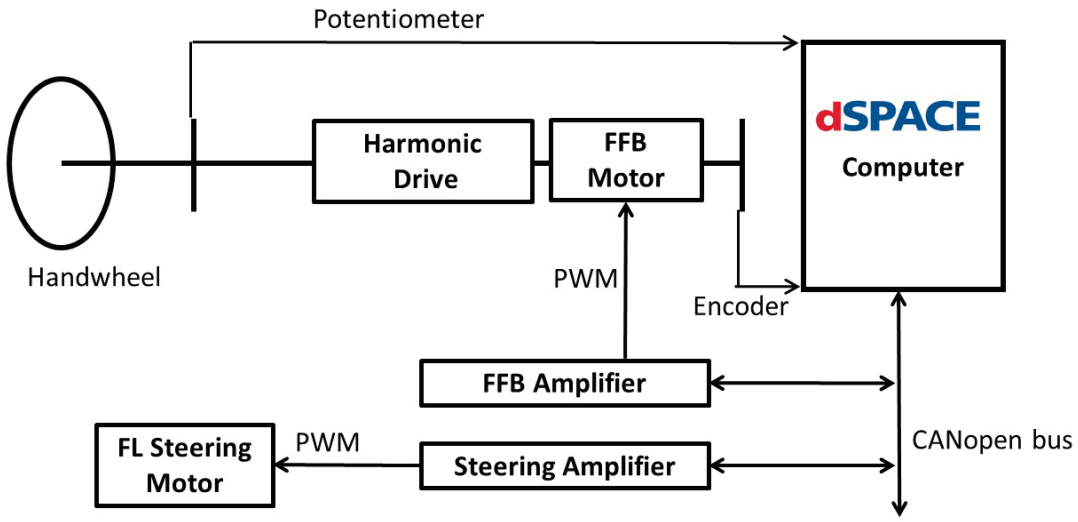

Figure A.3: Electrical schematic for FFB steering system

sweeps over the frequency range 0.05 [Hz] to 5 [Hz]. Using the measured system output of handwheel angle (δ_{hw}), parameters for the model presented in Equation (A.1) can be tuned to match the actual system response for the same input. Figure A.4 illustrates this comparison after the model has been tuned. This figure demonstrates that the tuned model clearly matches the actual response very well. Based on this, the inherent system parameters for the FFB system can be obtained and are displayed in Table A.2. Note that the value of the coulomb friction term (F_s) is found to be small when compared to the average expected torque of 2 [Nm] indicating that the driver should not feel much of the friction in the system during general operation.

Table A.2: System Parameters of FFB System

Parameter	Quantity	Units
Inherent system inertia (J_{system})	0.0011	kgm^2
Inherent system damping (b_{system})	0.012	$\frac{Nm}{rads^{-1}}$
System coulomb friction (F_s)	0.045	Nm

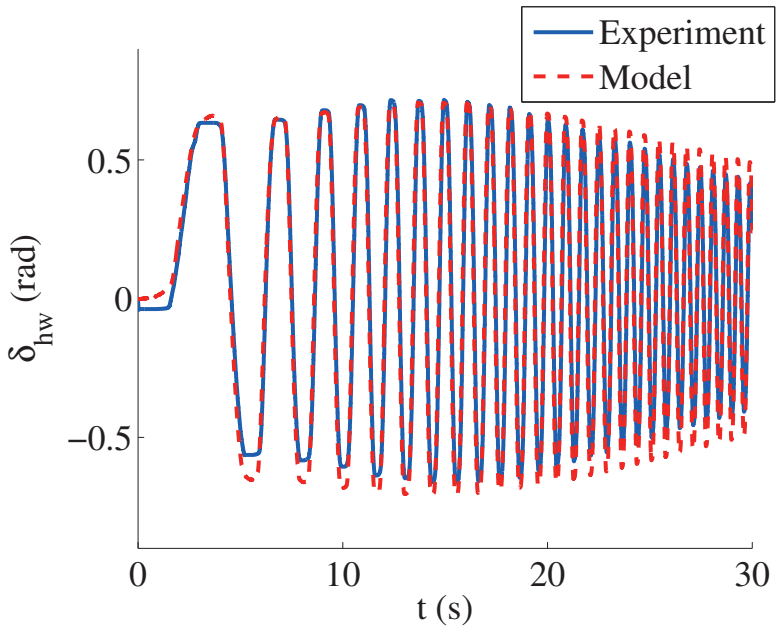

Figure A.4: System identification chirp response with simulated model

Bibliography

[1] David A. Abbink, Mark Mulder, and Erwin R. Boer. Haptic shared control: smoothly shifting control authority? *Cognition, Technology & Work*, 14(1):19–28, November 2011.

[2] J Ackermann, D Odenthal, and T Bunte. Advantages of active steering for vehicle dynamics control. *Proceedings of 32nd ISATA, Automotive Mechatronics Design and Engineering*, pages 263–270, 1999.

[3] FJ Adams. Power steering 'road feel'. *SAE 830998*, June 1983.

[4] Sanket Amberkar, Farhad Bolourchi, Jon Demerly, and Scott Millsap. A control system methodology for steer by wire systems. *Steering and Suspension Technology Symposium*, 2004(724), 2004.

[5] S J Anderson, S B Karumanchi, and K Iagnemma. Constraint-based planning and control for safe, semi-autonomous operation of vehicles. In *Intelligent Vehicles Symposium (IV), 2012 IEEE*, pages 383–388, June 2012.

[6] Sterling J. Anderson, Steven C. Peters, Tom E. Pilutti, and Karl Iagnemma. An optimal-control-based framework for trajectory planning, threat assessment, and semi-autonomous control of passenger vehicles in hazard avoidance scenarios. *International Journal of Vehicle Autonomous Systems*, 8(2/3/4):190, 2010.

[7] Suguru Arimoto, Fumio Miyazaki, H.G. Lee, and Sadao Kawamura. Rivival of lyapunov's direct method in robot control and design. *1988 American Control Conference*, pages 1764–1769, 1988.

[8] Shoji Asai, Hiroshi Kuroyanagi, Shinji Takeuchi, Toshihiro Takahashi, and Shoji Ogawa. Development of a steer-by-wire system with force feedback using a disturbance observer. *SAE International 2004-01-1100*, (724), 2004.

[9] Romuald Aufrère, Jay Gowdy, Christoph Mertz, Chuck Thorpe, Chieh Chih Wang, and Teruko Yata. Perception for collision avoidance and autonomous driving, 2003.

[10] A. Badawy, J. Zuraski, F. Bolourchi, and A. Chandy. Modeling and analysis of an electric power steering system. *Steering and Suspension Technology Symposium 1999*, 1999.

[11] Avinash Balachandran, Matthew Brown, Stephen M. Erlien, and J. Christian Gerdes. Creating predictive haptic feedback for obstacle avoidance using a model predictive control (MPC) framework. In *IEEE Intelligent Vehicles Symposium (IV2015)*, 2015.

[12] Avinash Balachandran, Stephen M. Erlien, and J. Christian Gerdes. The virtual wheel concept for supportive steering feedback during active steering interventions. *ASME 2014 Dynamic Systems and Control Conference, San Antonio, TX*, 2014.

[13] Avinash Balachandran and J. Christian Gerdes. Artificial steering feel design for steer-by-wire vehicles. In *7th IFAC Symposium on Advances in Automotive Control*, pages 404–409, September 2013.

[14] Avinash Balachandran and J. Christian Gerdes. Designing steering feel for steer-by-wire vehicles using objective measures. *IEEE/ASME Transactions on Mechatronics*, 20(1):373–383, February 2015.

[15] Karlin Bark, Jason Wheeler, Gayle Lee, Joan Savall, and Mark Cutkosky. A wearable skin stretch device for haptic feedback. In *Proceedings - 3rd Joint EuroHaptics Conference and Symposium on Haptic Interfaces for Virtual Environment and Teleoperator Systems, World Haptics 2009*, pages 464–469, 2009.

[16] Craig Earl Beal and J. Christian Gerdes. Model predictive control for vehicle stabilization at the limits of handling. *IEEE Transactions on Control Systems Technology*, 21(4):1258–1269, July 2013.

[17] M M Botvinick, T S Braver, D M Barch, C S Carter, and J D Cohen. Conflict monitoring and cognitive control. *Psychological review*, 108(3):624–652, 2001.

[18] Thorsten Brandt, Thomas Sattel, and Michael Bohm. Combining haptic human-machine interaction with predictive path planning for lane-keeping and collision avoidance systems. In *2007 IEEE Intelligent Vehicles Symposium*, pages 582–587. IEEE, June 2007.

[19] Carlos Canudas-de Wit, Hubert Bechart, Xavier Claeys, Pietro Dolcini, and John-jairo Martinez. Fun-to-drive by feedback. *European Journal of Control*, 11(4-5):353–383, January 2005.

[20] Samuel Y. Chang, Christopher R. Carlson, and J. Christian Gerdes. A lyapunov function approach to energy based model reduction. *Proceedings of 2001 ASME International Mechanical Engineering Congress and Exposition*, pages 1315–1322, 2001.

[21] Robert Charette. Nissan moves to steer-by-wire for select Infiniti models, October 17, 2012. *IEEE Spectrum*, 2012.

[22] Stephen M. Erlien, Susumu Fujita, and J. Christian Gerdes. Safe driving envelopes for shared control of ground vehicles. In *7th IFAC Symposium on Advances in Automotive Control*, pages 831–836, September 2013.

[23] C. Favre. Fly-by-wire for commercial aircraft: the Airbus experience. *International Journal of Control*, 59(1):139–157, 1994.

[24] E Fiala. Lateral forces on rolling pneumatic tires. *Zeitschrit V.D.I*, 96, 1954.

[25] Benjamin A C Forsyth and Karon E Maclean. Predictive haptic guidance: intelligent user assistance for the control of dynamic tasks. *IEEE Transactions on Visualization and Computer Graphics*, 12(1):103–113, 2006.

[26] Christopher D Gadda, Shad M Laws, and J Christian Gerdes. Generating diagnostic residuals for steer-by-wire vehicles. *IEEE Transactions on Control Systems Technology*, 15(3):529–540, 2007.

[27] Thomas D. Gillespie. *Fundamentals of vehicle dynamics*. SAE International, 1992.

[28] Donald A. Gordon. Experimental isolation of the driver's visual input. *Human Factors: The Journal of the Human Factors and Ergonomics Society*, 8(2):129–138, 1966.

[29] Weston B. Griffin, William R. Provancher, and Mark R. Cutkosky. Feedback strategies for telemanipulation with shared control of object handling forces. *Presence: Teleoperators and Virtual Environments*, 14(6):720–731, 2005.

[30] Paul G. Griffiths and R. Brent Gillespie. Sharing control between humans and automation using haptic interface: Primary and secondary task performance benefits. *Human Factors: The Journal of the Human Factors and Ergonomics Society*, 47(3):574–590, October 2005.

[31] Vincent Hayward and Juan Manuel Cruz-Hernandez. Tactile display device using distributed lateral skin stretch. *Proceedings of the haptic interfaces for virtual environment and teleoperator systems symposium*, pages 1309–1314, 2000.

[32] Robert C. Hoffman, Jeffrey L. Stein, S S. Louca, and Kunsoo Huh. Using the milliken moment method and dynamic simulation to evaluate vehicle stability and controllability. *International Journal of Vehicle Design*, 48(1/2):132, 2008.

[33] Y H J Hsu and J C Gerdes. A feel for the road: A method to estimate tire parameters using steering torque. In *International Symposium on Advanced Vehicle Control*, 2006.

[34] Yung-Hsiang Judy Hsu, Shad M Laws, and J Christian Gerdes. Estimation of tire slip angle and friction limits using steering torque. *IEEE Transactions on Control Systems Technology*, 18(4):896–907, July 2010.

[35] M Husain, B Ashrafi, and G Stout. Generating steering feel for steer-by-wire systems. *US Patent Office, US 6,678,596*, 2004.

[36] S. Inagaki, I. Kshiro, and M. Yamamoto. Analysis on vehicle stability in critical cornering using phase-plane method. *Proceedings of the International Symposium on Advanced Vehicle Control*, 1994.

[37] ISO13674-1:2010. Road vehicles - Test methods for the quantification of on-centre handling - Part 1: Weave Test. 2010.

[38] Matthew J Jensen, A Madison Tolbert, John R Wagner, Fred S Switzer, and Joshua W Finn. A customizable automotive steering system with a haptic feedback control strategy for obstacle avoidance notification. *IEEE Transactions on Vehicular Technology*, 60(9):4208–4216, November 2011.

[39] D. Katzourakis, M. Alirezaei, J. C F De Winter, M. Corno, R. Happee, A. Ghaffari, and R. Kazemi. Shared control for road departure prevention. In *Conference Proceedings - IEEE International Conference on Systems, Man and Cybernetics*, pages 1037–1043, 2011.

[40] Diomidis Katzourakis, Efstathios Velenis, Edward Holweg, and Riender Happee. Haptic steering support when driving at the tires cornering limits. *Proceedings of the 11th International Symposium on Advanced Vehicle Control 2012, AVEC12*, 2012.

[41] T. Kawabe, H. Nishira, and T. Ohtsuka. An optimal path generator using a receding horizon control scheme for intelligent automobiles. In *Proceedings of the 2004 IEEE International Conference on Control Applications, 2004.*, volume 2, pages 1597–1602. IEEE, 2004.

[42] Philip Koehn and Michael Eckrich. Active steering - The BMW approach towards modern steering technology. *SAE International 2004-01-1105*, March 2004.

[43] Dale A. Lawrence. Stability and transparency in bilateral teleoperation. *IEEE Transactions on Robotics and Automation*, 9(5):624–637, 1993.

[44] John Leonard, Jonathan How, Seth Teller, Mitch Berger, Stefan Campbell, Gaston Fiore, Luke Fletcher, Emilio Frazzoli, Albert Huang, Sertac Karaman, Olivier Koch, Yoshiaki Kuwata, David Moore, Edwin Olson, Steve Peters, Justin Teo, Robert Truax, Matthew Walter, David Barrett, Alexander Epstein, Keoni Maheloni, Katy Moyer, Troy Jones, Ryan Buckley, Matthew Antone, Robert Galejs, Siddhartha Krishnamurthy, and Jonathan Williams. A perception-driven autonomous urban vehicle. *Journal of Field Robotics*, 25(10):727–774, October 2008.

[45] Jesse Levinson, Jake Askeland, Jan Becker, Jennifer Dolson, David Held, Soeren Kammel, J. Zico Kolter, Dirk Langer, Oliver Pink, Vaughan Pratt, Michael Sokolsky, Ganymed Stanek, David Stavens, Alex Teichman, Moritz Werling, and Sebastian Thrun. Towards fully autonomous driving: Systems and algorithms. In *IEEE Intelligent Vehicles Symposium, Proceedings*, number Iv, pages 163–168, 2011.

[46] A. Liu and S. Chang. Force feedback in a stationary driving simulator. *1995 IEEE International Conference on Systems, Man and Cybernetics*, 2(2):1711–1716, 1995.

[47] A Liu and S Chang. Force feedback in a stationary driving simulator. In *1995 IEEE International Conference on Systems, Man and Cybernetics. Intelligent Systems for the 21st Century*, volume 2, pages 1711–1716. IEEE, October 1995.

[48] Uday B Mandhata, Matthew J Jensen, John R Wagner, Fred S Switzer, Darren M Dawson, and Joshua D Summers. Evaluation of a customizable haptic feedback system for ground vehicle steer-by-wire interfaces. In *Proceedings of the American Controls Conference*, pages 2781–2787, 2012.

[49] Kenji Matsumoto and Keiji Tanaka. Neuroscience. Conflict and cognitive control. *Science (New York, N.Y.)*, 303(5660):969–970, 2004.

[50] J Mattingley and S Boyd. CVXGEN: A code generator for embedded convex optimization. *Optimization and Engineering*, 13(1):1–27, 2012.

[51] J Mattingley, Yang Wang, and S Boyd. Code generation for receding horizon control. In *2010 IEEE International Symposium on Computer-Aided Control System Design (CACSD)*, pages 985–992, 2010.

[52] P. Mitra and G. Niemeyer. Dynamic proxy objects in haptic simulations. *IEEE Conference on Robotics, Automation and Mechatronics, 2004.*, 2:1–3, 2004.

[53] M. Mulder, D. A. Abbink, and E. R. Boer. Sharing Control With Haptics: Seamless Driver Support From Manual to Automatic Control. *Human Factors: The Journal of the Human Factors and Ergonomics Society*, 54(5):786–798, May 2012.

[54] Mark Mulder, David A. Abbink, and Erwin R. Boer. The effect of haptic guidance on curve negotiation behavior of young, experienced drivers. In *2008 IEEE International Conference on Systems, Man and Cybernetics*, pages 804–809. IEEE, October 2008.

[55] Ba-hai Nguyen and Jee-hwan Ryu. Direct current measurement based steer-by-wire systems for realistic driving feeling. In *2009 IEEE International Symposium on Industrial Electronics*, number ISlE, pages 1023–1028. IEEE, July 2009.

[56] Kenneth D Norman. Objective Evaluation of On-Center Handling Performance. *International Congress & Exposition*, SAE 840069, 1984.

[57] Dirk Odenthal, Tilman Bunte, Heinza-Dieter Heitzer, and Eicker Christoph. How to make steer-by-wire feel like power steering. In Luis Basañez, editor, *Proceedings of the 15th IFAC World Congress*, pages 1497–1497, July 2002.

[58] Se-Wook Oh, Seok-Chan Yun, Ho-Chol Chae, Seok-Hwan Jang, Jae-Ho Jang, and Chang-Soo Han. The development of an advanced control method for the steer-by-wire system to improve the vehicle maneuverability and stability. *SAE 2003 World Congress & Exhibition, SAE2003-01-0578*, 2003.

[59] H.B. Pacejka. *Tire and vehicle dynamics*. Butterworth edition, 2012.

[60] Andrew J. Pick and David J. Cole. A mathematical model of driver steering control including neuromuscular dynamics. *ASME Journal of Dynamic Systems, Measurement, and Control*, 130(3):031004, 2008.

[61] William G. Redmond Jr. Fly-by-wire. *US Patent Office, US 3679156 A*, 1972.

[62] Diego Ruspini and Oussama Khatib. Haptic display for human interaction with virtual dynamic environments. *Journal of Robotic Systems*, 18(12):769–783, 2001.

[63] J Ryu and H S Kim. Virtual environment for developing electronic power steering and steer-by-wire systems. In *Intelligent Robots and Systems, 1999. IROS'99. Proceedings. 1999 IEEE/RSJ International Conference on*, volume 3, pages 1374–1379. IEEE, 1999.

[64] M K Salaani, G J Heydinger, and P A Grygier. Experimental steering feel performance measures. *SAE Transactions*, 113(6):680–683, 2004.

[65] M Kamel Salaani, Gary J Heydinger, and Paul A Grygier. Closed loop steering system model for the National Advanced Driving Simulator. *SAE 2004-01-1072*, 2004.

[66] Samuel B. Schorr, Zhan Fan Quek, Robert Y. Romano, Ilana Nisky, William R. Provancher, and Allison M. Okamura. Sensory substitution via cutaneous skin stretch feedback. In *Proceedings - IEEE International Conference on Robotics and Automation*, pages 2341–2346, 2013.

[67] Masaya Segawa, Shuuji Kimura, Tomoyasu Kada, and Shirou Nakano. A study on the relationship between vehicle behavior and steering wheel torque on steer by wire vehicles. *Vehicle System Dynamics 41*, pages 202–211, 2004.

[68] Yang Shengbing, Den Chunan, Ji Xuewu, and Chen Kuiyuan. Research on road feeling control strategy of steer-by-wire. *SAE International 2007-01-3652*, 2007.

[69] Yasuo Shimizu and Toshitake Kawai. Development of electric power steering. *SAE 910014*, 1991.

[70] Neville a. Stanton and Philip Marsden. From fly-by-wire to drive-by-wire: Safety implications of automation in vehicles. *Safety Science*, 24(1):35–49, 1996.

[71] M. Steele and R. B. Gillespie. Shared control between human and machine: using a haptic steering wheel to aid in land vehicle guidance. *Proceedings of the Human Factors and Ergonomics Society Annual Meeting*, 45(23):1671–1675, October 2001.

[72] Keisuke Suzuki. Analysis of driver's steering behavior during auditory or haptic warnings in lane departure situations. *Proceedings of the International Symposium on Advanced Vehicle Control (AVEC)*, JSAE 20024, 2002.

[73] Joshua P. Switkes, Eric J. Rossetter, Ian A. Coe, and J. Christian Gerdes. Handwheel force feedback for lanekeeping assistance: combined dynamics and stability. *ASME Journal of Dynamic Systems, Measurement, and Control*, 128(3):532, 2006.

[74] Kirstin L.R. Talvala, Krisada Kritayakirana, and J. Christian Gerdes. Pushing the limits: From lanekeeping to autonomous racing. *Annual Reviews in Control*, 35(1):137–148, April 2011.

[75] Mandhata Uday, John R Wagner, Fred Switzer, Darren M Dawson, and Joshua D Summers. A Customizable steer-by-wire interface for ground vehicles. In Trächtler Ansgar, editor, *Advances in Automotive Control*, pages 656–661, July 2010.

[76] D. E. Williams. Synthetic torque feedback to improve heavy vehicle drivability. *Proceedings of the Institution of Mechanical Engineers, Part D: Journal of Automobile Engineering*, 223(12):1517–1527, December 2009.

[77] Daniel E Williams and Kenneth A Sherwin. Artificial steering feel. *SAE International Journal of Passenger Cars Mechanical Systems*, 2(1):229–238, 2009.

[78] Fernando A. Wilson and Jim P. Stimpson. Trends in fatalities from distracted driving in the United States, 1999 to 2008. *American Journal of Public Health*, 100(11):2213–2219, 2010.

[79] A. Zaremba and R.I. Davis. Dynamic analysis and stability of a power assist steering system. In *Proceedings of American Control Conference*, volume 6, pages 4253–4257. American Autom Control Council, 1995.